UNIVERSITY OF CAPE TOWN

DEPARTMENT OF ELECTRICAL ENGINEERING

Ultrasonic spectroscopy of liquid filled piezoelectric tube

Bjorn Alexander Prenzlow

PhD

2006

Supervisor: Prof. J Tapson and Assoc. Prof. J Davies
Assessor:

Abstract

The characterization and classification of liquids through instrumentation is essential in many industries. As such, measuring the characteristics of liquids is not just useful as a control parameter within an industrial process; such measurements can also be used to classify the liquid. Such a sensor is especially practical if it can be connected in-line with the liquid to be measured, thus minimally influencing flow.

A piezoceramic tube was studied in an attempt to produce a sensor to encompass exactly those aims. Spectra were taken of liquid-filled piezoceramic tubes. Several models for this system, both for the piezoceramic tube and the liquid within it, were then studied to determine an accurate mathematical representation of the measured spectra. The model ultimately used was a derived equation for the dynamics of the liquid.

The simulated spectra were optimized to match the actual data, using several techniques ranging from simple search algorithms to breeder algorithms. The optimization technique used was based upon the complexity of the model implemented. The effect of the error calculation method is important and is discussed. From the optimization results, the speed of sound, density and viscosity of the liquid can be determined to accuracies of less than 0.2%, 3% and 10% respectively.

Contents

Contents 1

List of Figures 4

List of Tables 7

1 Introduction 1

2 Liquid properties and their measurement 3
- 2.1 Physical properties of liquids . . . 3
  - 2.1.1 Density . . . 3
  - 2.1.2 Bulk Modulus . . . 4
  - 2.1.3 Longitudinal Speed of Sound . . . 4
  - 2.1.4 Viscosity . . . 5
  - 2.1.5 Effects of frequency on parameters . . . 7
- 2.2 Vibrational measurement techniques . . . 8
  - 2.2.1 Ultrasonic Spectroscopy . . . 8
  - 2.2.2 Sensors based on liquid effect on transducer . . . 8
  - 2.2.3 Sensors based on the resonant behavior of the liquid . . . 9

3 System Description 13

4 Spectral response due to the piezoceramic tube 16
- 4.1 Piezoelectricity . . . 16
- 4.2 Polarization of tube . . . 17
- 4.3 Effect due to case capacitance and the cabling . . . 17
- 4.4 Dominant resonant modes in a piezoceramic tube . . . 19
  - 4.4.1 Radial modes . . . 20
  - 4.4.2 Length modes . . . 21
  - 4.4.3 Circumferential modes . . . 21
- 4.5 Effect of placing a liquid into piezoceramic tube . . . 21
- 4.6 Attempts to model the behavior of the piezoceramic tube . . . 23
  - 4.6.1 The Butterworth - Van Dyke model . . . 23
  - 4.6.2 Mason's model . . . 24
  - 4.6.3 Redwood's model . . . 26
  - 4.6.4 The KLM model . . . 26

4.6.5 Solving equations of state for a piezoceramic tube 28
4.7 Attempts to obtain and use the base spectrum of empty piezoceramic tube directly 31

5 Spectral response of the liquid-filled piezoceramic tube 35
5.1 How energy is coupled to liquids 35
5.2 Resonant response of Liquids 35
5.3 Effect due to the radial nature of the waves 36
5.4 Effect of viscosity on created modes 37
5.5 Models to represent the liquid 38
5.5.1 Transformer coupled RLC circuits 39
5.5.2 Electrical transmission lines and frequency offset transmission lines 40
5.5.3 Solution though continuum mechanics for a viscoelastic liquid 41
5.6 Effects on coupling 44
5.7 Integration of the liquid model with piezoceramic tube 46
5.8 Visualization of the simulated spectra 46

6 Model evaluation 50
6.1 Combining the models 50
6.2 Practical variations in case capacitance 51
6.3 The spectrum of the empty piezoceramic tube 52
6.4 Determination of the transformer values and loss components 52
6.5 The ranges of frequency analysed 52
6.6 Comparison with real spectra 53

7 System Implementation 56
7.1 Device description 56
7.2 The transducer 56
7.2.1 The piezoceramic tube 57
7.2.2 The piezoceramic tube housing 58
7.3 Thermal regulation 59
7.3.1 The thermal jacket 61
7.3.2 The thermal bath 61
7.4 Data capture 64
7.4.1 The impedance analyzer 64
7.4.2 The connecting cable 64
7.5 Sample preparation 65

8 Evaluation of Error 66
8.1 Difficulties in describing spectral error 66
8.2 Introducing tolerance to mode placement 68
8.2.1 Distance sum between nearest neighbour points 68
8.2.2 Match distance 69

9 Optimization to obtain liquid parameters **72**
9.1 Adaptive Mutation Breeder Algorithm 72
9.1.1 Basic Description of Breeder Algorithm 73
9.1.2 Methods of recombination 75
9.1.3 Adaptive mutation 76
9.2 Optimization of liquid's parameters 76
9.2.1 Determination of speed of sound 76
9.2.2 Analysis of remaining error space 77
9.2.3 Search to determine density and viscosity 79

10 Results **80**
10.1 Comparison of spectra after cable mode removal 80
10.2 Comparison between optimized spectra and actual spectra and error space for each liquid 80
10.2.1 Castor Oil 82
10.2.2 Glycerol (88%) / Water mixture 84
10.2.3 Olive Oil 87
10.2.4 Linseed Oil 87
10.3 Discussion 89

11 Conclusions **93**

12 Future work **95**

Bibliography **101**

List of Figures

2.1 Diagram showing interferometric technique for determining physical properties of gasses. 10
2.2 Diagram showing basic representation of impedance tube sensor. . . . 11

3.1 Diagram showing a pictorial view of sound travelling in a piezoceramic tube. 14
3.2 Admittance spectra of an olive oil filled piezoceramic tube over the tube's thickness resonance. 14

4.1 Spectra of empty piezo tube of dimensions: inner diameter 31.8 mm, outer diameter 38.0 mm and length 38.3mm. 18
4.2 Diagram of RLC circuit used to simulate the spectral response of the cable and the case capacitance. 18
4.3 Spectra of empty piezo tube with case capacitance and cable removed. 19
4.4 Spectra of empty piezo tube showing radial, length and circumferential modes. 20
4.5 Spectra of conductance and susceptance of a olive oil filled piezo tube. 22
4.6 Diagram illustrating the Butterworth - van Dyke model for a quartz resonator. 24
4.7 Diagram showing Mason's equivalent model for a piezo plate. 25
4.8 Diagram of Redwood's equivalent model of a piezo plate. 26
4.9 Diagram of the KLM equivalent model of a piezo plate. 27
4.10 Spectra of resistance and reactance of an empty and an olive oil filled piezo tube after removal of the cable impedance and case capacitance. 31
4.11 Spectra of olive oil sample, once the cable component had been removed and the piezotube subtracted. 33

5.1 Diagram representing the initial approximation of the sound travelling though the liquid cylinder. 36
5.2 Resistance spectra of several real liquids with piezoceramic tube and cable responses removed. 37
5.3 A closer look at the resistance spectra of liquids with the piezoceramic tube impedance and cable modes removed. 38
5.4 Diagram representing the RLC model originally attempted to replicate the liquid's spectra. 39

5.5 Diagram repesenting the transmission line model used to simulate a spectra. 40
5.6 Spectra of the simulated resistance of several liquids. 47
5.7 Simulated reactance of several liquids. 48
5.8 A closer look at simuated resistance shows the different spacing between modes due to variations in sound speed. 49

6.1 Diagram of completed model for filled piezoceramic tube. 50
6.2 Real and simulated spectra of resistance and reactance for an olive oil sample over the first thickness resonance mode of the piezoceramic tube. 53
6.3 Real and simulated spectra of resistance and reactance for an olive oil sample over the second thickness resonance mode of the piezoceramic tube. 54
6.4 Real and simulated spectra of resistance and reactance for an olive oil sample over the third thickness resonance mode of the piezoceramic tube. 54
6.5 Real and simulated spectra of resistance and reactance for an olive oil sample over the fourth thickness resonance mode of the piezoceramic tube. 55

7.1 Basic diagram showing the fundamental components of the system implementation. 57
7.2 A typical piezoceramic tube. This tube has dimensions: inner diameter 31.8mm, outer diameter 38mm and length 38.3mm. The electrode was made of fired screen printed silver. 58
7.3 Exploded view of the piezotube housing. The square cut-out on the inner lid houses the SMA connector. 60
7.4 Exploded view of thermal jacket. 62
7.5 Picture of the thermal bath. 63

8.1 These graphs to show how a slight difference in mode placement affects error calculations. 67
8.2 Comparison between nearest neighbour error and RMS distance error for a single reference point. 69
8.3 Flow chart of nearest neighbour distance algorithm. 70

9.1 Flow chart of a Breeder Algorithm [16]. 74
9.2 Surface plot of error in relation to density and viscosity. 78

10.1 Reactance spectra of empty piezoceramic tube, with case capacitance removed, and of the tube filled with different liquids. 81
10.2 Surface plot of the error vs simulated density and viscosity compared to castor oil sample at $30°C$. 82
10.3 Resistance and reactance spectra for actual and modelled castor oil sample at $30°C$ over the first thickness mode of the piezotube. 83
10.4 Resistance and reactance spectra for actual and modelled castor oil sample at $30°C$ over the second thickness mode of the piezotube. . . . 83

10.5 Resistance and reactance spectra for actual and modelled castor oil sample at $30°C$ over the third thickness mode of the piezotube. 84
10.6 Surface plot of the error vs simulated density and viscosity for a glycerol (88%) / water mixture sample at $30°C$. 85
10.7 Resistance and reactance spectra for actual and modelled glycerol (88%) / water mixture sample at $30°C$ over the first thickness mode of the piezotube. 85
10.8 Resistance and reactance spectra for actual and modelled glycerol (88%) / water mixture sample at $30°C$ over the second thickness mode of the piezotube. 86
10.9 Resistance and reactance spectra for actual and modelled glycerol (88%) / water mixture sample at $30°C$ over the third thickness mode of the piezotube. 86
10.10Surface plot of the error vs simulated density and viscosity for a olive oil sample at $30°C$. 87
10.11Resistance and reactance spectra for actual and modelled olive oil sample at $30°C$ over the first thickness mode of the piezotube. 88
10.12Resistance and reactance spectra for actual and modelled olive oil sample at $30°C$ over the second thickness mode of the piezotube. 88
10.13Resistance and reactance spectra for actual and modelled olive oil sample at $30°C$ over the third thickness mode of the piezotube. 89
10.14Surfance plot of the error vs simulated density and viscoity for a linseed oil sample at $30°C$. 90
10.15Resistance and reactance spectra for actual and modelled linseed oil sample at $30°C$ over the first thickness mode of the piezotube. 90
10.16Resistance and reactance spectra for actual and modelled linseed oil sample at $30°C$ over the second thickness mode of the piezotube. . . . 91
10.17Resistance and reactance spectra for actual and modelled linseed oil sample at $30°C$ over the third thickness mode of the piezotube. 91

List of Tables

5.1 Table of measured liquid properties 46

Chapter 1

Introduction

Industrial processes often benefit from the measurement of the physical characteristics of the liquids that they produce. Many sensors are available to determine density in-line in pipes; and the measurement of viscosity in-line is also feasible but less common or accurate. Most of these techniques, however, obstruct the flow of the liquid due to the intrusion of the sensor into the flow. This means that a liquid has to be pumped harder to overcome the pressure drop across the sensor. Also, the sensor is likely to suffer abrasive damage from the continuous flow of the liquid past it, especially if there are solids suspended in the liquid. It would thus be beneficial to have an in-line sensor that has no impact on the flow of the liquid in the piping in which it is being transported.

Over the past few years, the author and colleagues have been using radially polarized piezoceramic tubes to accurately measure the relative change in speed of sound in liquids as part of a non-linearity parameter () sensor [15][42]. As part of that work, the admittance spectra for several liquids placed inside these piezoelectric tubes were analyzed. These spectra had many resonant modes which were dependent on the physical parameters of liquid (density, viscosity, speed of sound, etc.). If an accurate model for these spectra could be produced, then the parameters of the liquid ought to be determinable.

Such a sensor would be very useful, as the diameter of a piezoceramic tube can be made the same as that of a pipe to which it could be connected, and thus it would make for a convenient in-line sensor. Also, it would have no moving parts that could suffer damage. Additionally, the admittance spectrum of a tube can be sampled at very low voltage, so sound waves being set up by the piezoceramic tube are of such a small amplitude that they are unlikely to damage or alter any sample.

Thus, this work is based on the idea of filling a piezoceramic tube with a sample liquid; measuring the admittance spectra of the liquid filled tube; removing the dy-

namics of the piezoceramic tube; and fitting a model to that data to determine the density, viscosity and speed of sound of Newtonian liquids.

The document is broken into four primary parts namely:

- The basic theory of liquids, within the scope of this sensor and the techniques used to measure the properties (Chapter 2).
- A discussion of the individual components that affect the spectrum of the tube (Chapter 3); techniques to model or overcome the mechanical and electrical response of the piezoceramic tube (Chapter 4); the derivation of a realistic model to represent the modal response of the liquid (Chapter 5); and evaluating how representative these models are, with respect to producing a reliable sensor (Chapter 6).
- The implementation of this sensor with respect to hardware (Chapter 7) and software. The software implementation can be broken down into two components, namely the evaluation of the spectral error (Chapter 8), and the optimization of the error function to fit simulated spectra to actual data (Chapter 9).
- The evaluation of the results for different liquids (Chapter 10), and the conclusions drawn from these results (Chapter 11).

Chapter 2

Liquid properties and their measurement

2.1 Physical properties of liquids

2.1.1 Density

The density of a liquid, ρ, is defined by the mass of a liquid, m, divided by the volume, V, that the mass of liquid fills, as shown in equation 2.1.

$$\rho = \frac{m}{V} \tag{2.1}$$

Several components can affect the density of a liquid, such as its temperature and the pressure that the liquid is under. These variables have a small effect on the density of the samples that will be studied in the project, however as the thermal dependence of other variables studied during this work is quite high, the temperature was stabilized and thus these effects can be ignored.

Density is most easily measured statically using a pycnometer. Here a glass flask is used to contain a fixed volume of liquid; the mass of this volume is then measured on a scale and Equation 2.1 is used to calculate the density. Density can also be measured by the amount of pressure that a height of fluid produces.

There are in-line processes that can be used to measure density. A Coriolis flow sensor measures mass flow rate. If the volume flow rate is measured using another technique, the density can be determined using the geometry of the pipe. There are also many vibratory measurement techniques that will be discussed later in this chapter (section 2.2).

2.1.2 Bulk Modulus

Although for most applications, a liquid is assumed to be incompressible, there is a definite change in the volume of a liquid when it is placed under pressure. Although this change is small, it has important consequences for the physical behaviour of a liquid, as it, along with density, establishes the speed of sound. A liquid acts like a spring: when a pressure is applied to it, it decreases in volume. The linear assumption of the relationship between pressure, p, and relative change in volume, V, is defined as bulk modulus, B, as seen in Equation 2.2.

$$B = -\frac{\Delta p}{\frac{\Delta V}{V}} \tag{2.2}$$

Bulk modulus is fairly dependant on temperature. It can be determined by measuring the pressure in a liquid that has experienced a known change in volume, however, most commonly it is measured through its relationship to the speed of sound.

2.1.3 Longitudinal Speed of Sound

The longitudinal speed of sound in liquids was one of the first liquid properties established. Careful measurement and use of the speed of sound has many medical, industrial and military uses. The speed of sound, c_l, for longitudinal waves travelling in a liquid is defined by the distance, d, travelled by the wave over a certain time, t, as can be seen in equation 2.3

$$c_l = \frac{\Delta d}{\Delta t} \tag{2.3}$$

Another definition for the speed of sound was mentioned in the discussion of bulk modulus. Here, the speed of sound of a liquid is defined by the density and bulk modulus of the liquid, as these components store energy with respect to momentum and the spring-like behaviour of the liquid, and thus delay the wave as it travels. This behaviour is defined by Equation 2.4.

$$c_l = \sqrt{\frac{B}{\rho}} \tag{2.4}$$

The speed of sound is very temperature dependant, and it is slightly pressure dependant. It can also be affected by the frequency of the sound in some liquids.

There are many methods available to measure it. Most methods use a fixed distance between an ultrasonic transmitter and receiver. The speed of sound is then determined by the time the transmitted wave takes to travel the fixed distance.

At this point, it is also important to mention the difference between group and phase velocity. Phase velocity is easily described by the scenario where a sine wave traveling through a media. The velocity, at which this wave moves past a point, is the phase velocity. Group velocity is the speed at which a modulated wave moves through the media. A good example of this is the sum of two similar frequency sine waves. This sum can produce beating. The speed of the beating wave through the media can be much slower than the speed of the two added waves. The speed of the beating wave would then be the group velocity, while the speed of the individual waves is the phase velocity. In this work only phase velocity was used.

Very accurate measurements of the speed of sound have been taken in the process of measuring the non-linearity parameter ($\frac{B}{A}$). This parameter describes the non-linear relationship between the density of a liquid and the pressure that is being applied to the liquid [7]. The many techniques for measuring this value use very accurate measurements of the speed of sound. These measurements are normally based on two types of techniques, namely pulse-echo and continuous wave techniques. With pulse echo, a small ultrasonic chirp is transmitted through the liquid towards a receiver. The time the chirp takes to travel from transmitter to the receiver is used to determine the speed of sound. The accuracy of this method is heavily dependent on the signal processing done on the received chirp to determine when exactly it arrived [21][38].

As part of the sensor that will be demonstrated in this work, the speed of sound will be measured using a continuous wave technique. This type of measurement involves setting up standing waves in the liquid, and determining the speed of sound by the placement in frequency space of the resonant modes that are formed by the standing waves. This technique is an extremely accurate measure of the speed of sound, or of relative changes in the speed of sound [48][20][15][42]. It requires either an admittance spectrum to be sampled, or additional signal processing circuitry, such as a phase-locked loop or a resonant circuit to function.

As can be seen from Equation 2.4, bulk modulus can be determined by measuring the density and speed of sound of a liquid.

2.1.4 Viscosity

In all liquids, there are resistance forces between moving molecules. This can be observed in the resistance of a liquid to flow. Viscosity, η, is thus defined as the ratio of shear stress, τ, over shear strain rate, $\dot{\gamma}$, applied to a liquid as can be seen in equation 2.5.

$$\eta = \frac{\tau}{\dot{\gamma}} \tag{2.5}$$

Viscosity is slightly pressure dependant, but very temperature dependant. For example, castor oil halves its viscosity from $30°C$ to $40°C$. This dependence on temperature implies that most viscosity readings should be taken with known temperature values. Viscosity can also be dependent on the shear flow rate of the liquid. Liquids such as starch solution increase in viscosity with shear flow rate, and solutions such as tomato sauce decrease in viscosity with shear flow rate. All samples that are used for testing this sensor are based on liquids that behave linearly with shear rate; which are so-called ideal viscous liquids.

For compressional fluids, viscosity becomes a bit more complicated. Here Navier-Stokes equation is used to define a liquid. Within which Volume (Bulk) viscosity is defined. It can be described as a measurement for the resistive forces between particles as the fluid is compressed. In such a situation shear viscosity is also introduced. Shear Viscosity is the same as normal simple viscosity if the liquid is assumed to be incompressible. Some simplifications are later introduced to simplify these variables. And the liquids that are tested in this thesis are so that they are unaffected by such a simplification.

Several techniques are used to determine viscosity of liquids. Most of them are designed for static testing, i.e. a liquid is removed from the process and placed into a testing system. By far the most versatile, accurate and common, within research laboratories, is the coaxial measurement system. It uses a bob and cup arrangement. The liquid is poured into a cup and a bob is inserted into the liquid. The bob is then spun at various speeds and the torque required to get the bob to spin at a specific speed is used to determine the viscous behavior of the liquid at that speed. Some sensors also used a spinning cup, with the bob fixed; however, thermal control of the sample was found to be problematic when using this technique.

Several different bob shapes are implemented for different viscosity ranges and different types of tests [41]. It is important to note that viscometers measure the friction caused by the liquid, and, as such, careful care is taken in these types of sensors to reduce friction caused by other external sources, such as bearings [56]. Also, variations in cup and bob shape are used, such as the double gap measuring system for less viscous samples. The benefit of this system is that the sample can be accurately controlled with respect to temperature, and its viscous behaviour can be determined for a variety of shear strain rates. All samples used for comparison purposes in this work were calibrated using such a system.

Many other techniques are also available, but they tend to be more crude. Several timing techniques are used; some of these involve timing how long a volume of liquid takes to drain though a small orifice. Another variation is the falling ball technique, where a heavy ball is dropped into the liquid and the time taken for the ball to drop

a fixed distance is measured. These techniques depend on the shapes of the objects used, and they can normally only determine relative viscosity. They are also not independent of the density of the liquid.

There are two main methods to measure viscosity in-line. One uses the coaxial system placed in-line in the pipe. This system has a large effect on the flow of the liquid that is being tested, and it has several moving parts, so requires regular maintenance. A variation of this technique uses a ball placed in the pipe, that is either spun at a specific speed or oscillated, and the resistance to the movement is measured. Another popular in-line measurement is simply determining the drop of pressure along a fixed length of pipe. If laminar flow is established, the drop of pressure per unit length of pipe can be defined and is dependent on the viscosity of the liquid. However, establishing laminar flow requires a very long section of accurately machined pipe before and behind the sensor, and for the liquid to be transported at a slow enough speed in relation to its Reynold's number. Also this sensor is dependent on the speed of flow in the pipe, so a flow sensor would need to be implemented as well.

Another less practical method of measuring viscosity involves transmitting a beam of ultrasound into the medium and measuring the streaming that occurs away from a transmitter [23]. The velocity of the streaming is inversely proportional to the viscosity of the liquid. The speed is measured through the Doppler shift detected by a receiver. This method is non-intrusive; however, it will be affected by the flow of the liquid, and the real benefit of having a non-intrusive system would be that the liquid could flow past the sensor.

Later in this chapter, vibrational techniques for measuring viscosity will be discussed (section 2.2).

2.1.5 Effects of frequency on parameters

Both speed of sound and viscosity can be affected by the frequency of the sound in a liquid. This is especially apparent in polymers and suspensions, where these changes can be used to determine the particle size within the suspension [13]. This behaviour is commonly described by the use of Maxwell's model for a liquid, which is defined by a spring and dashpot in series. The relaxation time is defined as the inverse of the cutoff frequency for this arrangement. Most liquids do relax slightly; however, this effect can be minimal and it will not be further studied in this work, thus a test solution will be chosen to avoid these effects. However, the measurement of these terms should be within the limitations of the sensor discussed in this work, especially in relation to the speed of sound.

2.2 Vibrational measurement techniques

The oscillatory behaviour of a liquid is defined by the physical parameters of a liquid. Thus, it stands to reason that the effect that a liquid has on the sound waves travelling through it can be used to determine the parameters of the liquid. This is easily stated, but much more difficult to implement, as the measurement of these waves is as much dependent on the sensing method as it is on the liquid. Several techniques are available in literature for measuring various liquid parameters. Since the sensor design in this work falls within this category of sensor, it is important to mention these techniques in more detail. They can be broadly broken down into two types: those that measure the effect that a liquid has on the resonant behaviour of a transducer, and those that measure the effect on the resonant behaviour of the liquid.

2.2.1 Ultrasonic Spectroscopy

Ultrasonic spectroscopy is the study of the frequency spectra of attenuation and phase of sound traveling through a media. This media can be a solid, liquid or Gas. The Spectra can indicate several properties of the media, including fundamental material properties, particle size and density in suspensions and material defects like surface roughness and cracks Over the past few years there have been several advances in Ultrasonic Spectroscopy. These can be mostly accredited to an improvement in computing power and digital electronics to be able to handle the rather complicated equations that are required to compute [8] The sensor designed in this work falls into this group of research. As it uses the acoustic spectra of a liquid in an attempt to determine the physical properties of the liquid. However, it does not use the classical attenuation model, and rather uses a electrical equivalent models.

2.2.2 Sensors based on liquid effect on transducer

A vibratory transducer has a resonant behaviour, at which point standing waves of a specific type, such as axial, shear or torsional waves, are set up in the device. The frequencies of the waves are defined by the characteristics of the material used to construct the transmitter, such as the speed of sound, the density and the internal damping. These resonant modes are quite constant and there is normally only a slight variation due to temperature.

When such a transducer, in the form of a reed element, is submerged in a liquid, the liquid interacts with the dynamics of the transducer and changes its resonant behaviour. By measuring these changes, some of the parameters of the fluid, such as density and viscosity, can be determined.

Many variations of this technique exist, either using a vibrating probe in shear mode [45][55][5][19][32], in torsional mode [33][37][29] or in flexural mode [30][27]. The flexural mode is more suited to measure changes in density, as the vibration of the reed displaces a volume of liquid. Thus, the effective mass of the reed is increased, thereby decreasing the resonant frequency of the reed. These techniques have the benefit of reduced moving parts and thus less maintenance. However, the dynamics of these sensors need to be accurately determined and regularly calibrated.

Measurements of the effect of shear motion on the outside of the probe, which is the effect of both the shear mode and the torsional mode, are more suited for measuring viscosity, as the drag of the probe due to the liquid has the larger impact on the mode. The drag that the liquid has on the probe reduces the Q of the probe's resonant mode. The probe also entrains a volume of liquid; this increases the effective mass of the probe and decreases the frequency of the resonant mode. The amount of mass that is entrained is dependent on the viscosity of the probe.

These techniques formulate relationships that relate the density and viscosity of the liquid to the changes in the resonant behaviour. There are other factors that also change the behaviour of the probes, and these will incur a measurement error that will not be easily be discovered. These probes are also not very accurate compared to the bob and cup system and they are not well suited for in-line application for liquids, where the flow of the liquid will change the behaviour of the reed.

A sensor to measure bulk modulus based on the changes of the resonant characteristics of a piezoceramic spherical shell, with a sample of liquid inside it, has also been implemented. This method was used to measure the relaxation of a sample of glycerol. The effect of the glycerol was to stiffen the shell. The bulk modulus can be determined though the changes in the shell's electrical capacitances [12].

2.2.3 Sensors based on the resonant behavior of the liquid

With these techniques, an attempt is made to generate standing waves within the liquid. Our System allows the behaviour of those standing waves to be measured, and from that the characteristics of the liquid are determined. These measurement systems are the most similar to the system implemented in this study.

A popular technique for determining fluid properties, especially in gases, is the interferometric technique [24]. Here a piezoceramic actuator is placed a variable distance from a reflecting surface as can be seen in Figure 2.1.

The transducer is excited at a fixed frequency and the path length is changed. The current that the transducer draws is measured and as the distance from transducer to the reflecting surface is increased, the column of liquid will go through resonance. As

Figure 2.1: Diagram showing interferometric technique for determining physical properties of gasses. A fixed frequency of sound is produced by the transmitter. Then the distance between the reflecting surface and the transmitter is increased. Each time a standing wave is produced, the current through the transducer increases and the relative change in current can be used to determine the properties of the fluid.

the length is extended further, a resonant mode will form again and again. Thus as the length is increased, the current flowing through the transducer increases at resonance and decreases again during anti-resonance. The behaviour between the length of the fluid column and the current can be mathematically modelled with respect to the fluid's characteristics.

This technique is not suitable for in-line applications as it requires a specialized, accurate test environment; the measurements take time to do, and the changes in the column length required are quite substantial. It is also more suitable for gases than for liquids, as in this method the effects of the walls that encase the system were not taken into account. One benefit of the system, however, is that the fluid properties are calculated from relative electric currents and thus the sound coupling and transducer modelling are less critical.

A similar technique has been implemented for the measurement of liquid viscosity and speed of sound. This system includes a model for the relationship that a liquid has with the walls that encase it. The liquid is placed in a thick-walled steel tube. On one side, a piston is connected to a shaker, which can be oscillated at a fixed range of frequencies (<4kHz). The other side is either exposed to air [40] or is sealed with another piston connected to an accelerometer [39]. The basic concept is shown in figure 2.2.

With this implementation, the resonant behaviour of the fluid with respect to frequency is measured. Then, the dynamics of the piston, with respect to its mass, damping and spring constant, are removed from that impedance to leave only the impedance of the liquid.

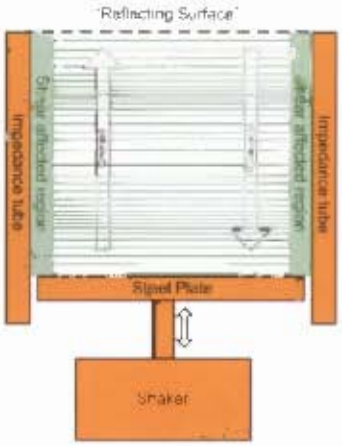

Figure 2.2: Diagram showing basic representation of impedance tube sensor. Here an axial sound wave is transmitted in a pipe towards a reflecting surface. The amount of energy lost by the sound moving past the wall surface as standing waves are formed is used to determine the viscosity of the sample.

There are two components to that impedance, namely that of the sheared liquid region and that of the rigid body liquid region [39]. Within the rigid body region the plane waves travel from the piston to the reflecting surface and back. However, the walls of the tube remain stationary, thus if it is assumed that there is no slip, the fluid at that interface must be stationary as well. This implies that there is a transition area between the still fluid and that in the rigid body liquid region. This region is where the shear behaviour of the fluid affects the wave. The length of this region is dependent on the viscosity of the liquid. Thus, if the behaviour due to these two regions is modelled, the viscosity and speed of sound of the liquid can be determined.

This system is ideal only for testing static samples of liquids. It produces very similar spectra to that produced by the work discussed in this project, and it also seems to exhibit a similar coupling effect as is discussed in section 5.6, where the simulated modes have a slightly higher Q and mode size than the actual data. This could be due to the surface roughness of the impedance tube used [47].

The techniques that employ the modal behavior of liquids produce very accurate measurements for the speed of sound, as long as the distance that the sound waves needs to travel is well defined. In one implementation, a piezoceramic tube is placed an accurate distance from another, and the frequency distances between the modes of the liquid are used to determine the speed of sound [15]. However, the use of a piezoceramic tube to determine the speed of sound should also be mentioned with respect to this research. The frequencies at which the liquid modes are formed in a radial coordinate system are not linearly related as they are in a Cartesian coordinate

system. However these systems have been successfully used to determine the speed of sound in liquids [4][15][42].

As mentioned, most systems for measuring density or viscosity are not ideal for in-line applications. Many contain moving parts and require a static environment to complete the tests. Also, few allow for a sensor that does not protrude into the flow of the liquid. It would be beneficial for a sensor to be able to determine the parameters of a liquid without affecting the transport of that liquid.

Chapter 3

System Description

The proposed sensor consists of a radially polarized piezoceramic tube. The inside of the piezoceramic tube is filled with the sample liquid and the outside is left exposed to air. When the piezoceramic material of the tube is subjected to a potential difference, the wall of the tube expands or contracts, primarily radially, depending on the direction that the voltage is applied. This movement is coupled into the liquid. A basic diagram showing this can be seen in figure 3.1.

As the frequency of the applied voltage is increased, the sound travelling in the liquid eventually starts to form a standing wave. At this point, the total electrical impedance from both the piezoceramic tube and the liquid systems decreases and a resonant mode becomes apparent. When the frequency is further increased, the harmonics of that liquid standing wave frequency are also apparent. However, the effect on the spectrum of the piezoceramic tube is relatively small at these low frequencies, compared to other standing waves formed in the tube, such as the length modes.

As the frequency is further increased, the wall thickness resonance of the piezoceramic tube is excited. Since this is in the primarily polarized direction of the tube, the mode that is generated is very dominant. However, this mode also excites the harmonics of the liquid modes in its vicinity. Essentially, this low impedance domain of the tube acts as a window onto the dynamics of the liquid. The response of the piezoceramic tube - liquid system can be seen in figure 3.2. This figure shows the real and imaginary parts of the inverse of impedance. Thus, a spike in conductance in this figure shows a low impedance frequency of the sensor. The liquid modes visible in this area of the thickness resonance (at about 6.5MHz), and the areas of its harmonics, are the subject of this work, to determine the physical parameters of the liquid.

This system can be separated into two sections: the first is the study of the resonant response of the piezoceramic tube, which makes the dominant impact on the spectra (Chapter 4). This part also includes the impact of the case capacitance and the wiring

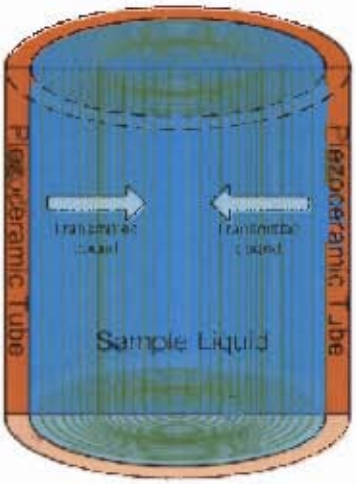

Figure 3.1: Diagram showing a pictorial view of sound travelling in a piezoceramic tube. This a basic repesentation of what the sensor system looks like.

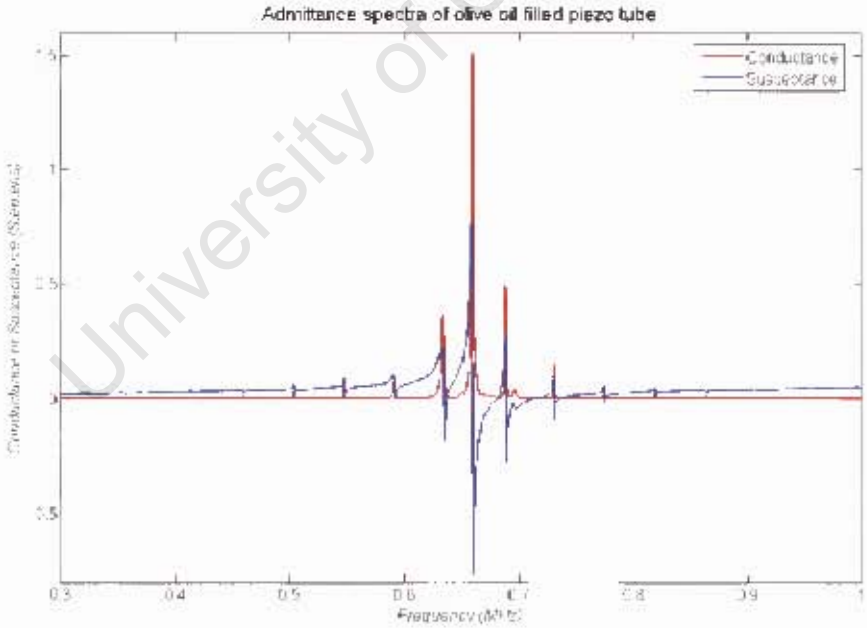

Figure 3.2: Admittance spectra of an olive oil filled piezoceramic tube over the tube's thickness resonance. The resonant modes of the liquid are easily visible under the response of the thickness mode of the piezo tube. Also note the effect of case capacitance as the susceptance rises for higher frequencies.

to the tube, whose impact becomes more apparent with spectra at higher frequencies. Secondly, the study of the response of the liquid will be formulated (Chapter 5), as an accurate determination of this response is fundamental to the use of the sensor.

The primary benefit of the implementation of such a sensor is that it could be applicable for use in an in-line application, as a liquid flowing in the middle of it would not be restricted by the sensor. Also, the wear on such a sensor will be limited as it does not intrude into the flow. However, wear will occur, and further work on the effect of a protective lining should be done.

This work, however, aims to produce a proof of concept of this idea. It will attempt to produce a static sensor, whereby a sample of liquid is loaded into the tube, set to a specific temperature and a spectrum is taken. That spectrum is then analyzed in an attempt to determine the liquid's physical parameters inside the tube.

Chapter 4

Spectral response due to the piezoceramic tube

The piezoceramic tube was the most challenging part of the system to model in practice. Since the liquid modes were coupled to this model, it had to very accurate, and it had to span several resonant modes of the piezoceramic tube to achieve the bandwidth requirements for viscosity measurements, as later described in section 5.4.

4.1 Piezoelectricity

A piezoceramic is a material that, in addition to obeying normal mechanical stress-strain relationships, also has the ability to couple electrical behaviour into mechanical behaviour. Thus, if this material is placed with an electrical field across its polarized axis, it will strain; and conversely, if it is placed under strain in the polarized axis, the material will induce an electrical field. This behaviour is approximated by the following equations:

$$\sigma_{ij} = C^{E}_{ijkl}\varepsilon_{kl} - e^{\varphi}_{mij}E_m \tag{4.1}$$

$$q_i = e^{\varphi}_{ijk}\varepsilon_{jk} + D^{\varphi(\varepsilon)}_{ij}E_j \tag{4.2}$$

where σ is stress, ε is strain, C^E is the stiffness matrix of the piezoceramic material, e^{φ} is the matrix of piezoelectric constant, $D^{\varphi(\varepsilon)}$ is a matrix of dielectric constants, E is the electric field, and q is charge density. The subscript notations indicate the axis of reference for the material; the numbers 1, 2 and 3 indicate the primary axes (e.g. x,y,z). The first term on the right of the equations shows the standard mechanical influences and the second term shows the electrical influences. This equation allows that defined values for all the axis for the piezoceramic actuator can be defined and

used in the calculation of the movements of the piezoceramic. This was not very practical though, and since most of the non primary axis variables a rather small compared to the primary operation of the tube, they where are set to zero for the calculations that follow. This simplification will add an error to the results. However since the final solution used did not apply this equation, it was decided that a study of this system with additional degrees of freedom would not be of much additional benefit to the work. These equations will be discussed in more detail in section 4.6.5.

4.2 Polarization of tube

Piezoceramics are polarized by heating them to high temperatures and then allowing them to cool while exposed to a electric field in the desired polarization direction. The piezoceramic tubes that were used for this project were polarized in such a way that their primary strain was though the radial thickness of the tube. Thus, when a voltage is applied to the piezoceramic tube the distance between the outer and inner diameters will increase or decrease depending on the polarity of the voltage. It is important to be aware that there will be some smaller additional piezoelectric behaviour in the other non-polarized directions. These additional effects are significant in size; however, the resonance modes in those directions occur at much lower frequencies than the thickness resonance mode used for this work and so can be ignored.

4.3 Effect due to case capacitance and the cabling

Since the piezoelectric effect is driven through the creation of an electric field between two electrodes, the piezoceramic obviously has significant capacitance. When analyzing the admittance spectra of the tube, the first noticeable mode is that of the case capacitance coupled with the cable. This can be seen at 11MHz in figure 4.1. In order to be able to compare the simulated data in later sections, it was important to remove this mode from the spectra. This can be a little more complicated than it seems, owing to harmonics of the thickness modes of the piezoceramic tube, which interfere with the cable mode, as is visible in the dip occurring at 11MHz in figure 4.1.

Two methods were attempted to remove this mode. The one was a simple RLC circuit model, and the other was to use an actual transmission line model for the cable. It was found that if the cable was kept as short as possible (in this case, that was 25mm) an RLC model, as shown in figure 4.2, was sufficient. Note that since the capacitance of the cable and that of the piezoceramic tube are in parallel, they can be considered as one capacitance for removal purposes.

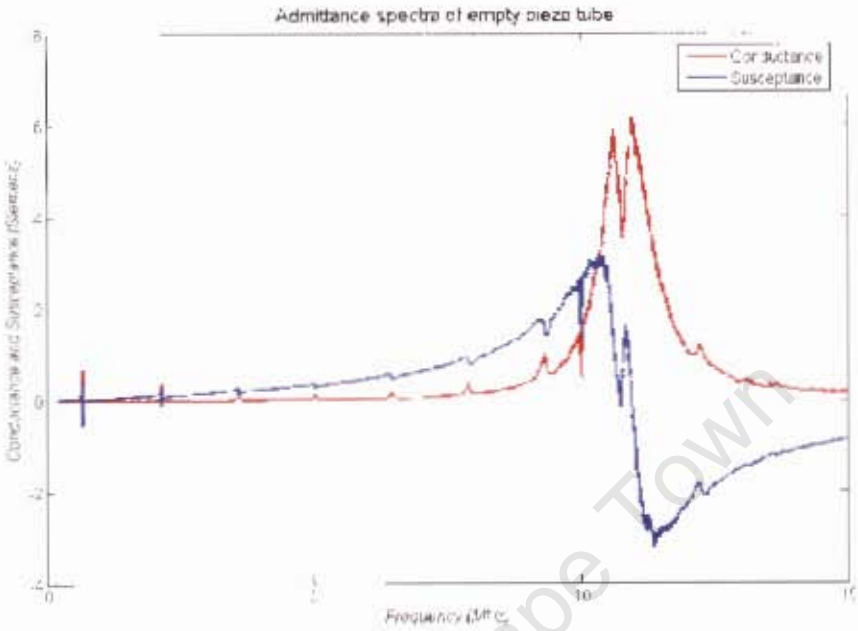

Figure 4.1: Spectra of empty piezo tube of dimensions: inner diameter 31.8 mm, outer diameter 38.0 mm and length 38.3mm. The main mode occuring at 11MHz is the resonance of the case capacitance and the cable. The smaller, sharper, modes seen at 1.5MHz intervals are the thickness resonances of the tube. The dip seen at 10MHz is a measurement error visible on all spectra.

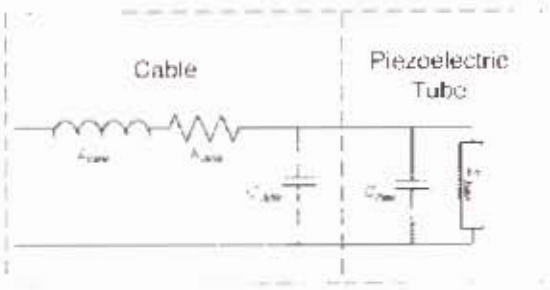

Figure 4.2: Diagram of RLC circuit used to simulate the spectral response of the cable and the case capacitance. The case capacitor of the piezo tube and the capacitance of the cable can be considered as one, since they are in parallel.

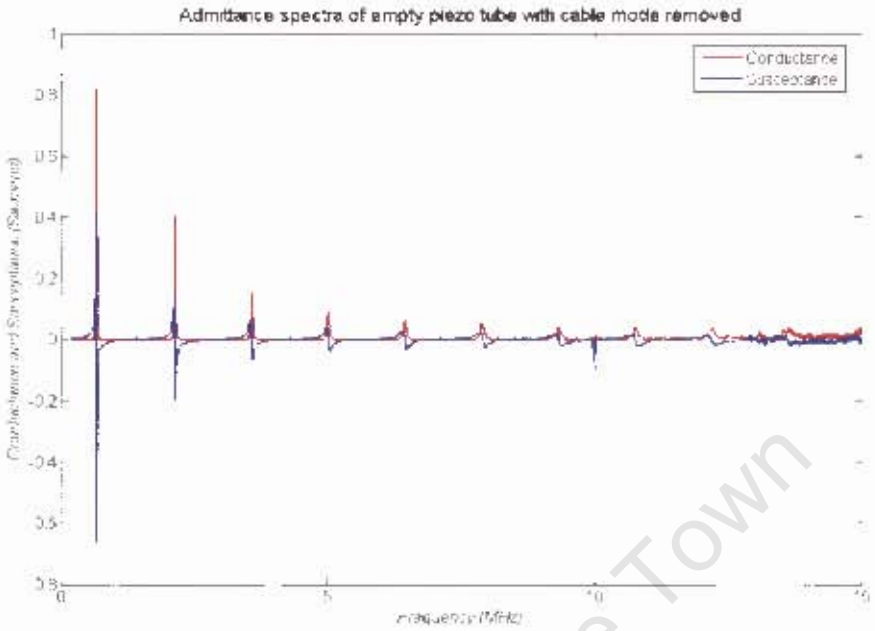

Figure 4.3: Spectra of empty piezo tube with case capacitance and cable removed. The thickness resonances of the tube have become more visible and are now centered around zero.

Implementing an accurate cable removal algorithm was complicated by the behaviour of the modes that distort the resonance of the cable. The resistance was straightforward to obtain from an admittance - susceptance circle. However, the exact placement of the mode and the Q of the mode were more difficult to obtain through optimization, as the answers tended to vary depending on which model was used for the interfering mode. However, once the cable mode was removed, the spectra appeared as in figure 4.3. For this spectrum shown, the values were $R = 0.16\Omega$, $L = 25.05nH$, $C = 8.6nF$.

4.4 Dominant resonant modes in a piezoceramic tube

As mentioned when discussing equation 4.1, the behaviour of the piezoceramic tube is dependant on both the normal mechanical response and the additional electrical response of the piezoceramic tube. Thus, when the piezoceramic tube goes through mechanical resonance, this behaviour will be coupled into the electrical response. This becomes especially apparent when considering the admittance spectrum of the piezoceramic tube. For a tube, the dominant modes are the radial (thickness), length and

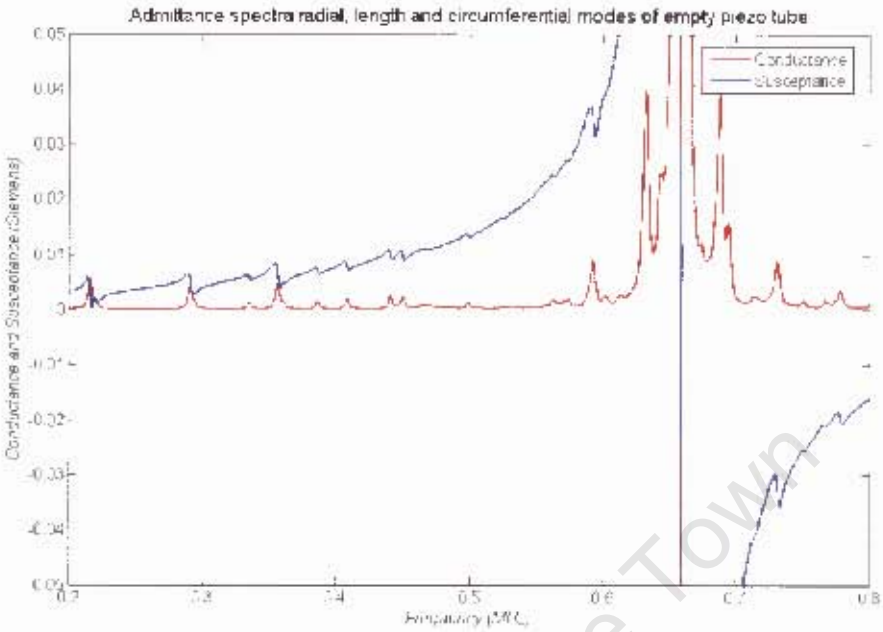

Figure 4.4: Spectra of empty piezo tube showing radial, length and circumferential modes. Notice the smaller modes on the left of the spectra. These modes are substantially smaller than the radial mode at 650kHz which has a peak of 1 Siemens. However, their effect does become more significant on the edges of the radial mode.

circumferential modes [1]. When the frequency of the driving voltage is near that of the resonant mode of the piezoceramic tube, it becomes easier to drive, and thus the electrical impedance of the tube reduces. This is because the returning wave of movement in the tube contributes to producing the next wave.

4.4.1 Radial modes

These modes are formed by setting up standing waves though the thickness of the tube and they can initially be approximated by the following equation:

$$f_r = \frac{N_t}{r_o \quad r_i} \tag{4.3}$$

Where f_r is the resonant frequency and N is a frequency constant. This equation holds only if the tube wall is substantially thinner than its inner diameter. It also only defines the fundamental mode of the tube. Other more detailed models are available and are discussed in section 4.6.

4.4.2 Length modes

These modes are set up in the length of the tube. For the dimensions of the tubes used, in this work, the modes are at a much lower frequency than the thickness mode; however, some of the higher length modes do sometimes interfere in the fundamental thickness mode as can be seen in figure 4.4. They are defined by:

$$f_r = \frac{N_{31}}{L} \tag{4.4}$$

Where L is the length of the tube and N_{31} is the frequency constant for length modes.

4.4.3 Circumferential modes

These modes occur through the diameter of the tube and are at also at a low frequency. They had little impact on the system. They are defined by:

$$f_r = \frac{N_c}{r_o + r_i} \tag{4.5}$$

Where N_c is the frequency constant for circumferential modes.

4.5 Effect of placing a liquid into piezoceramic tube

When a liquid sample is loaded into the piezoceramic tube, it interacts with the movement of the tube. Thus, the spectral response of the combined system is a function both of the behaviour of the piezoceramic tube and of the liquid. This can be observed in figure 4.5. For each frequency at which a standing wave is formed in the liquid, a mode is coupled into the response of the piezoceramic tube. Some of these modes are barely visible, while others are superimposed on the thickness resonances of the piezoceramic tube. These modes are clearly visible in the spectrum as the smaller, sharp, satellite modes interfering with the large thickness modes visible in figure 4.3.

The exact locations of the liquid modes are also slightly displaced by frequency pulling over the thickness mode of the piezoceramic tube[15]. Frequency pulling is an effect influencing the liquid modes that are on top or very close to the thickness resonance of the cylinder. The frequency intervals between modes deviate from the linear relationship when they lie over the thickness resonance, while the modes before and after the thickness resonance are still at the same frequency interval.[42] This effect gets nullified by the piezoceramic tube removal technique used at the end of this chapter.

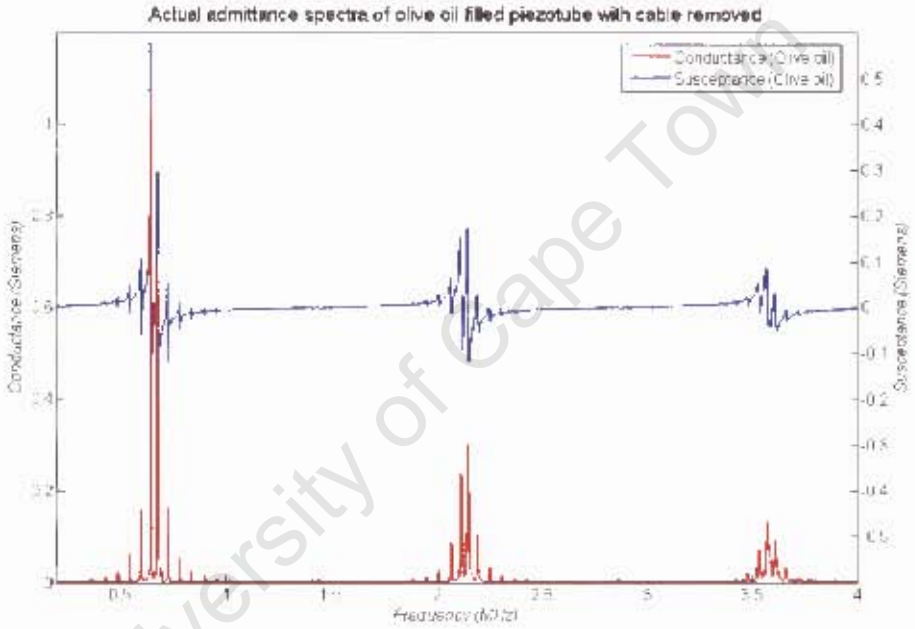

Figure 4.5: Spectra of conductance and susceptance of a olive oil filled piezo tube. Note the sharp satellite modes that have been created over the region of the primary thickness modes of the piezotube.

The remainder of this chapter describes the investigation into a method to either find a model for the piezoceramic tube that would allow, in conjunction with a model for the liquid, the approximation of a real spectrum as seen in figure 4.5 with that of a simulated model, or, preferably, the removal of the response of the piezoceramic tube so that a model response of the liquid can be compared directly with an actual spectrum of the liquid.

4.6 Attempts to model the behavior of the piezoceramic tube

Piezoelectric equations can be complicated and rather cumbersome to solve (an example of a piezoceramic plate can be seen in [10]). Several techniques described in the literature have been used to model the behaviour of piezoceramic plates using electrical equivalent circuits. Such modeling allows the use of commonly known electrical components and network theory to create equivalent systems which are substantially easier to solve; graphical techniques may possibly be used also [11]. However, many assumptions and simplifications are made to obtain these circuits, and the effect of these on the system studied had to be examined to determine if such a simplified circuit could usefully be implemented. These models include the Butterworth - Van Dyke [9], Mason's [34], Redwood [44] and the KLM models [28] (which seek to remove some of the physical ambiguities from Mason's model, such as the negative capacitor). The complexity of these models is largely dependent on the accuracy required for the problems being studied.

4.6.1 The Butterworth - Van Dyke model

The Butterworth-van Dyke model is by far the simplest model that can be implemented for a piezoelectric resonator. It consists of a series RLC resonator in parallel with the case capacitance of the piezoceramic plate. Normally this model is used to represent empty or coupled systems, and because there would be nothing to restrict the movement of the outer walls, the outer port can be short circuited. Since the component values can be calculated from a spectrum, this system is often used to determine what the physical constants are that define the piezoceramic material used.

As can be seen from figure 4.6, the Butterworth - van Dyke model [9] for a quartz resonator only represents one mode of the resonator and it makes no allowance for its harmonics. It also only represents linear systems, whereas the system in the study is defined by a radial coordinate system, since the piezoceramic actuator has the form of a tube. Beneficially though, this model is extremely simple and computationally

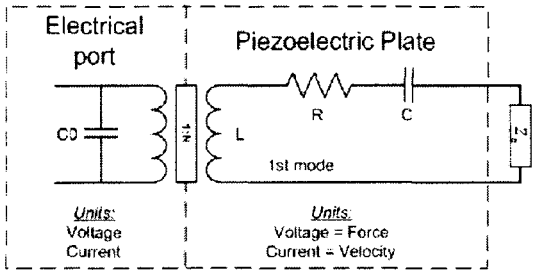

Figure 4.6: Diagram illustrating the Butterworth - van Dyke model for a quartz resonator. Where C_0 is the case capacitance of the piezoceramic place and the RLC cicuit componants represent the thickness resonant mode of the plate.

inexpensive and thus would have been ideal for optimization purposes. Some improvements are available on this model whereby a complex capacitor and inductor are used, and the resister is set to zero [51].

4.6.2 Mason's model

This model was the first network theory-based model implemented to ease the cumbersome problem of analytically deriving the equations for a piezoceramic plate in contact with a specific acoustic impedance. It was derived for a one dimensional case, assuming that the piezoelectric characteristics in the non-polarized directions were negligible. Several other assumptions were made to reduce the complexity of the end result. The component values that have been illustrated in figure 4.7 are defined as follows:

$$C_0 = \frac{\varepsilon_{33}^s A}{t} \tag{4.6}$$

$$N = C_0 h_{33} \tag{4.7}$$

$$Z_0 = A\sqrt{\rho c_{33}^D} \tag{4.8}$$

$$\Gamma = \omega\sqrt{\frac{\rho}{c_{33}^D}} \tag{4.9}$$

$$Z_s = -iZ_0 \csc(\Gamma t) \tag{4.10}$$

$$Z_t = iZ_0 \tan\left(\Gamma\frac{t}{2}\right) \tag{4.11}$$

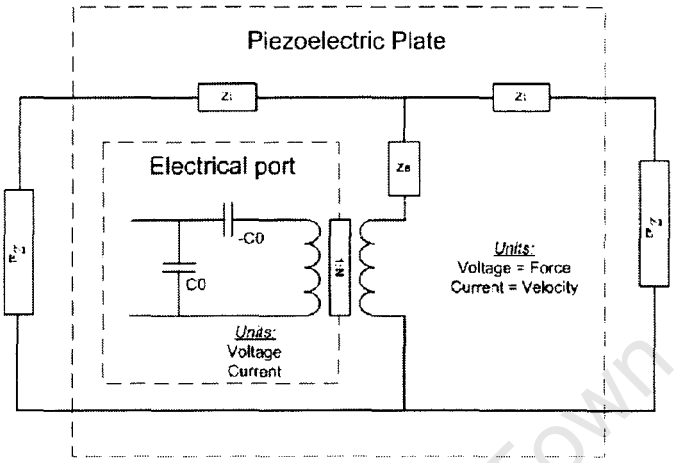

Figure 4.7: Diagram showing Mason's equivalent model for a piezo plate. Three regions are indicated. The electrical region is where the case capacitor and the characteristic negative capacitance are. The transformer couples this system into the mechanical domain of the piezo plate. Beyond that domain are the impedances of the acoustic enviroment with which the outer surfaces of the plate make contact.

where A is plate area, t is plate thickness, ε_{33}^{s} is clamped permittivity, h_{33} is a piezoelectric constant, ρ is the density of the piezoelectric ceramic, c_{33}^{D} is the speed of sound in the ceramic and ω is angular frequency. Many of these variables are frequency dependant and complex to allow for losses and damping.

Mason's model [34] consists of a T-network. The acoustic impedances are simply added to the end of the network. Thus, for this model, the impedance of the individual components in the T - network (i.e. Z_s and Z_t) are not dependent on the acoustic load; nor is the turns ratio of the transformer(N).

This model and the other two models mentioned below worked relatively well to represent the behaviour of the liquid-filled piezoceramic tube for a single harmonic of the tube. However, once the system was extended to multiple modes, they failed to align the harmonics of the tube correctly. This is due to the radial nature of the sound waves travelling inside the piezoceramic tube. If a sufficiently thin tube is used (instead of the tube that was implemented), the behaviour of that tube will tend towards the behaviour of this system. Many piezoceramic tube implementations have been based on this type of thin tube approximation.

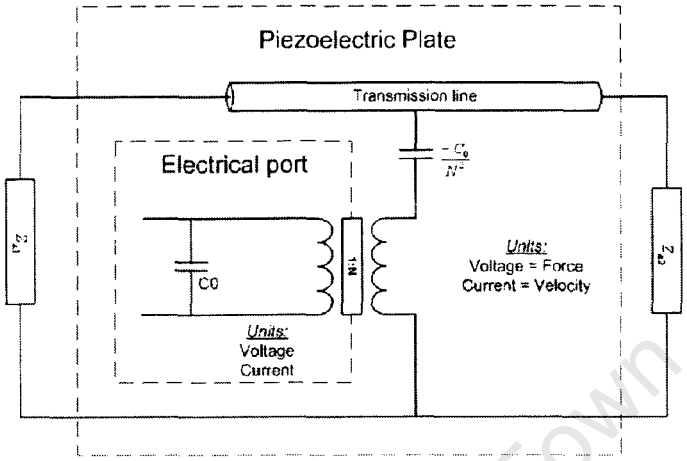

Figure 4.8: Diagram of Redwood's equivalent model of a piezo plate. The three impedances of Mason's model have been replaced with a transmission line, and the negative capacitance has been moved across the transformer.

4.6.3 Redwood's model

Redwood's model [44] aimed to improve some of the physical inconsistencies of Mason's model, such as the negative resistance and the load independence of the impedances, as can be seen in figure 4.8. He achieved this through replacing the T-network with a transmission line and by shifting the capacitor to the other side of the transformer. This model is essentially an intermediate step between Mason's and the KLM model and it was not implemented in this study as being inappropriate for the same reasons as the Mason's model.

4.6.4 The KLM model

The KLM model [28] is commonly used to design high frequency transducers, especially for medical purposes. There are several differences between it and Mason's model (section 4.6.2). Firstly, there is no parallel case capacitance, but only a capacitance in series. Secondly, a different transformer ratio is used. One of the most interesting differences between the models is that two transmission lines were used to simulate the mechanical characteristic of the piezoelectric plate. The variables in this model, as seen in figure 4.9, are defined as follows:

$$C_0 = \frac{\varepsilon_{33}^S A}{t} \tag{4.12}$$

$$Z_0 = A\sqrt{\rho c_{33}^D} \tag{4.13}$$

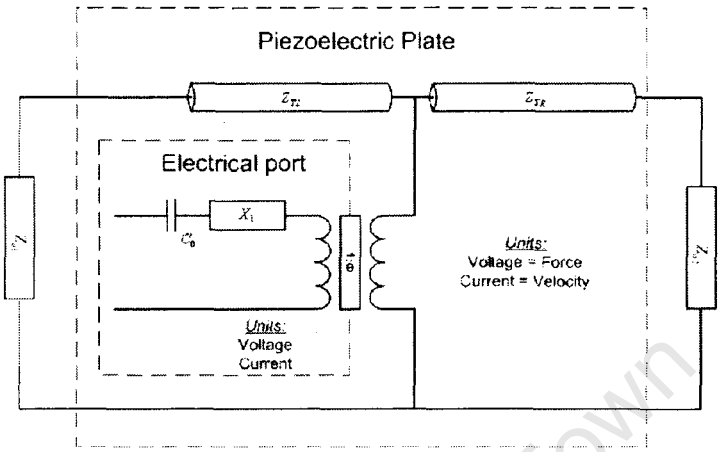

Figure 4.9: Diagram of the KLM equivalent model of a piezo plate. This model has many differences to Mason's model. There is no negative capacitor. The transformer's value is frequency dependent and there are two transmission lines leading to the acoustic impedances at the exposed plate area.

$$M = \frac{h_{33}}{\omega Z_0} \tag{4.14}$$

$$\Gamma = \omega \sqrt{\frac{\rho}{c_{33}^D}} \tag{4.15}$$

$$X_1 = iZ_0 M^2 \sin(\Gamma t) \tag{4.16}$$

$$\phi = \frac{1}{2M} \csc\left(\Gamma \frac{t}{2}\right) \tag{4.17}$$

$$Z_{TL} = Z_0 \left(\frac{Z_{a1} \cos\left(\Gamma \frac{t}{2}\right) + iZ_0 \sin\left(\Gamma \frac{t}{2}\right)}{Z_0 \cos\left(\Gamma \frac{t}{2}\right) + iZ_{a1} \sin\left(\Gamma \frac{t}{2}\right)} \right) \tag{4.18}$$

$$Z_{TR} = Z_0 \left(\frac{Z_{a2} \cos\left(\Gamma \frac{t}{2}\right) + iZ_0 \sin\left(\Gamma \frac{t}{2}\right)}{Z_0 \cos\left(\Gamma \frac{t}{2}\right) + iZ_{a2} \sin\left(\Gamma \frac{t}{2}\right)} \right) \tag{4.19}$$

Where the variable definitions are the same as in section 4.6.2. ϕ is the transformer ratio in figure 4.9.

Owing to the transmission line definition of this system, the impedance of the piezoceramic tube has a dependence on the acoustic load. This type of system should be more representative of what is to be expected in real life. However, it has been

shown that if a comparison is done between the KLM model and Mason's model, the results are equivalent for a variety of boundary conditions [50].

Unfortunately, these models proved to be unsuccessful at describing the resonant behavior of the piezoceramic tube over several thickness modes. This was accredited to the radial nature of the of the sound waves created. So, other techniques were attempted to solve this deficiency.

4.6.5 Solving equations of state for a piezoceramic tube

As a last resort at modelling this system, the analytical approach was attempted. The hope was that the equation obtained by solving the characteristic equations of the piezoceramic tube could be simplified and used to obtain the admittance spectra of a liquid filled tube analytically, to compare to an actual spectra with the cable impedance and case capacitance removed. This section first describes the derivation of the equation for the impedance of the tube, then it discusses possible difficulties involved in actually using the derived equation. Some derivations for tubes [22] for other applications have been previously published, such as for a fully submersed tube [18] [52].

The behaviour of a piezoceramic tube can be accurately determined by solving the Navier equation for a solid, and the equations of state for a piezoelectric crystal.

$$(\lambda + \mu)\, u_{k,ki} + u_{i,kk} + F_i = \rho \frac{\partial^2 u_i}{\partial t^2} \tag{4.20}$$

where u is displacement and ρ is density.

This equation assumes a linear, elastic, isotropic material, where λ and μ are Lamé constants for the material. Rewriting this equation in cylindrical coordinates for a sinusoidal input, and analyzing the behaviour only in the radial (polarized) direction, gives

$$r^2 \frac{d^2 y(r)}{dr^2} + r \frac{dy(r)}{dr} + \left(r^2 B^2 y(r)\right) = 0 \tag{4.21}$$

$$B = \sqrt{\frac{\omega^2 \rho}{(\lambda + 2\mu)}} \tag{4.22}$$

where $\frac{dy(r)}{dr}$ is radial displacement.

The solution to this differential equation is

$$y = C_1 J_0(Br) + C_2 Y_0(Br) \tag{4.23}$$

where C_1 and C_2 are constants to be solved for using the boundary equations, and J_0 and Y_0 are Bessel's equations.

The equations of state for a piezoelectric material in the e- form are

$$\sigma_{ij} = C^E_{ijkl}\varepsilon_{kl} - e^{\varphi}_{mij}E_m \quad (4.24)$$

$$q_i = e^{\varphi}_{ijk}\varepsilon_{jk} + D^{\varphi(\varepsilon)}_{ij}E_j \quad (4.25)$$

where σ is stress, ε is strain, C^E is the stiffness matrix of the piezoceramic material, e^{φ} is the matrix of piezoelectric constants, $D^{\varphi(\varepsilon)}$ is a matrix of dielectric constants, E is the electric field and q is charge density. The subscript notations indicate the axis of reference for the material; the numbers 1, 2 and 3 indicate the primary axes (e.g. x,y,z).

By introducing the boundary equations of the piezoceramic tube, the acoustic impedance at the inner surface produces a relation between stress and strain at that radius. The equation is now converted to cylindrical equation system due to the tube nature of the piezoceramic actuator. This substantially simplifies the mathematics. Thus, substituting these boundary equations for stress into the equation of state above, assuming sinusoidal input equations, and again assuming linear, elastic, isotropic material, the boundary conditions for the piezoceramic tube are

$$Z_i A_i j\omega \frac{dy(r_i)}{dr} - \lambda\left(\frac{d^2y(r_i)}{dr^2} + \frac{1}{r_i}\frac{dy(r_i)}{dr}\right) - \mu\frac{d^2y(r_i)}{dr^2} + e_{33}E_{amp} = 0 \quad (4.26)$$

$$Z_o A_o j\omega \frac{dy(r_o)}{dr} - \lambda\left(\frac{d^2y(r_o)}{dr^2} + \frac{1}{r_o}\frac{dy(r_o)}{dr}\right) - \mu\frac{d^2y(r_o)}{dr^2} + e_{33}E_{amp} = 0 \quad (4.27)$$

where Z_i and Z_o are the effective acoustic impedances at the inner and outer surfaces, A_i and A_o are the inner and outer surface areas, r_i and r_o are inner and outer radius, e_{33} is a piezoelectric constant in the polarized direction, and E_{amp} is the amplitude of the sinusoidal electric field applied.

The derivative of y gives the radial displacement. The current produced though a sinusoidally changing electric field can thus be calculated by putting the strain components into the second equation of state of the piezoceramic tube, and integrating the charge density over the volume of the tube.

$$\therefore q_r = e_{33}\frac{d^2y}{dr^2} + \frac{e_{22}}{r}\frac{dy}{dr} + DE \quad (4.28)$$

$$i = \frac{d}{dt}\int_{r_i}^{r_o} q_r dV = 2\pi l\frac{d}{dt}\int_{r_i}^{r_o} q_r dr \quad (4.29)$$

Also, $V = E(r_0 - r_i)$ assuming that the electric field is constant in the wall. This assumption ensures that the final answer consists only of Bessel's functions, whereas if a radially changing electric field is used the final impedance also includes a Lommel function term, which makes the equation more computationally expensive to optimize. Finally, the outer impedance was set to zero, since the outer surface was always only exposed to air and it was decided that in relation to the acoustic impedance of the water, this assumption would be reasonable.

These equations where then input into a differential equation solver and the solution was as follows in equation 4.30.

$$Z\_piezo = \frac{-\frac{1}{2}i}{\left(\omega\pi l\left(e_{33}^2\left(\frac{Nom}{Denom}\right) + D_{ij}^{\varphi(\varepsilon)}\frac{(log(r_o)-log(r_i))}{log\left(\frac{r_o}{r_i}\right)}\right)\right)} \tag{4.30}$$

$$\begin{aligned} Nom &= B(2\mu+\lambda)\left(\begin{array}{l} -r_o(J0oY1o) + r_o(J0oY1i) + r_i(J0iY1o) - r_i(J0iY1i) \\ +r_o(J1oY0o) - r_i(J1oY0i) - r_o(J1iY0o) + r_i(J1iY0i) \end{array}\right) \\ &\quad + Z_i A_i \omega i r_i (J1oY1i - J1iY1o) \end{aligned}$$

$$\begin{aligned} Denom &= log\left(\frac{r_o}{r_i}\right) B^2 r_i r_o (2\mu+\lambda)^2 (J0iY0o - J0oY0i) \\ &\quad + (2\mu+\lambda)(Br_o 2\mu + Z_i A_i \omega r_i r_o Bi)(J0oY1i - J1iY0o) \\ &\quad + Br_i 2\mu(2\mu+\lambda)(J1oY0i - J0iY1o) \\ &\quad + 2\mu(2\mu + iZ_i A_i \omega r_i)(J1iY1o - J1oY1i) \end{aligned}$$

Where $J0o = J_0(Br_o)$, $J1o = J_1(Br_o)$, $J0i = J_0(Br_i)$, $J1i = J_1(Br_i)$, $Y0o = Y_0(Br_o)$, $Y1o = Y_1(Br_o)$, $Y0i = Y_0(Br_i)$ and $Y1i = Y_1(Br_i)$.

The first aspect that should be noted about the answer is its complexity. Computationally, this solution was impractical to optimize for different solutions, especially since the spectra that were normally taken contained 150000 sample points, to ensure that there was sufficient resolution to capture the low frequency liquid modes adequately.

This model was implemented in order to determine how effective it was. Although this system aligned to the resonant modes of the actual spectra, it performed poorly with respect to the damping of those modes, even when frequency dependent damping was introduced to limit the Qs of the modes. Later, it was determined that the

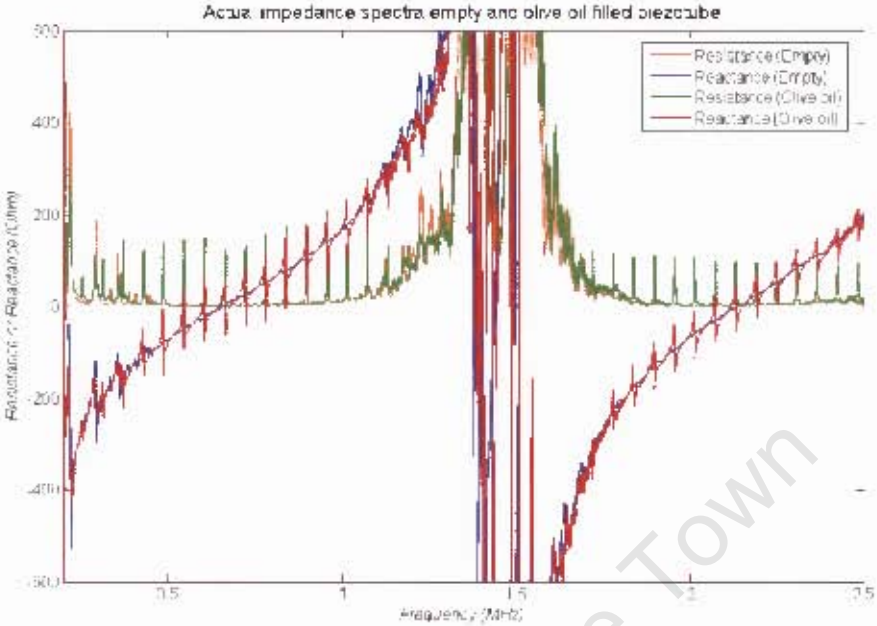

Figure 4.10: Spectra of resistance and reactance of an empty and an olive oil filled piezo tube after removal of the cable impedance and case capacitance. Note that around the resonance of the piezo tube (at 600KHz and 2.2MHz) the impedance of the liquid seems to be just added onto the impedance of the empty tube. At the antiresonance of the tube (at 1.4MHz) the behaviour seems to be swamped by noise. Also, note that both spectra contain low frequency modes not caused but damped by liquid.

dynamics of the silicone used to fix and seal the tube to its housing had a greater impact than was initially assumed. Also, spectra taken at different temperatures showed variations in mode placement. This essentially implied that all the piezoceramic tube's variables and their thermal characteristics, and those of the sealing agent would need to be known in order to create an accurate representation of the piezoceramic tube's response.

4.7 Attempts to obtain and use the base spectrum of empty piezoceramic tube directly

Eventually, the author decided on a simpler approach. Once the cable's impedance and the case capacitance of the system had been removed, and the impedance of the system had been plotted, the response of the liquid was quite visible on the impedance of the piezoceramic tube, as can be seen in figure 4.10.

This figure shows the resistance and reactance of the piezoceramic tube, thus showing the real and imaginary components of the inverse of figure 4.3 and figure 4.5, for an empty piezoceramic tube and for a sample of olive oil inside the tube. In figure 4.10, the thickness resonance of the piezoceramic tube occurs when the reactance of the empty tube's spectrum passes though zero from negative reactance to positive reactance. This is also the point at which the resistance is at a minimum value. Thus for this spectrum, resonance occurs at about 600kHz and 2.2 MHz.

The large spike in the centre of this spectrum, at about 1.4MHz, is the point where the admittance spectrum, its cable mode removed, will be at its minimum. Theoretically, this point should have zero admittance, thus ensuring that the conductance-susceptance circle is correctly placed. Practically, the impedance only needs to be substantially larger over this point. The size of the impedance over this region is so large that the spectrum was trimmed to allow other behaviour to be observed. Since the relative admittance is so small over this area, and since the impedance analyzer which was used took readings of conductance and susceptance, the signal-to-noise ratio of this area is poor, and becomes worse as higher modes are analyzed.

At lower frequencies of both spectra, some smaller modes are visible that are not due to the formation of standing waves in the liquid, although they are definitely affected by the presence of the liquid. These are some of the non-dominant modes described in sections 4.4.2 and 4.4.3. Several sensors have been designed over the years that exploit the damping and the shift of frequency of these types of modes to measure density or viscosity.

If the spectrum for the empty piezoceramic tube and that for the olive oil sample are now compared, it seems as if the impedance of the liquid has simply been superimposed on that of the liquid. This can only be an approximation; however, several models described in section 4.6, such as the Butterworth-van Dyke and Mason's models, simply add the acoustic impedance to that of the piezoceramic tube. If superposition is used it does solve several of the problems that plagued some of the other models evaluated. Firstly, the actual piezoceramic tube's mechanical parameters, except for piezoelectric coupling, do not need to be evaluated. Empty spectra can be taken for several temperatures, and thus thermal effects, complex variable components and the frequency dependence of the variables do not need to be approximated and evaluated. Also, the effects of the sealer between the piezoceramic tube and its housing will be represented in both the empty and the filled spectra. The correctness of this assumption is assumed to be best over the resonance of the piezoceramic tube, and thus modes used in later the optimization are in frequencies near that resonance. This is because the liquid will damp away most other non-primary modes of the piezoceramic tube. Also, the resolution of the spectrums is much improved over resonance than it

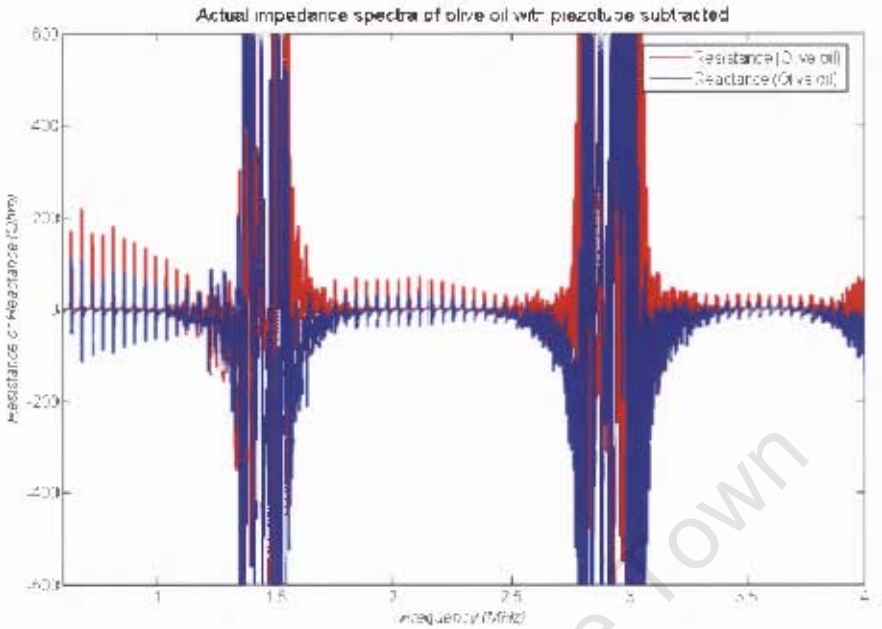

Figure 4.11: Spectra of olive oil sample, once the cable component had been removed and the piezotube subtracted. The response of the liquid is quite clearly visible in the open areas where the resonances of the piezotube were. The large noise bands, at 1.5MHz and 3MHz, are where the two antiresonances were. These areas tend to be noisy and substantial in size.

is over non-resonant areas. After subtraction, the lower frequencies will still have many spurious modes that interact with those of the liquid, so low frequencies are also ignored.

Once the two spectra have been subtracted, what remains can best be described as a spectrum that has some windows onto the response of the liquid. The size of the antiresonance in figure 4.10, and the level of noise over those ranges makes a perfect subtraction impossible. Also, to get the antiresonance modes to coincide perfectly would require both spectra to have the cable impedance and case capacitance to be known exactly. Unfortunately, that degree of accuracy was unachievable, especially with the variation in case capacitance experienced. Nonetheless, if the regions away from those zones are studied, they do produce a relatively consistent spectrum to that of the simulated spectrum of the same liquid as will be discussed in the next chapter.

Careful analysis of the liquid modes as they come closer to the edges of the antiresonance zones reveals a slight decay in amplitude. This shows one of the limitations of the subtraction technique. If the frequencies of the liquid modes in figure 4.10 are projected across the antiresonance, they do however tend to line up. However, close

to the antiresonance, the liquid modes tend to rise out of the impedances of the piezoceramic tube rather than be added to it. When subtraction occurs, they lose some of the amplitude. Again, frequency ranges for optimization were chosen to minimize this error.

Chapter 5

Spectral response of the liquid-filled piezoceramic tube

The effect on the spectral response due to the liquid inside the tube is the most critical part of this study, as it reveals the parameters of the liquid that are to be determined. This section discusses how this energy is coupled into the spectral response of the tube and how the spectral response of the liquid can be described.

5.1 How energy is coupled to liquids

The way that motion though a liquid is normally defined is by the pressure on an area of a liquid, and the volume of liquid that flows though that area. In this case, the boundary of this moving volume is the wall of the piezoceramic tube. Thus, the movement of the walls of the piezoceramic tube is coupled though the exposed area of the liquid, and this sets up the pressure waves inside the liquid. This connection between the piezoceramic tube and the liquid is not necessarily ideal and there are several factors that can limit the coupling of the motion to the liquid. These include wall roughness, small bubbles of air trapped on the wall surface, and the actual thickness of the electrodes. However, ideally the force and velocity of the wall of the piezoceramic tube is coupled by area to the liquid and it is transformed to pressure and volume flow rate.

5.2 Resonant response of Liquids

An initial approximation of the sound travelling though the liquid cylinder is to imagine that the centre axis of the tube is a reflector, and that at the radius of the tube away from this axis is a plate transmitter/receiver with the same surface area as the inner

Figure 5.1: Diagram representing the initial approximation of the sound travelling though the liquid cylinder.

electrode of the tube, as shown in figure 5.1. As the transmitter vibrates, the sound it produces travels in the liquid away from the plate toward the reflector, and then back towards the transmitter. Thus standing waves can be set up by transmitting at a frequency that will ensure that the returning signal will aid the production of the next wave. These frequencies can be calculated from the speed of the sound of the liquid, and the distance that the liquid has to travel. For this scenario, the equation for obtaining the frequencies at which resonant modes occur is given by:

$$f_n = \frac{nc}{d} \tag{5.1}$$

Where n is the number of the mode, f_n is the frequency at which the nth mode occurs, c is the speed of sound and d is the inner diameter of the tube. However, analysis of spectra for different liquids showed that the equation does not exactly express the behaviour of a liquid in a tube.

5.3 Effect due to the radial nature of the waves

In practice, although the distance between the modes is basically as indicated by equation 5.1, the modes are offset, from zero Hz, by approximately a quarter wavelength. Also, the size of offset varies for different liquids. As the wave travels from the outside of the volume toward the inside, the radial nature concentrates the pressure wave and this affects the relative behaviour of the modes. When the continuum equations are solved later in this chapter (section: 5.5.3), it is shown that the equivalent impedance

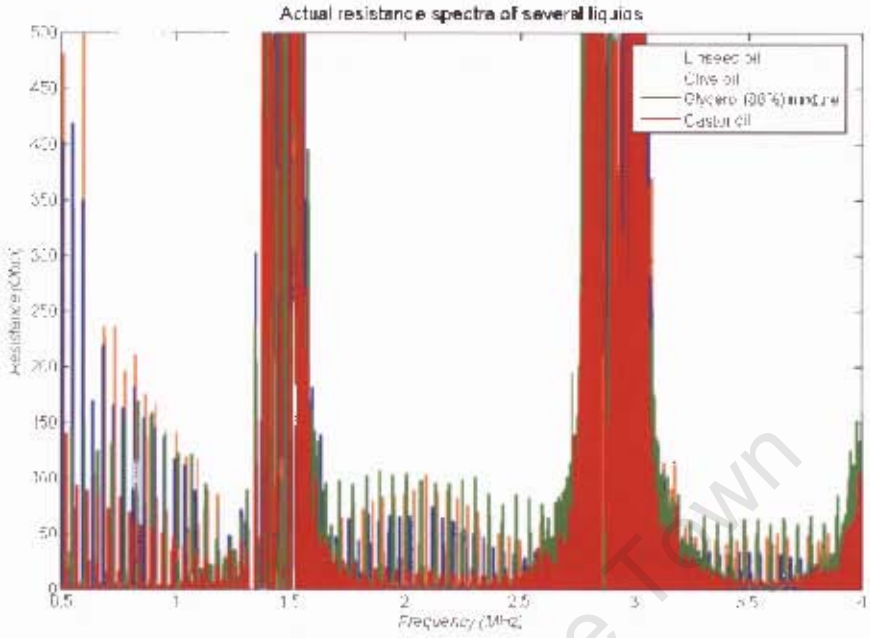

Figure 5.2: Resistance spectra of several real liquids with piezoceramic tube and cable responses removed. While the piezoceramic tube goes through its thickness resonance, the behaviour of the liquid is visible. During antiresonance this behaviour becomes obscured by noise.

for the liquid is the ratio of Bessel's functions [31], and that derived equation also exhibits the characteristics mentioned above.

5.4 Effect of viscosity on created modes

As previously discussed in the fundamentals of liquids (section 2), the density and bulk modulus are primarily responsible for producing the speed of sound in a liquid. They are also responsible, in conjunction with viscosity, for producing the Q of the resonant modes. However, the effect of viscosity on the Q and the magnitude of the modes was not obvious, in comparison to other effects, such as coupling efficiency. So a characteristic of the liquid within the spectrum, caused exclusively by the viscosity, had to be determined.

This factor was found by extending the examined spectrum to higher modes of the piezoceramic tube, as can be seen in figure 5.2. It became apparent that more highly viscous liquids have a decrease in Q and amplitude at higher frequencies, since attenuation due to viscosity is dependant on frequency [25]. Although this effect is due

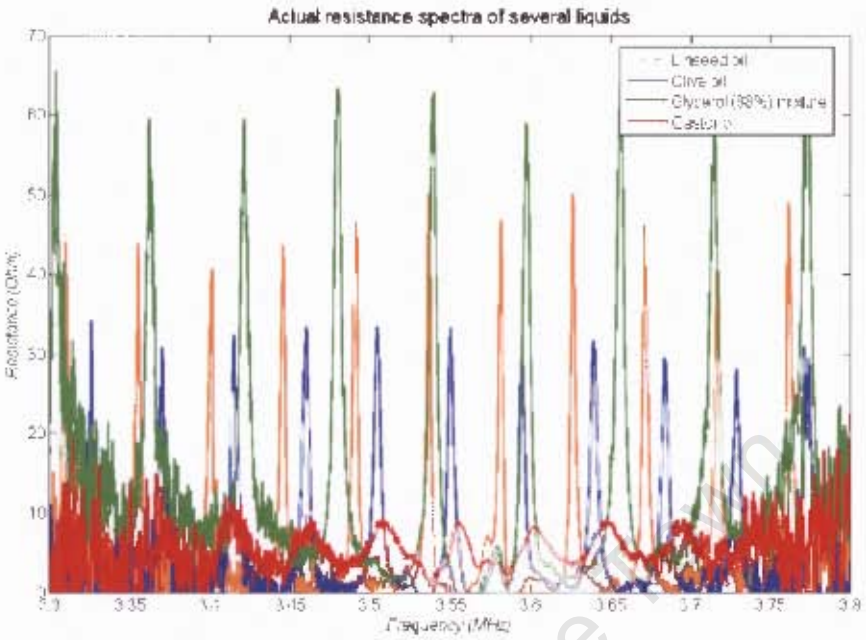

Figure 5.3: A closer look at the resistance spectra of liquids with the piezoceramic tube impedance and cable modes removed. Note the increase in offset resistance of the castor oil, and the lower Q modes on the glycerol(88%) sample.

to both density and viscosity, it is important to note that this might be a relatively good measure of the viscosity-density product, however only in liquids in which the relationship between density and viscosity makes for a reasonable decay rate of modes. The behaviour is defined by both viscosity and density. However the Qs of the decaying equations are much lower for more viscous samples, as seen in the Glycerol (88%) sample in figure 5.3. Another issue that should be noted is that there is a increase in the non modal offset of impedance of the castor oil sample (figure 5.3). Finally, some liquids do not behave like this at all, one case like this is water, which has Qs substantially higher that which it's viscosity should allow. However, the liquids studied in this work to behave as the classical theory suggests.

5.5 Models to represent the liquid

A lot of work has been done on the transmission of sound down circular tubes. In order to produce an equivalent model admittance spectrum for the liquid, several mathematical techniques were tested. Various methods were tried, from simple RLC circuits to transmission lines. Eventually, a continuum model based upon a viscoelastic

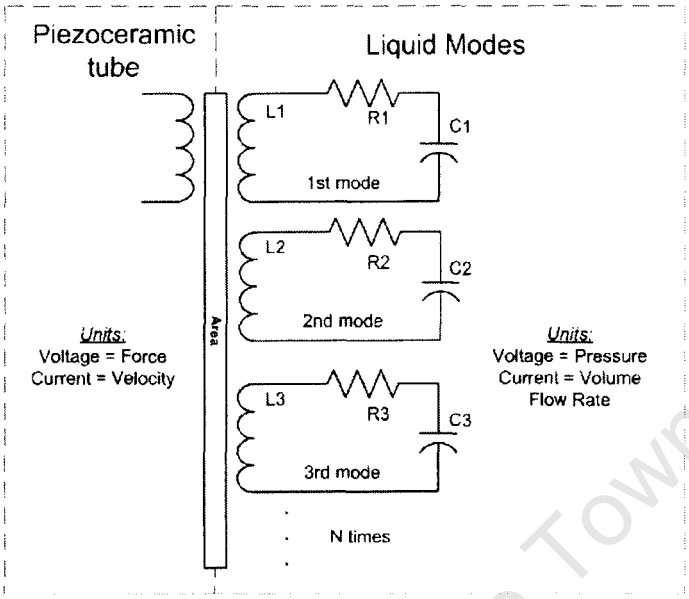

Figure 5.4: Diagram representing the RLC model originally attempted to replicate the liquid's spectra.

liquid was used.

5.5.1 Transformer coupled RLC circuits

Initially, it was hoped that modelling the modal behavior of the liquid using coupled RLC circuits would give an insight into the behaviour of the liquid. In this method each mode of the liquid is modeled by a RLC circuit, as can be seen in figure 5.4. These individual circuits are then coupled into the same transformer. The coupling ratio of the transformer was scaled to the area of the internal electrode of the piezoceramic tube (Figure 5.4). The resonant frequencies of all the simulated modes were set to be integer scaled values of the fundamental frequency of the liquid, as seen in equation 5.1, and the resistances were set to be the same. This was done in an attempt to ensure that the model tried to fit a common system, and not just the individual modes.

This model gave a relatively poor fit, and almost no inherent properties of the liquid could be extracted. Also, the calculation times required for this system seemed excessive. This system has the most degrees of freedom, and if unrestricted it will optimize to a spectrum with the closest fit to any real data; however, the practical problem remained that evaluating the liquid's properties from these results was not viable. Due to the vast number of variables used to define this system, optimization was only attempted using the breeder algorithm defined in section 9. A reasonable fit took a lot computational time and offered little insight into the liquid.

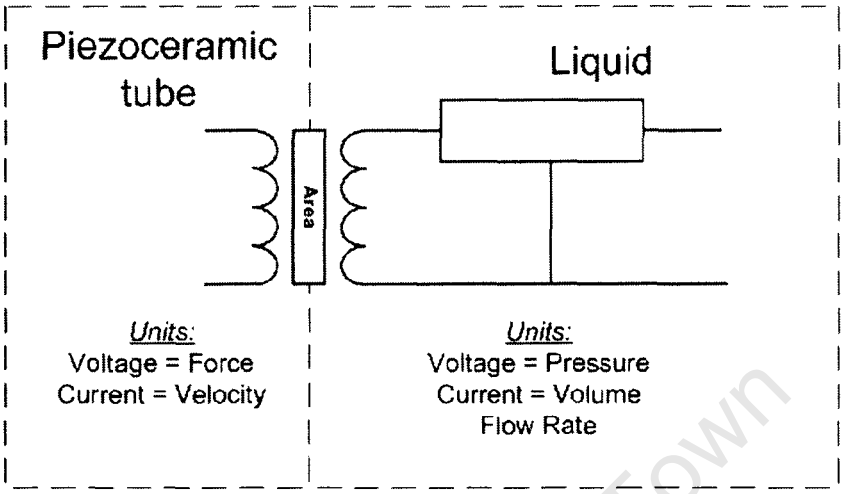

Figure 5.5: Diagram repesenting the transmission line model used to simulate a spectra.

5.5.2 Electrical transmission lines and frequency offset transmission lines

A transmission line model for the liquid has several advantages over the RLC model and it can be used in complicated linear systems [17]. The system has substantially fewer independent variables, and one equation produces all the modes. The independent variables are line resistance (Ω/m), capacitance (F/m), inductance (H/m) and the length of the cable. This system saves both in computational time and it makes for a more robust model, as shown in figure 5.5.

The movement of the piezoceramic tube is still coupled to the system through the area of the inner electrode. However, this transformer is now connected to an open circuit transmission line as long as the inner radius of the piezoceramic tube. The transmission line is open circuit, as in the centre of the liquid the movement from all sides cancels out and thus the net volume flow rate at the middle of the tube is zero. This indicates that no current will flow from or into the end of the transmission line, and therefore it is open circuit. The equations for an open circuit transmission line are:

$$Z_0 = \sqrt{\frac{(R + j\omega L)}{j\omega C}} \tag{5.2}$$

$$\gamma = \sqrt{(R + j\omega L)\, j\omega C} \tag{5.3}$$

$$Z_{liquid} = Z_0 \coth(\gamma r_i) \tag{5.4}$$

However, this model still had a slight error with respect to the fundamental frequency offset mentioned in section 5.3. To overcome this, an imaginary constant was added to inside the *coth* function. This offsets all the modes according to the value of the constant.

$$Z_{liquid} = Z_0 \coth(\gamma r_i + jK_{phase\_offset}) \tag{5.5}$$

This model was implemented with the same breeder algorithm as used in section 5.5.1, and worked much more effectively as fewer variables were required to be optimized. The breeder algorithm had a gene pool of 100 instances and took up to 60 iterations to obtain a result.

The results showed an excellent fit for the first mode of the piezoceramic tube, and the values for L and C changed proportionally with changes in density and bulk modulus. However, the reductions in Q and mode size, as mentioned in section 5.4, were not shown in this model; and the value for the offset could not be calculated from the liquid's material properties. At this point it was decided that if a true reflection of the behaviour of the liquid was to be produced, the fundamental equation for the liquid would need to be evaluated.

5.5.3 Solution though continuum mechanics for a viscoelastic liquid

The dynamics in a liquid of a cylindrical shape have been well defined [54] [35] [18] [52] [43] [31], however much of this research was aimed at longitudinal waves in the cylinder [6] and many do not take account of viscosity. The work of Vollmann [54] is adjusted to allow for no length effects, and it establishes what the impedance will be, rather than the stresses in the liquid. The liquid will be described as a viscoelastic material. This is because it can be assumed that, other than the movement of the sound waves through the tube and liquid, the system is at rest. This implies that there is no net volume flow rate of the liquid into or out of the tube. Since in the study only static samples will be tested, this assumption holds true. It also assumed that for future applications this assumption will work as long as the volume flow rate of the liquid is kept substantially lower than the speed of sound of the liquid tested. Thus, for a linear elastic material:

$$\sigma_{ij} = \lambda^*(\omega)\delta_{ij}\varepsilon_{kk} + 2\mu^*(\omega)\varepsilon_{ij} \tag{5.6}$$

where σ is stress, ε is strain, δ is the Kronecker delta and λ, μ are the Lamé constants or this case the viscoelastic constants. These constants are defined to be

complex and dependent on frequency. The viscoelastic constants for this application were defined as:

$$\mu^*(\omega) = j\omega v \tag{5.7}$$

$$\lambda^*(\omega) = k + \frac{2}{3}\mu^*(\omega) \tag{5.8}$$

where v is the viscosity of the liquid and k is its bulk modulus. This equation ignores bulk viscosity. The simplification will add some error to the final answer. However this assumption is quite commonly made [3]. And although it has been shown that this error can be small in ultrasonic range [26], it is very much dependant on the liquids samples that are used. For the samples used in this thesis this assumption did not have a large impact. However, For other liquids this simplification could produce a larger error.

It is also assumed that waves that are produced are entirely radial, and thus that there is no variation with respect to the angle or length within the cylinder. Also this implies that no sound energy is lost in the open ends of the tube. For this system, a displacement field is defined by:

$$u^f = \nabla\varphi \tag{5.9}$$

where u^f is the displacement of a point in the liquid with respect to r, and φ is the displacement field. For the above defined system, Navier's equation for a solid can be reduced to the Helmholz equation. This is the equation that will be solved to produce the solution.

$$-\omega^2\rho_f\varphi - (\lambda^*(\omega) + 2\mu^*(\omega))\,\triangle\varphi = 0 \tag{5.10}$$

where ρ_f is the density of the liquid. $\triangle\varphi$ can be derived, with respect to cylindrical coordinates and for a system that only changes with respect to radius as follows:

$$\triangle\varphi = \frac{d^2\varphi}{dr^2} + \frac{1}{r}\frac{d\varphi}{dr} \tag{5.11}$$

Since these equations are being used to produce a spectra, all equations can be assumed to be sinusoidal. Thus

$$\varphi = f(r)e^{j\omega t} \tag{5.12}$$

So equation 5.10 becomes:

$$-\omega^2\rho_f f(r)e^{j\omega t} - (\lambda^*(\omega) + 2\mu^*(\omega))\,(f''(r)e^{j\omega t} + \frac{1}{r}f'(r)e^{j\omega t}) = 0 \tag{5.13}$$

This can be simplified to become the differential equation for the defined system under study

$$r^2 f''(r) + r f'(r) + r^2 B_f(\omega) f(r) = 0 \tag{5.14}$$

$$B_f(\omega) = \sqrt{\frac{\omega^2 \rho_f}{(\lambda^*(\omega) + 2\mu^*(\omega))}} \tag{5.15}$$

The solution to equation 5.14 can be found by use of Bessels functions. Thus

$$f(r) = c_1 J_0(B_f(\omega) r) + c_2 Y_0(B_f(\omega) r) \tag{5.16}$$

Where J_0 is the Bessel's function of the first kind, and Y_0 is the Bessel's function of the second kind. However Bessel's functions of the second kind are infinite at zero, and since this would be impossible for the defined system, c_2 must be zero. Thus substituting this into equation 5.12 and then differentiation with respect to r, gives

$$\varphi = c_1 J_0(B_f(\omega) r) e^{j\omega t} \tag{5.17}$$

$$u_r = \varphi_{,r} = -c_1 B_f(\omega) J_1(B_f(\omega) r) e^{j\omega t} \tag{5.18}$$

Thus, since strain is the derivative with respect to radius of displacement:

$$\varepsilon_{rr} = u_{r;r} = -c_1 B_f(\omega)(B_f(\omega) J_0(B_f(\omega) r) - \frac{1}{r} J_1(B_f(\omega) r)) e^{j\omega t} \tag{5.19}$$

ε_{kk} is defined as the sum of the diagonal of the strain matrix, E. Since the equation for the strain matric will be dealing with a cylinder of liquid, cylindrical coordinated will be used. Strain in the theta direction and in the length direction are ignored in an attempt to keep the equations simple. The effect due to theta will be truely negligible, however ignoring the effects due to length will remove the possibility for the model to handle the sound waves that escape through the top and bottom of the tube. In a final implementation of such a sensor, a longer tube should be picked to minimize this error between model and real life. Thus, for the cylindrical solution with no effects due to angle or length, this matrix is:

$$E = \begin{matrix} u_{r;r} & 0 & 0 \\ 0 & \frac{1}{r} u_r & 0 \\ 0 & 0 & 0 \end{matrix} \tag{5.20}$$

$$\therefore \varepsilon_{kk} = -c_1 B_f(\omega)^2 J_0(B_f(\omega) r) e^{j\omega t} \tag{5.21}$$

Thus from equation 5.6, radial stress can be calculated:

$$\sigma_{rr} = -c_1 e^{j\omega t}((\lambda^*(\omega) + 2\mu^*(\omega))B_f(\omega)^2 J_0(B_f(\omega)r) - 2\mu^*(\omega)B_f(\omega)\frac{1}{r}J_1(B_f(\omega)r)) \tag{5.22}$$

From the derivative with respect to time of equation 5.18, volume flow rate can be evaluated:

$$V = area \times u_{r,t} = A(-c_1 j\omega B_f(\omega)J_1(B_f(\omega)r)e^{j\omega t}) \tag{5.23}$$

Finally, the impedance due to the sound travelling in the liquid at the inner diameter of the piezoceramic tube can be calculated:

$$Z_l = \frac{\sigma_{rr}(r_i)}{V(r_i)} \tag{5.24}$$

$$Z_l = \frac{-((\lambda^*(\omega) + 2\mu^*(\omega))B_f(\omega)^2 J_0(B_f(\omega)r_i) - 2\mu^*(\omega)B_f(\omega)\frac{1}{r_i}J_1(B_f(\omega)r_i))}{A_i(-j\omega B_f(\omega)J_1(B_f(\omega)r_i))} \tag{5.25}$$

Several assumptions have been made in the derivation of this equation. Firstly heat flux in the liquid was ignored. Inclusion of it would have meant that the relationship between temperature and the liquid's parameters would have needed to be known. It is assumed that the movement due to the piezoceramic tube in this application will produce so little displacement that heat flux is negligible. Also the movement in Length was ignored. Thus sound escaping out of the sides of the tube will not be taken into account. It is also assumed that the wall of the piezoceramic actuator contracts perfectly parallel to the liquid. This will also not be likely to occur. However, in the primary mode of operation, of the piezoceramic tube, most of the sound generated will be in the tube's primary mode of movement.

This equation is then coupled into the model for a piezoceramic tube, and the simulated impedance is calculated. It exhibits the behaviour required for the location and amplitude of the liquid modes, and it also exhibits the decay behaviour due to viscosity as mentioned in section 5.4.

5.6 Effects on coupling

In a perfect situation, all displacement and pressure will be coupled though the area of the inner surface of the piezoelectric tube into the sample liquid. However, in reality this seldom happens. This effect should not be confused with the wave reflections caused by a density mismatch between the piezoceramic material and the liquid, as

this effect can be simulated though the impedance mismatches between the sample liquid and the piezoceramic tube. In previous work using the piezoceramic tubes to measure speed of sound, it was found that when a sample liquid was placed in a dry piezoceramic tube, the liquid coupled very poorly to the piezoceramic tube [15]. However, when the author washed the piezoceramic tube with a soapy liquid and allowed it to dry before placing a sample liquid into the tube, the liquid's effect on the spectrum of the piezoceramic tube became much greater.

It is the opinion of the author that this can be explained as follows: as the liquid is placed in the tube, tiny air bubbles remain against the surface of the tube. These bubbles act to reduce the effectiveness with which the piezoceramic tube couples to the liquid. The soapy liquid reduces the surface tension and releases the bubbles from the surface, and coats the surface with a thin film. Thus when the sample liquid is placed in the piezoceramic tube, the liquid contact is established with the thin film, and thus there are fewer air bubbles present.

Additionally, there are other effects on the Q of the liquid modes. These include surface finish, the accuracy of the inner diameter, and the solder joint required to connect a cable to the inner electrode.

These effects were modelled though an electrical equivalent circuit in parallel with the impedance of the liquid. The equivalent circuit consists of a capacitor in parallel with a resistor. The capacitor simulates the elastic behaviour of the bubbles, and the resistor simulates the energy lost in the bubbles, and losses due to any other additional causes. The resistor and capacitor are placed in parallel with the impedance of the liquid. They are placed in parallel because the bubbles will simply get compressed to the applied pressure in the liquid and thus do not reduce the pressure on the liquid. However, the bubbles have a significant impact on the displacement that will be coupled.

After some difficulties obtaining consistent spectra, it was noticed that one of the samples being measured, namely linseed oil, had an effect that impaired the ability of the soapy solution to improve coupling to a new sample. When the piezoceramic tube was left in water for a day, the response of the piezoceramic tube coupled with a liquid returned to what it was before. This shows that the surface effect between the piezoceramic tube and the liquid is very much affected by the material that was last in contact with the tube. Further work on the implementation of this sensor will have to contend with techniques of stabilizing this problem.

Sample	Density	Speed of sound	Viscosity
30°C	$kg.m^{-3}$	$m.s^{-2}$	$Pa.s$
Olive Oil	909.8	1424	0.0526
Linseed Oil	926.6	1439	0.0332
Castor Oil	957.0	1481	0.456
Glycerol(88%)/Water mixture	1225	1869	0.0993

Table 5.1: Table of measured liquid properties

5.7 Integration of the liquid model with piezoceramic tube

The methods used to couple the equations that define the piezoceramic tube, and those for the liquid, depend on how the equation for the piezoceramic tube have been defined as described in section 4.6. For equations based on the constitutive relations the impedance can simply be inserted into equation 4.30. When the approximation method is used, the impedance due to the liquid will first need to be correctly scaled, to ensure that when it is added to the impedance of the piezoceramic tube, they are of the same scale. This difference in application is due to the definitions of the models. The constitutive equation model is defined in such a way that the pressure and the volume flow rate of the liquid are used. Thus the impedance of the liquid can be directly applied. Whereas in the case of the impedance method, the equivalent impedance of the piezoceramic is already in ohms, thus the impedance of the liquid needs to be transferred across the equivalent transformers to convert it to the same units.

To do this, the impedance of the liquid is converted to its equivalent actual impedance and it is placed in series with that of the piezoelectric tube.

5.8 Visualization of the simulated spectra

Several different liquids were placed in the piezoceramic tube to obtain comparable spectra. They varied in density between $900kg.m^{-3}$ to $1200kg.m^{-3}$ and in viscosity between 0.02 $Pa.s$ to 0.5 $Pa.s$. They were chosen for their variety in an attempt to show what the full domain of spectral possibilities might be. The viscosity was kept above 0.02 $Pa.s$ in an attempt to keep the Q of the modes down. This was for practical reasons, to restrict the resolution of the spectra in order that a sufficient number of sample points on each liquid mode was taken.

The liquids listed in table 5.1 were tested on a thermally controlled viscometer and had their densities measured on a pycnometer. These measurements were used as a

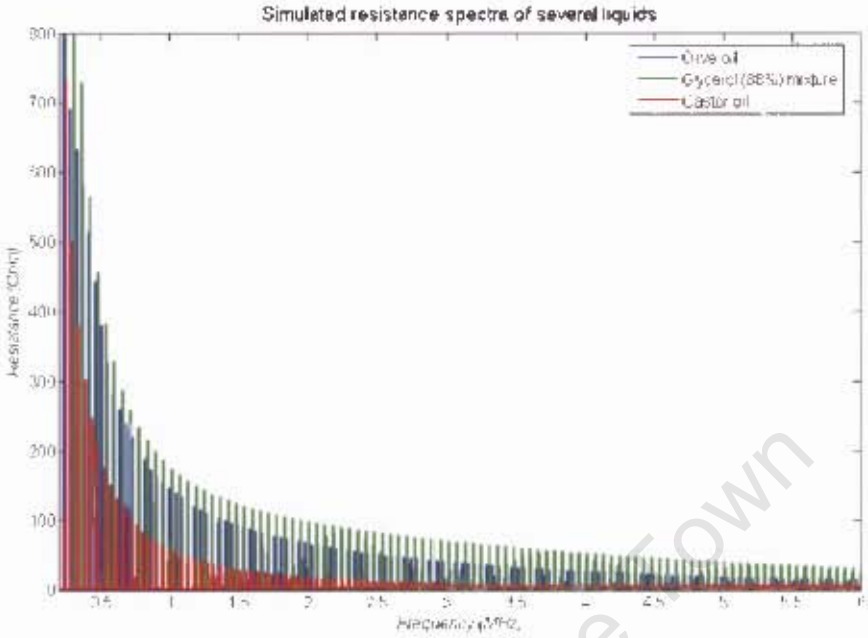

Figure 5.6: Spectra of the simulated resistance of several liquids. Note that the liquids decay in frequency at different rates. The glycerol (88%) sample is larger than the olive oil sample which is much more viscous, due to its greater density.

reference for comparison with the real spectra. To keep variations in oil down, Samples where taken from a single container of medical grade oil. Measurements where taken on the same day. Some variation between these values and literature values for these oils is to be expected since many factors can effect the eventual quality of the oils. This is most noticeable in viscosity values.

As can be seen in figure 5.6 and 5.7, the equation produces a modal behaviour similar to that of the real data seen in figure 5.2. It obviously does not suffer with the noise issues of the real data. Also its response at low frequencies (<800kHz) is difficult to compare to actual data, as the actual data contains a lot of spurious modes at the lower frequencies (as explained in section 4.4.2 and 4.4.3). Also as is visible in figure 5.8, the simulated equation develops an offset resistance for the castor oil sample, and has lower Q modes in the glycerol (88%) sample as mentioned in section 5.4. Closer comparisons of individual spectra are visible in the results chapter (chapter 10).

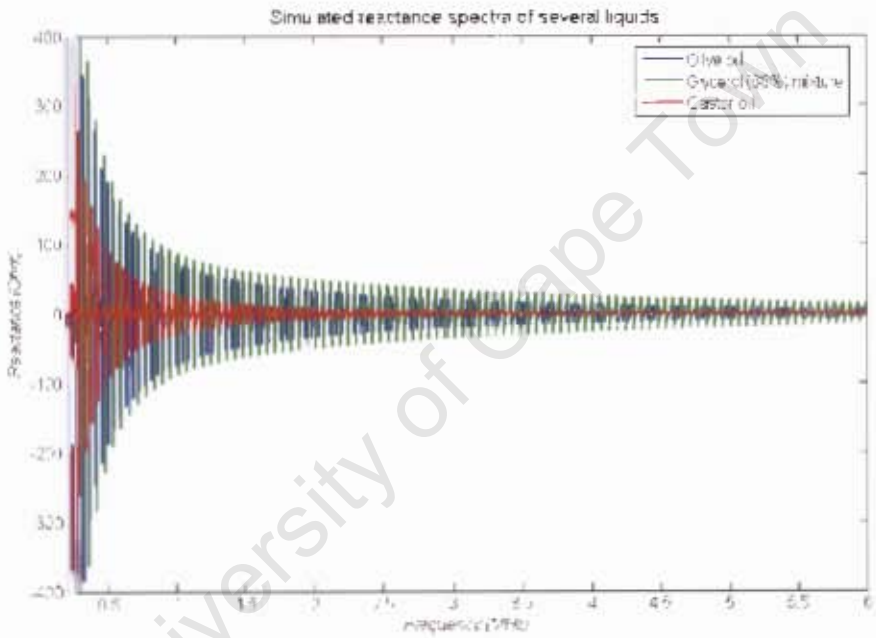

Figure 5.7: Simulated reactance of several liquids. This spectra shows the same decays as in figure 5.6. Note that all the modes are centered around zero siemens.

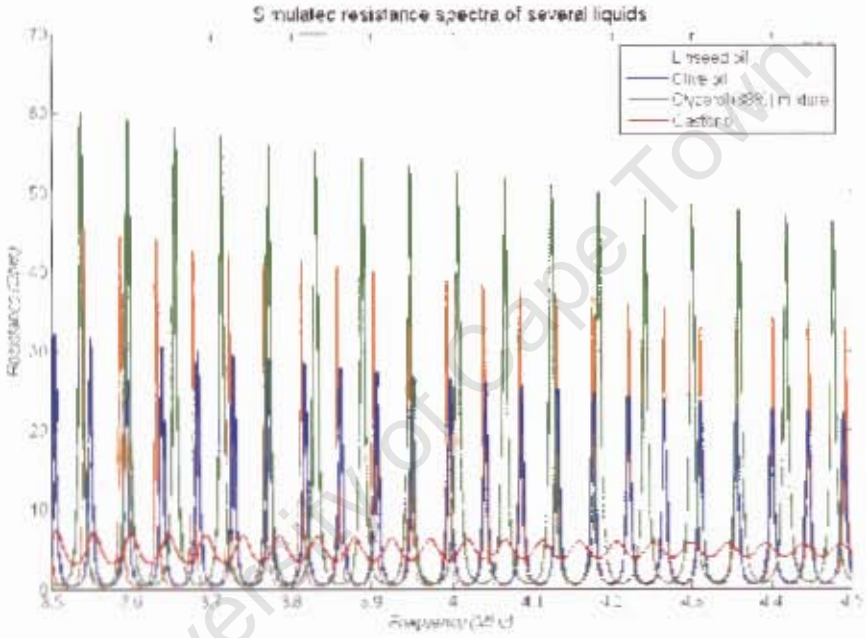

Figure 5.8: A closer look at simuated resistance shows the different spacing between modes due to variations in sound speed. Also, the density and viscosity effects become more apparent with the offset resistance of the castor oil sample, and the difference in mode Qs between the olive oil and glycerol (88%) samples.

Chapter 6

Model evaluation

Since the basic equations that will be used to simulate the fluid and the piezoceramic tube have been established, it is now important to discuss how these equations will be implemented. The peizoceramic tube system, the liquid, and the cable are used to produce a simulated spectrum. This chapter aims to show how accurate and representative these equations and simplifications prove to be.

6.1 Combining the models

In the previous two chapters, the author has discussed how the impedance of the peizoceramic tube and the liquid were determined. This section shows how the different impedances are coupled together.

As can be seen in figure 6.1, the basic simulated circuit consists of 3 components, namely the cable, the peizoceramic tube and the liquid. The impedance for the liquid was determined by the division of pressure and volume flow rate. These units need

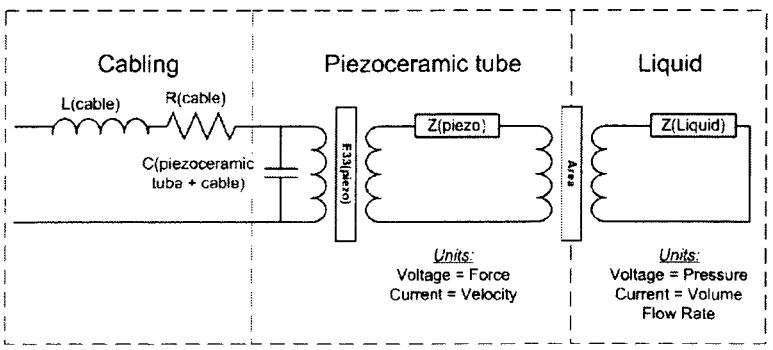

Figure 6.1: Diagram of completed model for filled piezoceramic tube.

to be converted to force and velocity so that they can be converted to the impedance of the peizoceramic tube. This is done using the electrical analogy of a transformer. The turns ratio of the transformer is the area of the inner electrode of the peizoceramic tube. Similarly, the force and velocity experienced by the peizoceramic tube are transformed to voltage and current through a transformer, with coupling proportional to the piezoelectric constant.

Several options are available for which particular spectrum will be compared with respect to the sensor, e.g. one could simulate the entire spectrum from liquid to peizoceramic tube and cable and compare that to the actual spectrum taken. However this will prove unwise as the dominance of a cable mode on a spectrum, as can be seen in figure 4.1, will drown out the actual response of the liquid and thus make the system especially sensitive to variables of no interest. It was decided to compare spectra of simulated impedances of the liquids to that of measured spectra with the cable and the peizoceramic tube's modes removed.

These are obtained by removing the cable impedances and case capacitance from the spectra, as described in section 4.3, and then subtracting the impedance of an empty tube spectrum (with the case capacitance removed) taken at the same temperature, as described in section 4.7. The remnant spectra will act as the reference model to which simulated models for the liquids, described in section 5.5.3, will be optimized. It should be noted that the simulated spectra of the liquids are transferred across both transformers, as indicated in figure 6.1, before a comparison can be performed.

6.2 Practical variations in case capacitance

Unfortunately, the liquid has an effect on the resistance and capacitance parameters of the cable resonance mode. In an attempt to reduce the effect that the internal solder joint has on the acoustic response of the liquid, only a tiny connection was made. The liquid is filled over the connector, and it aids in the conduction of electricity. Thus the cable resistance decreases slightly depending on the conductance of the liquid. The magnitude of this effect is normally smaller than $10m\Omega$.

Since the liquid is filled beyond the ends of the tube in an attempt to ensure planar acoustic waves, the liquid slightly increases the capacitance of the system. This is due to the liquid effectively increasing the surface area of the inner electrode. If the top ring (see figure 7.3), that was used to ensure that liquid can be filled to beyond the length to the tube, had been made from metal and had been grounded, this effect could have been minimized. Normally this capacitance increases by less than $40pF$.

Both of these changes are large enough that a single set of cable properties could not be used for all the spectra taken. Each spectrum had to have its cable parameters

calculated. The accuracy to which these variables are measured has a great impact on the final spectrum of the liquid, since errors in the cable mode alter the location of the antiresonance mode discussed in section 4.7.

6.3 The spectrum of the empty piezoceramic tube

Although the response of the peizoceramic tube does not change drastically with changes in temperature, there is a very slight variation of the location of the thickness modes. This variation can be seen as an offset in the reactance of the final liquid mode spectrum. It also acts to reduce the usable frequency window at the antiresonance, discussed in section 4.7.

6.4 Determination of the transformer values and loss components

As stated, the coupling ratio of first transformer on the right, in figure 6.1, is the area of the inner electrode. The ratio for the second transformer was derived from a finite element model that was previously developed for this tube [15]. Changing this value has a similar effect to changes in density of the liquid with respect to the Qs of the liquid modes. Thus, this variable could have been used to calibrate the sensor for density measurement. The other value that has an important impact on the measurement of density is the resistor used to simulate losses in coupling, as discussed section 5.6. This resistance and capacitance were aligned by eye to an actual spectrum to obtain a good fit. The actual value of the capacitor becomes unimportant, as the fundamental thickness mode of the tube is not used in the optimization and since the capasitor's effect on the spectra is minimal by the second harmonic. Both the values of the resistor and the capacitor are held constant for all liquids used, although slight variations in these values are to be expected each time a different sample is placed into the peizoceramic tube.

6.5 The ranges of frequency analysed

Only two thickness modes of the peizoceramic tube were used to determine liquid properties. They were the second and third thickness modes. The fundamental mode was ignored, as at such a low frequency the liquid modes were extremely sharp and normally consisted of only a couple of sample points. Also, if a spurious length or circumferential mode of the tube happens to align with such a sharp liquid mode,

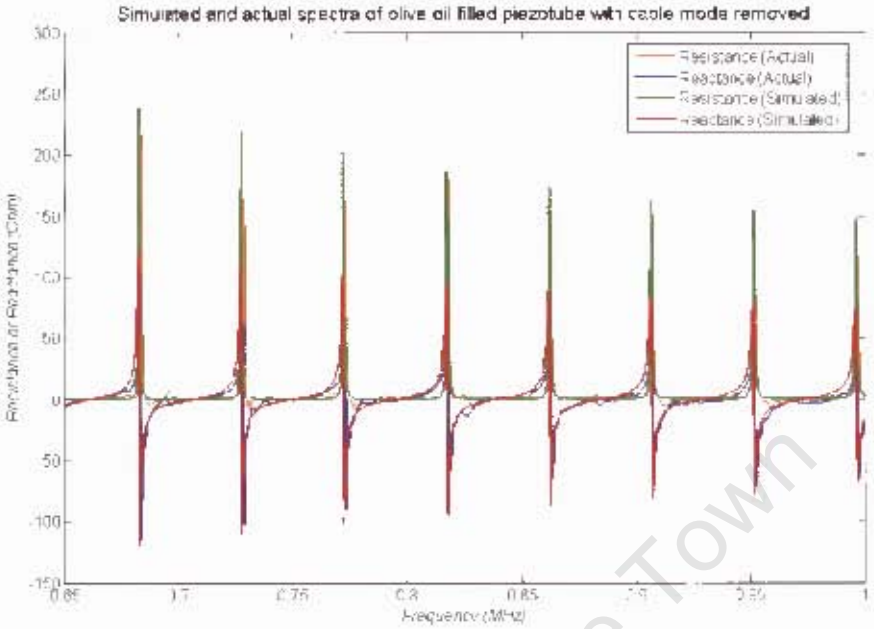

Figure 6.2: Real and simulated spectra of resistance and reactance for an olive oil sample over the first thickness resonance mode of the piezoceramic tube. Olive oil is shown as its lower viscosity makes its modes more apparent on the fourth thickness harmonic of the tube. It is very important that the placement, peaks and shape of the modes align.

the distortion of the liquid modes is quite extreme. Higher thickness modes of the peizoceramic tube, such as the fourth or fifth etc., tend to be more noisy and thus were also ignored. Filtering was attempted to allow for a greater operating area; however, the reward with respect to noise at high frequencies needed to be traded off with the distortion that the filter creates on the extremely sharp low frequency modes. It was decided to keep filtering to a minimum.

6.6 Comparison with real spectra

Comparisons between actual data and simulated spectra, derived from measured constants, described in table 5.1, for the first four thickness harmonics of the peizoceramic tube, in figures 6.2, 6.3, 6.4 and 6.5, show good fits. Across the fundamental radial mode, shown in figure 6.2, the effect of the capacitance, mentioned in section 6.4, is visible with the rise in the mode sizes. Also noticeable is a large degree of fluctuation in mode peaks. By the third and fourth thickness modes, noise tends to creep in from the edges of the resonant band. The reduction in liquid mode Q due to viscosity can

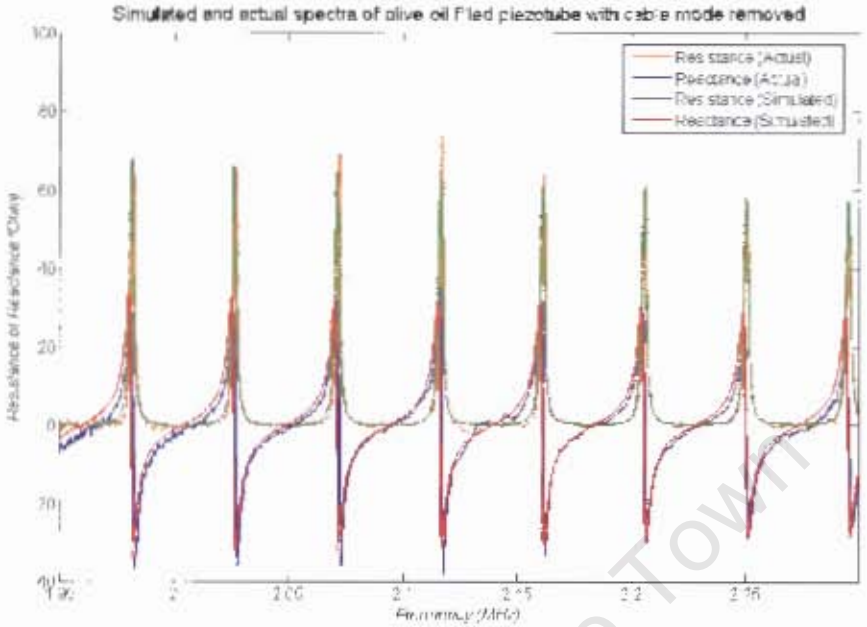

Figure 6.3: Real and simulated spectra of resistance and reactance for an olive oil sample over the second thickness resonance mode of the piezoceramic tube.

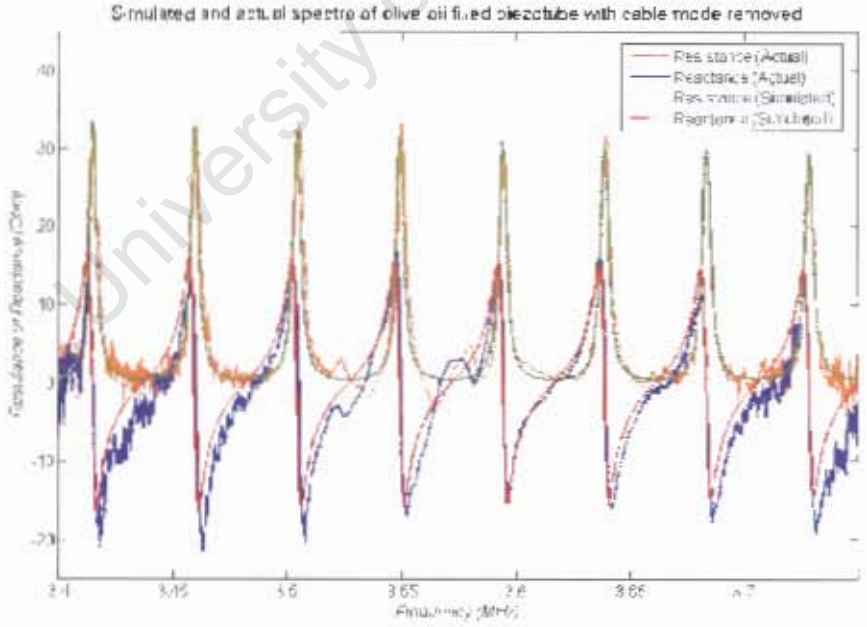

Figure 6.4: Real and simulated spectra of resistance and reactance for an olive oil sample over the third thickness resonance mode of the piezoceramic tube.

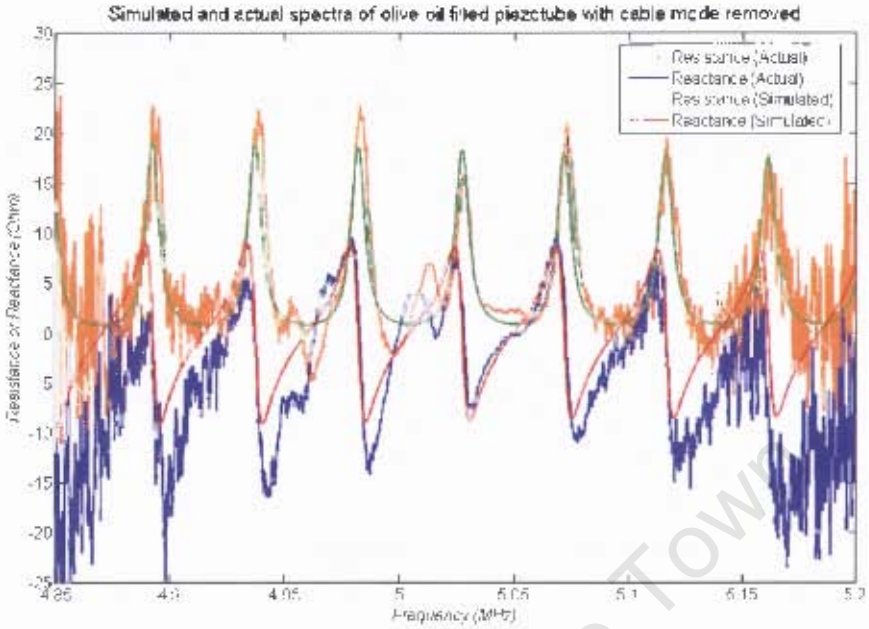

Figure 6.5: Real and simulated spectra of resistance and reactance for an olive oil sample over the fourth thickness resonance mode of the piezoceramic tube.

also be observed, in comparison with the second thickness mode. Finally, there is an offset error forming on the sides of the reactive part in figure 6.5. This is due to slight inaccuracies in the calculation of the RLC components used for cable impedance and case capacitance removal.

Future chapters will describe how these spectra are evaluated to determine the error between them, and how the values for the liquid are determined by reducing that error algorithmically.

Chapter 7

System Implementation

Now that the theoretical components of obtaining spectra have been discussed, the practical implementation should be mentioned. Since the system that was implemented was only to be a proof of concept for an analytical spectrometer, an attempt was made to reduce possible causes of error before any measurements were taken. This was done by measuring samples in a regulated environment and by using a standard impedance analyzer. The system also needed to be thermally controlled, to ensure that all samples could be taken at the same temperature and that the sample temperature did not change during the process of taking a spectrum.

7.1 Device description

Since a versatile implementation was required to ensure that when design flaws became apparent, the system could be easily altered without a complete redesign, a modular approach was chosen for the implementation. The basic system consists of three sections: the piezotube and its housing (this is the heart of the sensor and any modification made to this had an impact on a measured spectra), the thermal regulation system (which consists of a brass jacket and a thermal bath) and the impedance analysis system. A basic diagram of the implementation is shown in figure 7.1.

7.2 The transducer

The transducer is of course at the heart of the project. It consists of a piezoceramic tube that is bonded to a housing which seals the base and allows for a short cable to be connected to the tube.

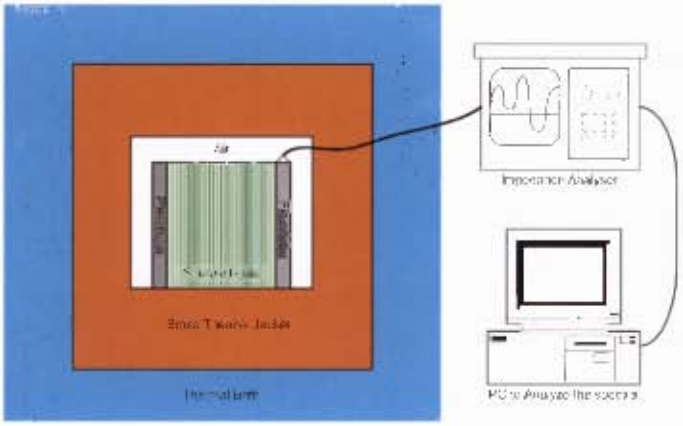

Figure 7.1: Basic diagram showing the fundamental components of the system implementation.

7.2.1 The piezoceramic tube

Several piezotubes of different sizes and properties were tested during the initial iterations of the system. There were several design choices that needed to be made when considering the tube to be chosen for such a sensor. The dynamics of the tube were discussed in chapter 4. However, some of the practical compromises that have to be made still need to be mentioned.

The dimensions of the tube chosen do not only affect its own impedance spectrum, they also affect that of the liquid as discussed in chapter 5. A tube with a small inner diameter, in relation to its thickness, will benefit in the measurement of more viscous liquids, as the decay in mode size with frequency will occur more slowly. With the same line of thinking, if measurement of many very inviscous liquids is to be done in the optimum tube, a piezotube with a relatively large inner diameter in comparison to its thickness is recommended. With a longer path length for the sound to travel, the viscosity of the liquid will have more time to attenuate the sound.

The thickness of the tube is chosen to set the frequencies of the thickness modes. This decision needs to be made in conjunction with the choice of inner diameter, since the placement of the thickness modes of the tube essentially locates windows onto what parts of the liquids' impedance spectra can be seen. Thus, the thickness modes need to be placed so that enough of the decay of the liquids' response can be seen to be able to fit a curve to it with sufficient confidence.

For this type of design, longer piezotubes should be beneficial, since this will mean that the length modes are further away from the zone of interest, and smaller. Also, the amount of sound that propagates from the ends of the tube becomes less significant

Figure 7.2: A typical piezoceramic tube. This tube has dimensions: inner diameter 31.8mm, outer diameter 38mm and length 38.3mm. The electrode was made of fired screen printed silver.

for longer tubes. Unfortunately, since piezoceramic tubes were purchased from manufacturers' standard stock, a relatively long piezotube, of the inner diameter desired, was never sourced.

It is also important that the piezoceramic material used was made of a relatively soft compound. Soft piezoceramics, which are normally used for sensors, produce lower Qs than hard piezoceramics, which are used for transmitters. Since the thickness resonance of the piezoceramic tube is the region of interest, a wider resonant zone will allow for more of the liquid modes to be seen.

No study was done on electrode material used for the piezoceramic; however, it stands to reason that the electrode could have an important impact on the losses experienced in coupling between the piezotube and the liquid. An electrode with minimal surface roughness is ideal.

The tube that was used had been previously used in a B/A study [15]. It consisted of NAVY 1 material and had dimensions: inner diameter 31.8mm, outer diameter 38mm and length 38.3mm, and is shown in figure 7.2 and had a small 50Ω coaxial cable soldered to it. It was less that 3cm long.

7.2.2 The piezoceramic tube housing

Although the mechanics of the piezotube are the primary influence on its spectral response, the method of housing the tube in a structure that allows a liquid to be held inside it had secondary affects on its behavior. The piezoceramic tube needs to be housed in a manner that allows it to be filled with a liquid so that the liquid column exceeds the piezotube's length both at the top and bottom. This ensures that the entire surface of the inner electrode is covered with a liquid. Also in previous work

[42], it was shown that the depth of the sample also influenced small length modes in the liquid; with a long sample column this effect is minimized. Consequently, a small plastic ring was bonded with a silicone sealer to the top of the tube. A recess was machined into the brass base used to seal off the bottom of the tube.

The base of the piezoceramic tube housing was constructed of brass to allow maximum thermal conduction between it and the thermal jacket, discussed in section 7.3.1, thus reducing the time the sample took to reach the same temperature as the inside of the jacket. It was machined to be of the some radius as the cavity in the thermal jacket. The plastic ring at the top of the tube had a slot cut in it to accommodate the cable to be soldered onto the tube, and it was constructed from plastic to minimize the likelihood of it shorting the cable circuit. However, in hindsight, it might have been better to make it from brass, similar to the base, and to short both of them to the inner electrode of the tube. This would have minimized the change in case capacitance experienced when the liquid was filled into the tube.

An additional plastic component of the housing was bolted above the piezotube. It held the SMA connector to which the cable, from the tube, was soldered. It had a hole in the middle to allow for the tube to be filled. Later, the plastic ring and this component were joined to reduce the likelihood of a spillage, and to allow for the cable to be fixed to the plastic ring, as it was found that moving the cable had an impact on the mode it produced.

A standard coaxial cable was used to connect the piezotube to the SMA connector. Its length was about 30mm. It was found that a longer cable brought the cable mode too close to the resonances of the piezoceramic tube. This increased the possibility of additional error at the measurement frequencies. If the cable was too short, it was very difficult to connect. Also, being able to study the cable mode made it possible to determine its values and its effect on the spectrum. If the mode was moved to a higher frequency, this ability was lost. This is because as the mode moved off to higher frequencies, a larger spectral bandwidth would be required to allow it to be viewed. This was becoming impractical with respect to how much time a spectrum took to sample, and how large the resulting data set became.

7.3 Thermal regulation

The thermal characteristics of the liquids to be measured made it important to regulate their temperature exactly. Both viscosity and speed of sound are very dependent on temperature. This implied that if the sensor output was to be compared to calibrated values, both these measurements would need to be taken at the same temperature; otherwise an error will be perceived that does not necessarily exist. The thermal

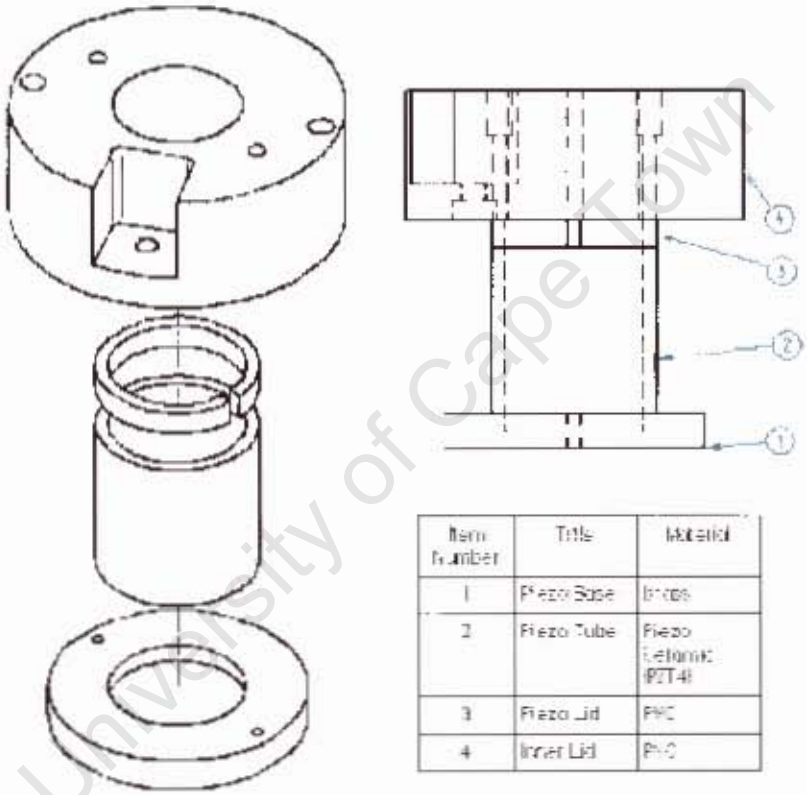

Item Number	Title	Material
1	Piezo Base	brass
2	Piezo Tube	Piezo Ceramic (PZT-8)
3	Piezo Lid	PVC
4	Inner Lid	PVC

Figure 7.3: Exploded view of the piezotube housing. The square cut-out on the inner lid houses the SMA connector.

regulation holds another important function. The impedance analyzer used to measure the impedance spectra takes a finite time to sample a spectrum. For the 148 000 sample points taken for a single spectrum, this impedance analyzer takes about 2 hours. This implies that the temperature of the sample needs to remain completely constant over this time to ensure that the same material constants of both the piezoceramic tube and the liquid do not change. It should be noted that if pulsed techniques were used to produce the spectrum, this time could be reduced to mere milliseconds and thus the constant temperature stabilization might no longer be needed.

7.3.1 The thermal jacket

The thermal jacket can best be described as a low pass filter between the temperature of the thermal bath and that of the sample liquid. It consists of a large brass cylinder with a cavity in the middle which houses the piezoceramic tube, and a brass lid that is bolted on top. The lid is sealed with an O-ring to the jacket, to ensure that water from the thermal bath does not get into the measurement areas. The lid has a hole at the top to which a pipe is connected. This pipe allows the cabling from inside the jacket to removed without allowing water to get into the system. Additionally four tapped holes were drilled into the bottom of the thermal jacket, into which four bolts where screwed to act as feet. This allowed for the jacket to be lifted off the floor thus allowing for water to flow under it.

Brass was chosen for the thermal jacket as it is a good conductor of heat and it is easy to machine. Also, it tends not to corrode in the water tank, but it does get a little tarnished. The thermal jacket took about 2.5 hours to reach thermal equilibrium at a set temperature. The determination of whether equilibrium had been reached was by examining a single liquid mode on the fourth harmonic of the thickness resonance of the tube. Depending on the sample this might be the 100th liquid mode harmonic. At this point of the spectrum the modes are extremely temperature sensitive. If the mode had not moved perceptively in forty minutes the system was considered to be at steady state.

7.3.2 The thermal bath

A thermal bath is used to set the temperature of the experiments. It aims to reduce the amount of heat that flows to or from the thermal jacket once steady state is reached. It also helps to isolate the system from external influences. This is especially important as the sample needs to remain at a fixed state for an extended period of time.

The design of this thermal bath was done by Davies [15]. Essentially the thermal jacket is submerged in water that is thermally controlled. The water is contained

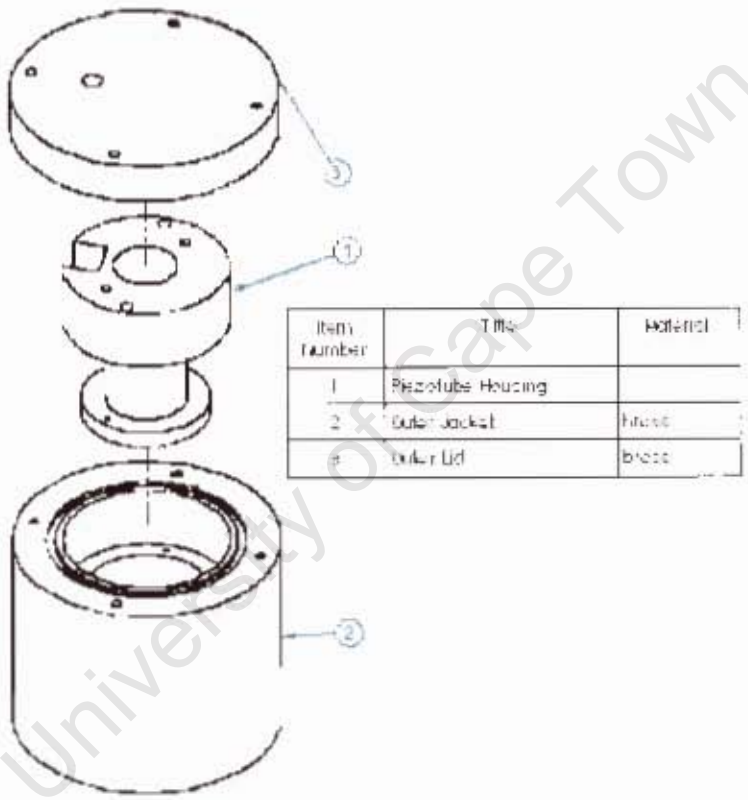

Figure 7.4: Exploded view of thermal jacket.

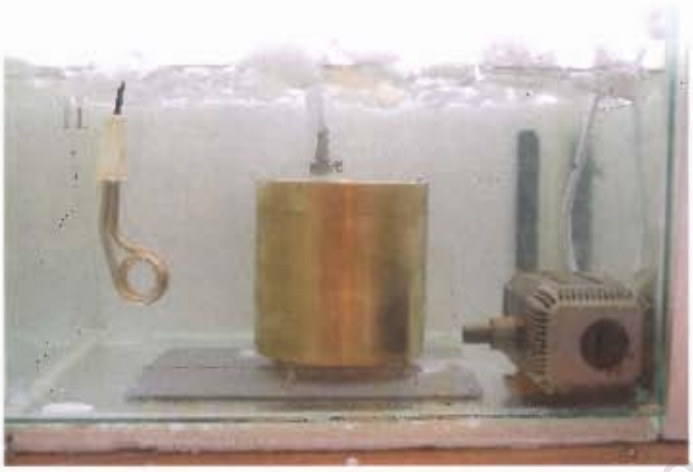

Figure 7.5: Picture of the thermal bath. In the middle can be seen the thermal jacket. The tank walls are covered by polystyrene sheets. At the top left corner the LM35 temperature sensor can be seen. One of the heating elements is visible on left centre of the picture and the submerged pump is in the bottom right corner.

in a glass tank with 5mm thick walls. The walls of the tank are covered by 25mm thick polystyrene foam sheets. These sheets help isolate the glass from changes in the room's temperature, and air movements in the room. They also ensure that no direct sunlight falls on the thermal jacket. The layer of polystyrene foam at the base of the tank also acts as a shock absorber for the system. Fragments of polystyrene have also been placed to cover the surface of the water.

Two $500W$ heating elements are submerged in the water, to allow the water to be heated above room temperature. No facility was used to cool the water, as this would have substantially increased the cost of the system without any fundamental benefits. An LM35 silicon temperature sensor was used to measure the temperature of the bath. The controller implemented a proportional integral control law and the elements were driven using triac and diac switches modulated at a controlled phase angle. The water in the bath was circulated using a submerged pump to ensure that no hot spots developed. The bath setup can be seen in figure 7.5.

The bath has been operated for temperatures of $25°C$ to $80°C$. However, the minimum operating temperature of the bath needs to be $2°C$ above the current room temperature. The bath had a temperature noise of less than $0.01°C$. It took 2.5 minutes to heat a full thermal bath through a $1°C$ change.

7.4 Data capture

As many external influences as possible should be eliminated if actual spectra are to be compared to simulated spectra. A network analyzer was used to capture the response of the tube, and with this system many uncertainties about the accuracies of the impedance measurement technique can be avoided. However, this has a side effect in that the measurement system was about $0.5m$ distant from the actual piezoceramic tube.

7.4.1 The impedance analyzer

An HP4195A network analyzer was used to measure the spectra. It was interfaced to a PC using a GPIB network. The computer ran an HPVEE routine that determined what the start and stop frequency should be, in order to have the correct resolution within the 400 point window that the network analyser sampled. The data was passed to the computer and saved to file. The HPVEE routine then moved up to the next frequency range until the whole spectrum was sampled.

The impedance analyzer was reasonably accurate (5 significant figures); however, it was extremely slow, as it took over two hours to sample a spectrum. This also made it impossible to attempt to measure more complicated liquids such as dynamic suspensions. Nonetheless, as a proof of concept, it allowed spectra to be sampled with high confidence in the results, as long as the analyzer was correctly calibrated.

7.4.2 The connecting cable

A $1m$ long coaxial cable was connected between the SMA connector, at the piezoceramic tube housing, and the impedance analyzer. This cable of course added substantially to the location and shape of the cable mode. To avoid this, the network analyzer was calibrated at the sensor end of the cable, thus making the SMA connector on the piezoceramic tube housing the location of the measurement. Spectra taken with the network analyzer calibrated on the piezoceramic tube side of cable tended to have more measurement noise than spectra taken from the network analyzer calibrated normally. An attempt was made to ensure that the cable took the same physical path to the network analyzer, to ensure that the change in cable response was minimal.

The cable ran from the network analyzer into a pipe and through a hole in the lid of the thermal jacket, and then it connected to the SMA connector in the housing, which in turn connected to the piezoceramic tube.

7.5 Sample preparation

The sampling process was carried out as follows:

First, the network analyzer was switched on and allowed to heat up to a steady condition. Then it was calibrated at the sensor end of the cable. After that, the cable was connected to the housing. The cable is not removed from the housing, until the network analyzer is calibrated again.

Before any sample was loaded into the piezoceramic tube, the tube was thoroughly washed with detergent and water. This ensured that any previous samples had been completely removed, and that there would be good coupling between the sample and the piezoceramic tube as mentioned in section 5.6. The tube was then rinsed out with water and wiped dry. The piezoceramic tube was then allowed to dry further for thirty minutes, after which a sample solution was poured into the measurement volume. The liquid was filled to more than 5mm above the top of the piezotube. Care was taken that any bubbles that were left in the solution were removed. Then the lid was closed and bolted shut.

Water was poured into the bath until it covered the temperature sensor, both the elements and the entire thermal jacket to at least 10cm depth. The submerged pump and the thermal regulator were turned on. At this stage the network analyzer was made to continuously sweep the drive to the piezoceramic tube. This was done to ensure that if the impedance measurements heated up the tube slightly, this effect would be close to steady state before measurements started. The system was then left to stabilize for two hours, after which it was checked to see whether it had reached steady state, as described in section 7.3.1.

The program was then started that triggered the impedance analyzer to sample a spectrum. This sampling process took about two hours. Over this time, care was taken not to disturb the setup. Once the program had finished, the water was drained, the sample was removed and the piezotube was cleaned to avoid sample residues caking onto it.

The spectra were then analyzed as is discussed in future chapters.

Chapter 8

Evaluation of Error

To be able to draw any mathematical comparison between data, some method is required to quantify their dissimilarity. There are many statistical methods of doing this; however, there is often a need to make a quantified error more sensitive to certain types of effects than others. For example, some methods for determining error are more sensitive to mode size that to mode placement. Simply analyzing the distances between individual points is not sufficient to give a true indication of the error. Spectral analysis is one of these cases.

8.1 Difficulties in describing spectral error

For initial attempts to calculate a metric for the error between the real and model spectra, a simple root-mean-square approach was taken, where error was calculated for the sum of all the point-to-point distances between simulated and real data points on the spectra. When optimization techniques were applied to the spectra using this error function, it was found to give poor results. It seemed that the author could produce a better fit visually than the optimizer. The difference lies in how error is perceived. The error function was:

$$d = \sqrt{\sum_i \left(Z_i^{actual} - Z_i^{sim}\right)^2} \tag{8.1}$$

where d is the error, and Z_i^{actual} and Z_i^{sim} are the impedance of the actual liquid and simulated liquid at a specific frequency. This method is a special case of Minkowski-form distance [46]. The subtraction occurs between points at the same frequency, determined by the value of i. These differences were summed to determine the error.

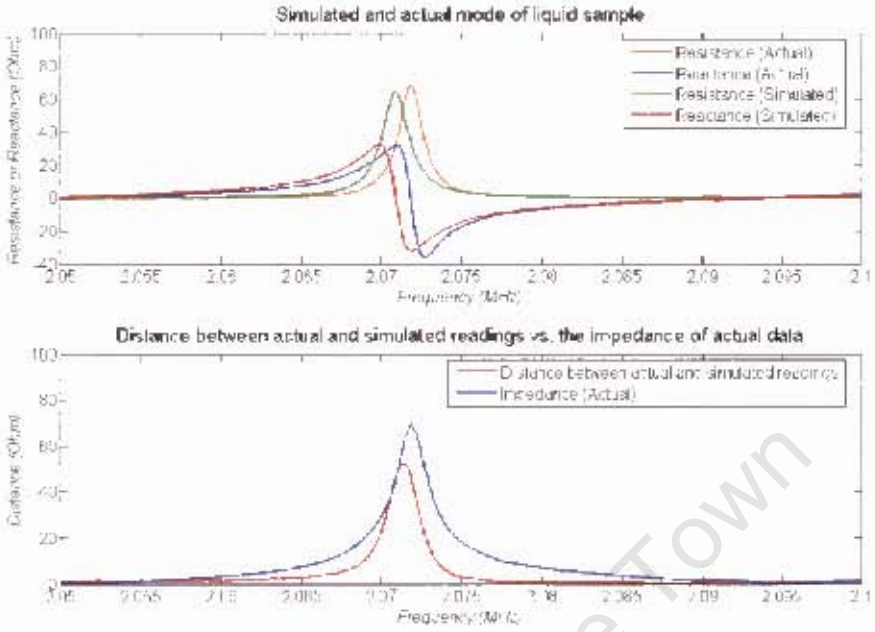

Figure 8.1: These graphs to show how a slight difference in mode placement affects error calculations. The top figure compares the spectra of an actual and a simulated mode. The bottom figure compares the distance between the two spectra with the actual impedance. Note how large the distances become with a slight variation in mode placement.

A spectrum for the liquid consists of several modes that occur at fixed intervals. Several factors, such as the relaxation time of the liquid, and slight thermal fluctuations, act on the mode placement. Thus some small variations in mode placement, compared to simulated data, do occur. This slight disparity has a large impact on error mathematically; however visually it was simple to see what made a relatively good fit.

This effect is best seen in a demonstration of a slight error in mode placement, as in figure 8.1. As can be seen, the simulated mode and the actual mode are roughly the correct size and Q. They are however 1kHz apart. On the lower plot, the absolute distance between the real and the simulated data has been shown. Note how large the spike in the error is: it is comparable in size to the impedance of the actual mode. If the two spectra were further apart, the error of the simulated mode, being slightly misplaced, will produce as much error as having no simulation mode at all. Since to obtain a noiseless actual spectrum is impossible, the error will tend always to be less for simulated data whose modes are smaller than the actual data. This is unacceptable, as it would affect the density and viscosity readings.

Changing to other error metrics that still only compare points at the same frequencies will not resolve this issue. The solution to this type of spectral comparison is to compare a measured data point at a specific frequency not only to the simulation at its own frequency, but to the frequencies around it too. This problem is common in several fields, and in particular in image processing [46].

8.2 Introducing tolerance to mode placement

More suitable error metrics can be found in so-called cross-bin dissimilarity measures. Here error is calculated not only from the point to point difference at a single frequency, but also from the difference between points around it. Several techniques are available for this, but only two techniques were implemented in this study. The technique that was implemented was a simple summing of the distance between nearest points. Match distance was also employed, and found to be less successful for this application. However, several more metrics are available, and might be optimal.

8.2.1 Distance sum between nearest neighbour points

Nearest neighbour classifiers [14] are quite common in many types of decision making applications. Here it will be used to determine the closest spectral point to the current reference point.

This technique was attempted as it includes the dimension of radial frequency into the calculation of distance, instead of only using the real and imaginary parts of impedance, thus allowing the effect of mode variations to be relaxed. This can be observed in figure 8.2. The blue line indicates the measurement of distance using nearest neighbours, whereas the dashed red line uses the difference between samples at the same frequency. For the nearest neighbour distance sum, only the nearest point with respect to absolute distance between the actual data at a specific frequency and any spectral frequency point is used. The radial frequency is used as the third dimension in this distance calculation. The difference in ω between the two points is scaled, to make it comparable in size with respect to the impedance values. This scale value can be rather important, as if the distance in ω between points is too small, the speed of sound will not be taken into account at all, and if it is too large, it is effectively back at an RMS distance system. This distance measure is always used in relation to the actual data spectrum and it cannot be called a metric, as if the simulated spectrum was to be used, a different result would be obtained.

A window range for comparison was introduced to reduce computation times. This window limits the number of points that are used, around the reference point, to find

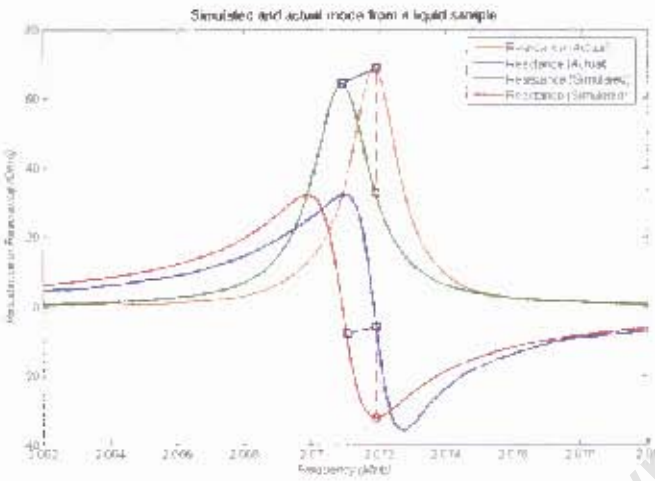

Figure 8.2: Comparison between nearest neighbour error and RMS distance error for a single reference point. The red dashed lines indicate the distance measured by simple subtraction. The blue line with square end points indicates what a nearest neighbour distance would be. The inclusion of ω as a third dimension improves the perceived error.

the nearest neighbour. This seems an obvious inclusion as the difference in ω between reference and current point will only get bigger the further they are from the reference point.

This algorithm works quite successfully, but it is more computationally intensive than potential alternative techniques. The value for the ω scaling, and the number of reference points used, depends on the properties of the liquid that were being determined. When the speed of sound is calculated, very few points are used in order to make the system extremely sensitive to speed of sound effects, and to reduce the calculation times. When density and viscosity are optimized, a large number of window points are used, to attempt to get as close a fit as possible onto the shape of modes, i.e. their size and their Q.

8.2.2 Match distance

Match distance [49] was attempted as a technique instead of the nearest neighbour distance measure, but it was not implemented in the final solution. Match distance is a special case of Earthmover distance [46], as it is one dimensional. It is based on the idea of comparing data by measuring the amount of work that would be required to turn the one spectrum into the other. It was decided that such an implementation might reduce operation times and improve the fit. The match distance is:

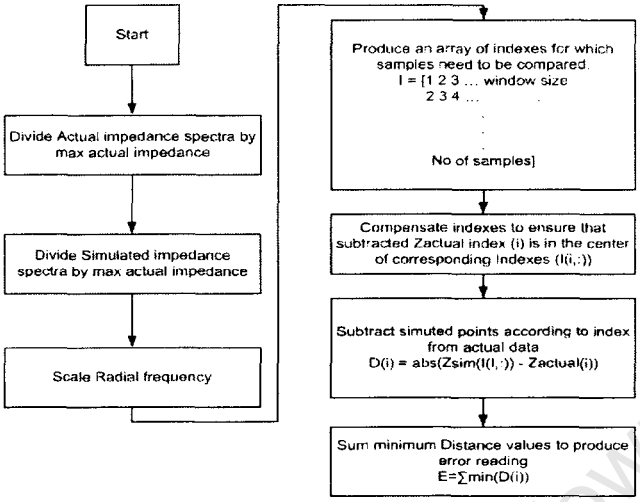

Figure 8.3: Flow chart of nearest neighbour distance algorithm.

$$d = \sum_i \left| \hat{Z}_i^{actual} - \hat{Z}_i^{sim} \right| \tag{8.2}$$

where $\hat{Z}_i^{actual} = \sum_{j \leq i} Z_j^{actual}$ and $\hat{Z}_i^{sim} = \sum_{j \leq i} Z_j^{sim}$

This distance technique accumulates the two spectra. As each frequency point is evaluated, the cumulative values for the simulated and real data are subtracted from each other. The distance is calculated by adding the differences between the cumulated values for the actual and simulated spectra, for each new frequency point. A helpful analogy would be to consider a bulldozer sculpting one landscape into another. As it drives it scrapes sand from the one area and puts it in another. The error is then calculated by how far it had to move the sand, and how much sand had to be moved.

In order for the match technique to work, both spectra have to be of the same area [46]. However, the simulated spectra cannot be normalized to make the areas equal, as this will distort the effect that density changes would have made. Instead it was decided to add or subtract a real and imaginary offset from the simulated spectra to make the area equal. This had an unfortunate consequence when the distance was optimized. Since different actual modes have slightly different sizes, this type of metric adds the distance to carry those slight size differences from the one mode to the next, to the error value. It was found that a smaller error would be produced, if all the simulated modes were made smaller, then a slightly larger offset would need to be added to make the areas of the real and imaginary data equal. The error metric

would exploit this added area, since as it would have to move less difference from one mode to the next, it could essentially sculpt the modes from an offset.

Other than the offset difficulties, this metric performed well and other variations of earthmover distance that did not require equal area could have been evaluated. It was decided that a detailed study into the effect of the metrics was outside the scope of this work.

Chapter 9

Optimization to obtain liquid parameters

Generating a simulated spectrum to represent the behaviour of the fluid, and removing the piezoceramic tube's response from the real spectrum allowed a comparison to be made between the actual and simulated spectra. However, if the physical values for the properties of the liquid are to be drawn from the actual spectrum a simulated spectrum must be able to fit accurately to an actual one, and it must be possible to determine how well such a fit can predict the value of the liquid's properties.

"Optimization is a procedure of finding and comparing feasible solutions until no better solution can be found" [16]. Many optimization techniques exist and different techniques are suitable for different problems, depending on the complexity of the error space and the number of input variables. Two techniques were implemented in this study, according to which models were being solved. They were a binary search, used for single or two input variable optimization when the error surface had only one minimum, and a breeder algorithm was used when there were many variables and the error surface had many local minima.

9.1 Adaptive Mutation Breeder Algorithm

The breeder algorithm was initially applied in fitting piezoceramic tube models to actual data when the sensor worked on the principle of comparing spectra of the piezoceramic tube coupled with the liquid, rather than that of just the liquid. This technique depends heavily on the parameters calculated for the piezoceramic tube. Thus optimization is needed to obtain those values. The piezotube model is defined by five basic piezoceramic properties, some of which are frequency dependent. Ultimately, a total of nine variables were used to define the behaviour of the piezoceramic tube.

Since the data set that was being fitted was modal in nature, the error space had several local minima. A breeder algorithm is well suited for this type of optimization.

9.1.1 Basic Description of Breeder Algorithm

Nature was the inspiration for breeder algorithms. They are based on the ability of a species to evolve to an optimum solution for its environment. The idea of evolution over several generations, where only the strongest of the species survives, is used. Evolutionary algorithms are a well-established method of optimization, and they have several advantages and disadvantages:

Advantages:

- They are very flexible
- They can get unstuck from local minima
- They can handle large numbers of input variables

Disadvantages:

- They require a lot of individual evaluations to obtain a solution, and hence can be very slow
- Due to the randomness included, the system does not always optimize to the same value or at the same rate.

All breeder algorithms follow the same form, which is shown in figure 9.1. First an initial population is established, on which the breeder algorithm will attempt to improve. In this initial population as much randomness as is practical should be included. The population should also be rather large - typically 100 individuals. This population is then evaluated. The determination of how well the individuals performed is critical, as mentioned in chapter 8. The individuals are sorted according to how well they performed. At this stage, a decision is made as to whether the optimization is complete. This decision can be based on the number of iterations, the error, a slow rate of improvement, etc. Thereafter, a new population is created based on those of the previous population which performed well (traditionally about 15% of the best performers in the last iteration are used). Several techniques can be used for this: some of them will be mentioned in section 9.1.2. Additionally, some randomness is added at this point ("mutation"). Without mutation, the chance of finding a good solution is vastly reduced. The addition of mutation allows for the solution space to be more thoroughly sampled. The new generation can then be evaluated again.

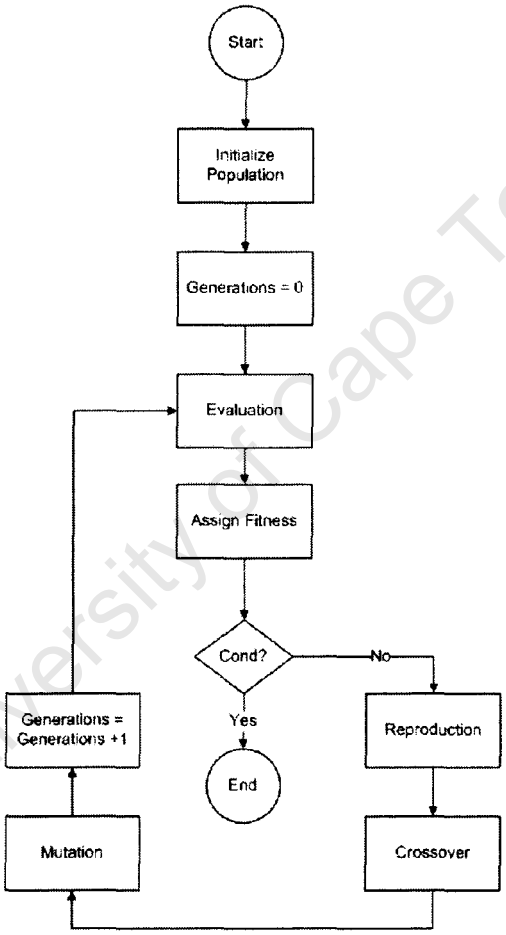

Figure 9.1: Flow chart of a Breeder Algorithm [16].

From this description it becomes apparent that for every iteration of the breeder algorithm, there will be as many evaluations of the equations used to describe the piezotube and the liquid inside it as the size of the population. Thus it can be very time consuming to iterate this type of algorithm, and it should only be used if a classical solver is unable to manage the number of variables in the solution space.

9.1.2 Methods of recombination

The choice of how the population that performed well in an evaluation should be combined to produce a new population has a significant impact as to whether an optimum solution is found, and how many iterations that will take. Several methods are available to combine pairs to form children. Three common methods are uniform crossover, line crossover and volume crossover.

- *Uniform Crossover*

  Here elements are chosen from one or other of the parents and are simply at random recombined to create the child.

- *Line Crossover*

  A straight line is drawn from the values for the one parent to the values of the other parent. Then a random point is chosen on the line. This point represents the values that will be used for the children. To prevent premature convergence, the line may be extended to be a bit longer on both sides of the parents, thus allowing data points to be on side of either parent.

- *Volume Crossover*

  The children are placed at a random location in a volume box defined by the location of the parents.

It should be noted that there are also several other, less common, techniques available to do the recombination.

The extended line crossover technique was implemented in this study. The amount of extension was also used to indicate the degree of mutation used. Also, about 10% of the next generation of children were produced by simply mutating 10% of the parents. This was found to be specially useful for obtaining the correct speed of sound for both the piezoceramic tube and the liquid as the error function is very sensitive to errors in that value. Both that mutation and the amount of line extension were linked to one variable, which allowed adaptive mutation (section 9.1.3) to be performed on both mutation values equally. Finally, the best solution from a previous iteration was

included in the next to ensure that the breeder algorithm's best solution could not get worse from one iteration to the next. This is called elitist insertion.

9.1.3 Adaptive mutation

The rate at which breeder algorithms converge to an optimal solution and the likelihood of them finding the true minimum are linked to the amount of mutation used. With a lot of mutation, the solution space is more heavily sampled, and one is more likely to find a point close to the true minimum. However, if the exact point is to be determined, a small mutation should be used around the best previous solution. Initially one would like a lot of mutation to track down as many of the local minima as possible, and as the program progresses, less mutation is desired.

However, the rate at which the best solution is found is not necessarily clear, so a routine to automatically determine which mutation rate is preferred would be beneficial to implement. This was done by mutating half of the gene pool slightly more, and the other half slightly less. When the solutions were evaluated, the mutation rate that produced the most suitable parents was used in the next iteration.

9.2 Optimization of liquid's parameters

When it was decided to optimize the spectra of the liquid directly to that of real data, the number of variables required to be optimized reduced to only those of the liquid. This implied that the use of a breeder algorithm, which tends to search for a solution rather slowly, was no longer required. A far simpler approach could be used. The speed of sound of the liquid was determined by comparing an actual sample to a simulated sample with fixed density and viscosity. This removed one degree of freedom, and thus the system was now only a two degree of freedom system, which can be optimized faster with a variety of techniques.

9.2.1 Determination of speed of sound

The speed of sound is largely responsible for the location of frequency of the liquid modes. Therefore, from the peaks of the modes it is possible to find an initial approximation. This is important to do, as every time a simulated mode corresponds with an actual one there will be a reduction in error. This reduction does not suggest that anything approaching the correct answer was found, but it is beneficial to at least be searching in the correct area in order to reduce the probability of it getting the optimizer stuck in a local minimum.

To do this, the peaks in the real spectra are found, and the frequencies of these peaks are recorded. The mean distance between peaks is used as the first approximation. Only the liquid modes around the second thickness mode of the piezoceramic tube were used for this. This approximation gave an answer that was within always 2 % of the correct answer.

However, it was found that to be close enough to be able to optimize to find an exact solution, the approximation had to be within 0.2% of the correct speed of sound. Thus, intervals of 0.2%, over a range of 2 % up and down from the approximated speed of sound were tested to find which of those solutions had the least error. This was done by setting the density and viscosity of the liquid to fixed values of $950kg.m^{-3}$ and viscosity to $0.03Pa.s$. These values were chosen at random and were only used in the optimization of the speed of sound. The viscosity was set low to ensure sufficient mode size. The values for density and viscosity were needed to calculate a simulated spectrum in order to compare it with the actual spectrum. For these calculations nearest neighbour distance was used an error function, using only a three sample point window. The two spectra that were compared were quite dissimilar, but when the liquid modes were lined up, there was still a minima at the correct speed of sound.

After the value was determined within 0.2 %, a search was performed to further resolve the speed of sound. This was done by evaluating points 0.2% above and below the previous best point, and determining which solution had the least error. This point would be the next point used, and the spacing between trial points was halved. This was iterated six times. The final speed of sound so determined proved to be adequate as a base line for further optimization.

9.2.2 Analysis of remaining error space

Now that a value for speed of sound had been defined, the nearest neighbour error was set to use a larger window (30 points). The link between density and bulk modulus can be exploited to reduce the problem to a two degree of freedom system. It was decided to link bulk modulus in further calculations to the speed of sound and the currently evaluated density. Thus, all further plots examine the behaviour between density, viscosity and error.

As can be seen from figure 9.2, a relatively smooth curve is formed for error as values for simulated density and viscosity are varied and the spectrum from the simulated liquid is compared to that of the actual liquid. It has one local minimum, although if the curve is analyzed with small enough changes in density and viscosity, some noise can be seen. It is important to note that variations in the chosen speed of sound can alter this curve, primarily in sharpness. Note also that the effect of viscosity on this

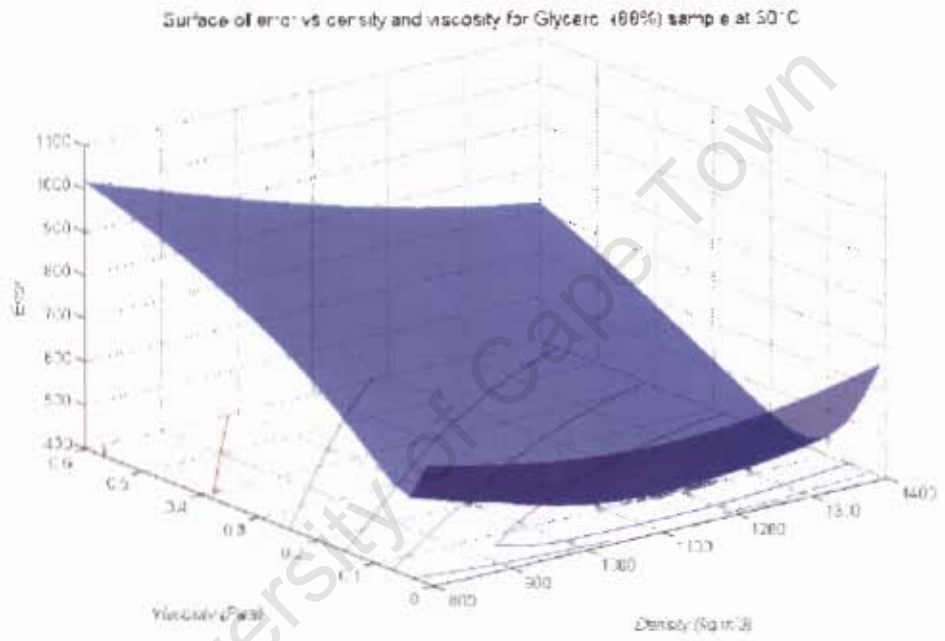

Figure 9.2: Surface plot of error in relation to density and viscosity. The plot was taken at an optimized speed of sound. Note the relative smoothness of the curve and also that it only has one minimum. Also note that the system is much more sensitive to changes in viscosity than changes in density. This surface is for a Glycerol (88%) water mixture at $30°C$.

plot is much more drastic than that of density. This is important as it indicates that measurements of density will be less accurate than measurements of viscosity. Another important factor that affects this curve is how well the cable mode has been removed.

9.2.3 Search to determine density and viscosity

Now that it was been established that this final stage of determining the liquid properties was essentially finding the minima of a bowl, many different search techniques became viable. For determining the minima, a simplex search could be used, and the final answer determined in about 100 evaluations of the simulations.

For the solutions applied here, though, it was decided to map the domain of the error, and determine the minima this way. This was done as it allowed a visual representation of how the error space changed with liquids, and also allowed for visual clues to check if a coding error had occurred. It took about 900 iterative evaluations of the liquid spectra to obtain a sufficiently accurate answer, however the system could produce a surface similar to figure 9.2 after execution.

Chapter 10

Results

The first results are presented as a set of spectra, comparing all the liquids mentioned in section 5.8, in order to show that the cable mode removal left all the spectra with the same peizoceramic tube characteristics as an empty peizoceramic tube. From there, each liquid sample's spectrum is modelled and comparisons of the simulated spectrum versus the actual spectrum will be presented for the first three peizoceramic tube thickness modes. Also, at this stage the error surface, mentioned in section 9.2, for each of the liquids will be shown. The liquids that were used, were chosen to have a high enough viscosity to ensure that the modes did not have too sharp Q. Otherwise the resolution on the Spectra would have needed to be very high, and this would have made the optimization extremely time consuming. Water was not used for this reason. Also the behavior of water often deviates from classical theory, and thus not suited this measurement technique.

10.1 Comparison of spectra after cable mode removal

Cable mode removal has to be done very accurately to allow the subtraction of the peizoceramic tube spectrum to occur with minimum error. To ensure that it is done accurately, the reactance of the liquid spectrum is lined up to that of an empty tube. This can be seen for all the liquids in figure 10.1.

10.2 Comparison between optimized spectra and actual spectra and error space for each liquid

In this study four liquids were tested. They were castor oil, a glycerol (88%) / water mixture, olive oil and linseed oil. All samples were taken at 30 degrees. Reference measurements were also made of viscosity at that temperature and of density, to

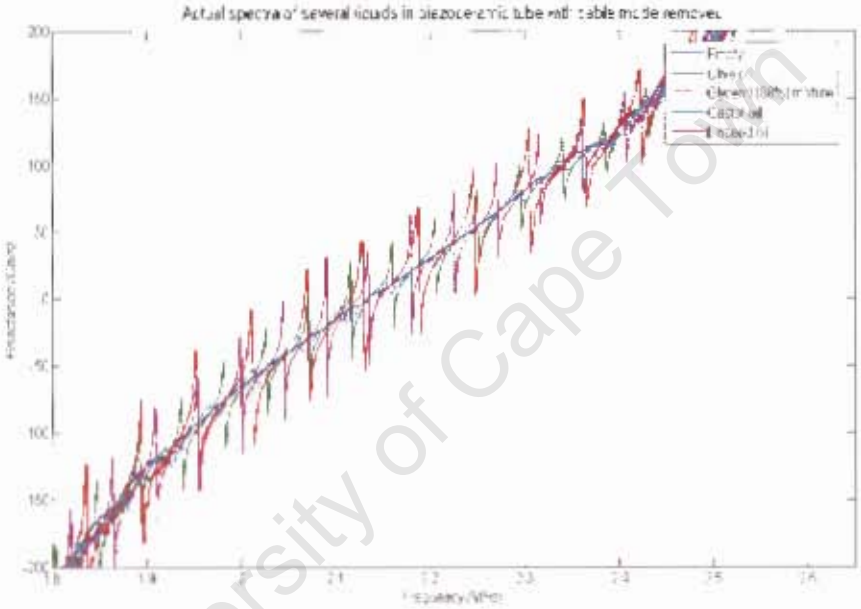

Figure 10.1: Reactance spectra of empty piezoceramic tube, with case capacitance removed, and of the tube filled with different liquids. These spectra are taken across the second harmonic of the tube. The reactance of the empty tube runs through the center of the of the reactance lines for the liquids, showing that the values of the case capacitance are acceptable.

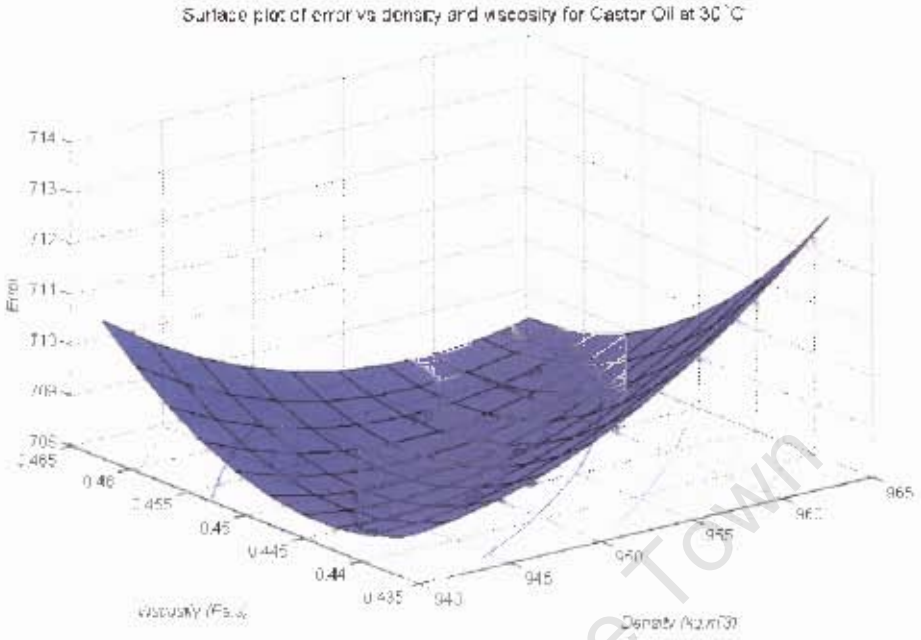

Figure 10.2: Surface plot of the error vs simulated density and viscosity compared to castor oil sample at 30°C.

allow for a comparison to be made. This was done using a Physica rheometer and a pycnometer.

All model optimizations were performed using the same transformer ratio of 2.25×10^6, a coupling resistance of 110Ω and a coupling capacitance of $1.6nF$.

10.2.1 Castor Oil

Castor oil was the most viscous sample tested. As can be seen from its spectrum in figures 10.3 to 10.5, most of the liquid modes' resonant response for the castor oil has been damped by the third peizoceramic tube mode. This means that fitting the resonant response to the third mode is more difficult, and it increases the possible error in measuring speed of sound substantially. And, as the mode sizes are much smaller, many more spurious modes are visible.

The speed of sound was determined to be $1482.8m.s^{-1}$ compared to a reference value of $1474m.s^{-1}$ [53]. For this speed of sound, the density optimized to $947.9kg.m^{-3}$ compared to a reference reading of $955kg.m^{-3}$ and the viscosity optimized to $0.4509Pa.s$ compared to a reference reading of $0.456Pa.s$.

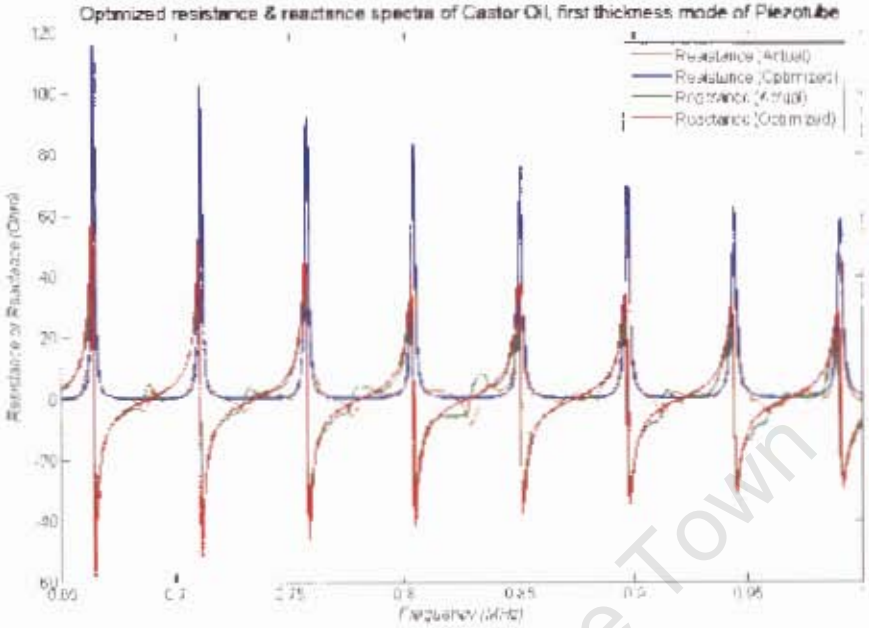

Figure 10.3: Resistance and reactance spectra for actual and modelled castor oil sample at $30^{\circ}C$ over the first thickness mode of the piezotube.

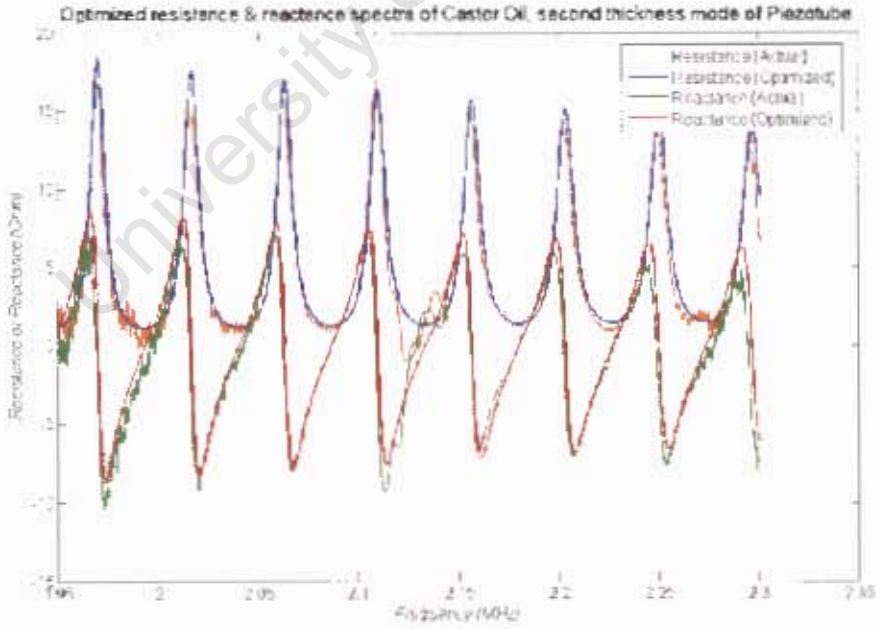

Figure 10.4: Resistance and reactance spectra for actual and modelled castor oil sample at $30^{\circ}C$ over the second thickness mode of the piezotube.

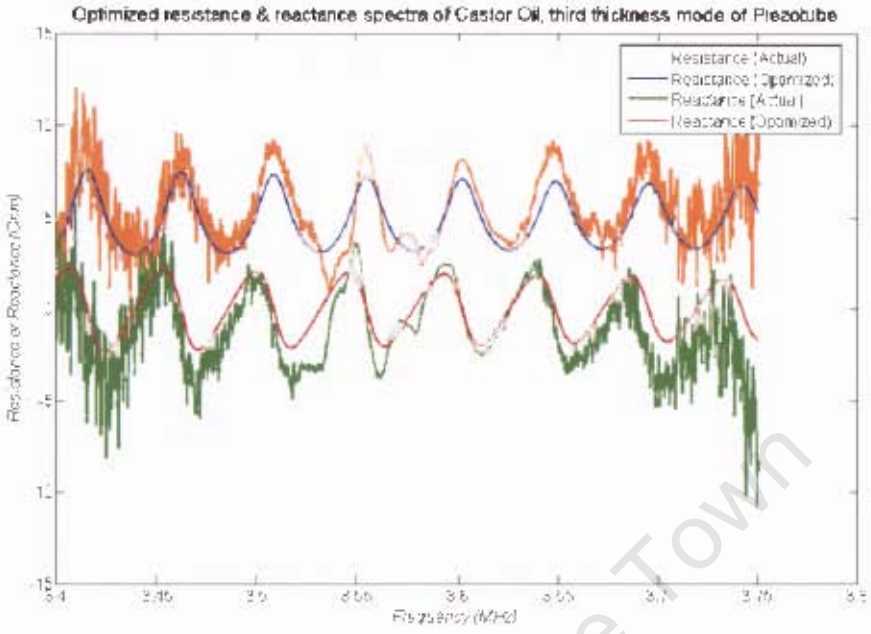

Figure 10.5: Resistance and reactance spectra for actual and modelled castor oil sample at $30°C$ over the third thickness mode of the piezotube.

10.2.2 Glycerol (88%) / Water mixture

This glycerol/water mixture was chosen as it was a sample of higher density in relation to other measured samples, and the intention was to determine whether this distinction could be determined. Unfortunately however, the bulk modulus of glycerol relaxes with an increase in frequency [12]. This acts to change the speed of sound with frequency, as can be seen in that the liquid mode placement over the first thickness mode of the peizoceramic tube, figure 10.7, does not fit as well as that over the second or third thickness modes, figures 10.8 and 10.9. However, this behaviour is normally most visible at low frequencies, and should not have a major impact on the liquid modes by the second or third thickness mode.

The speed of sound was determined to be $1868.2 m.s^{-1}$ compared to an interpolated reference value of $1892 m.s^{-1}$ [2]. For this speed of sound, the density optimized to $1262.8 kg.m^{-3}$ compared to a reference measurement of $1225 kg.m^{-3}$ and the viscosity optimized to $0.1163 Pa.s$ compared to a reference measurement of $0.0993 Pa.s$.

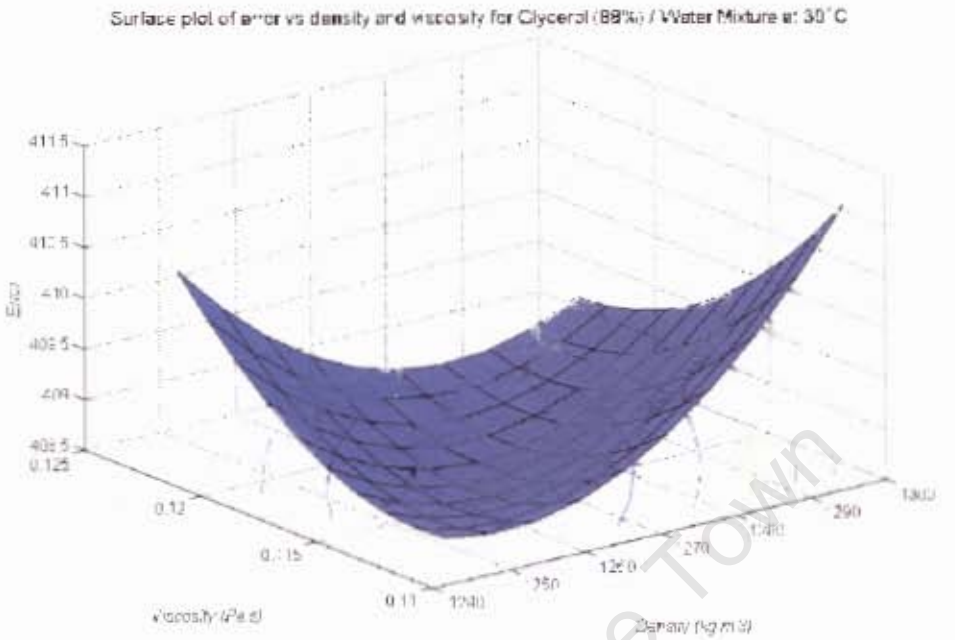

Figure 10.6: Surface plot of the error vs simulated density and viscosity for a glycerol (88%) / water mixture sample at $30°C$.

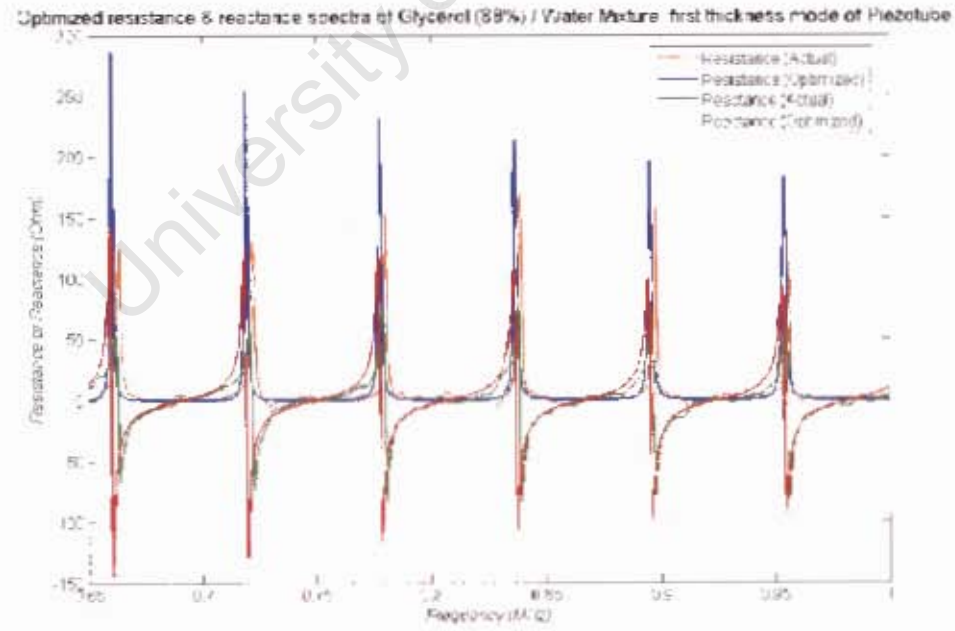

Figure 10.7: Resistance and reactance spectra for actual and modelled glycerol (88%) / water mixture sample at $30°C$ over the first thickness mode of the piezotube.

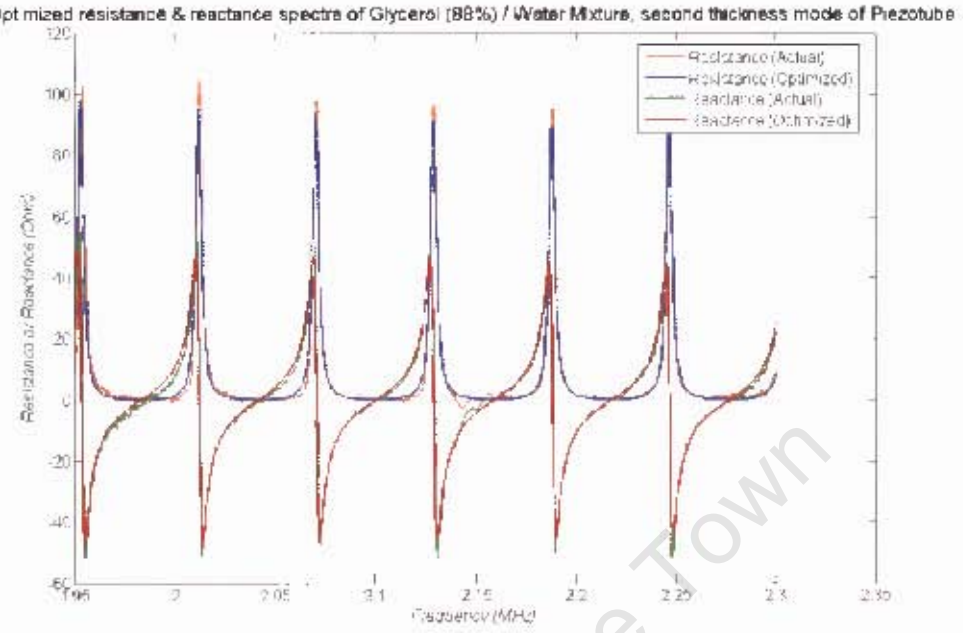

Figure 10.8: Resistance and reactance spectra for actual and modelled glycerol (88%) / water mixture sample at 30°C over the second thickness mode of the piezotube.

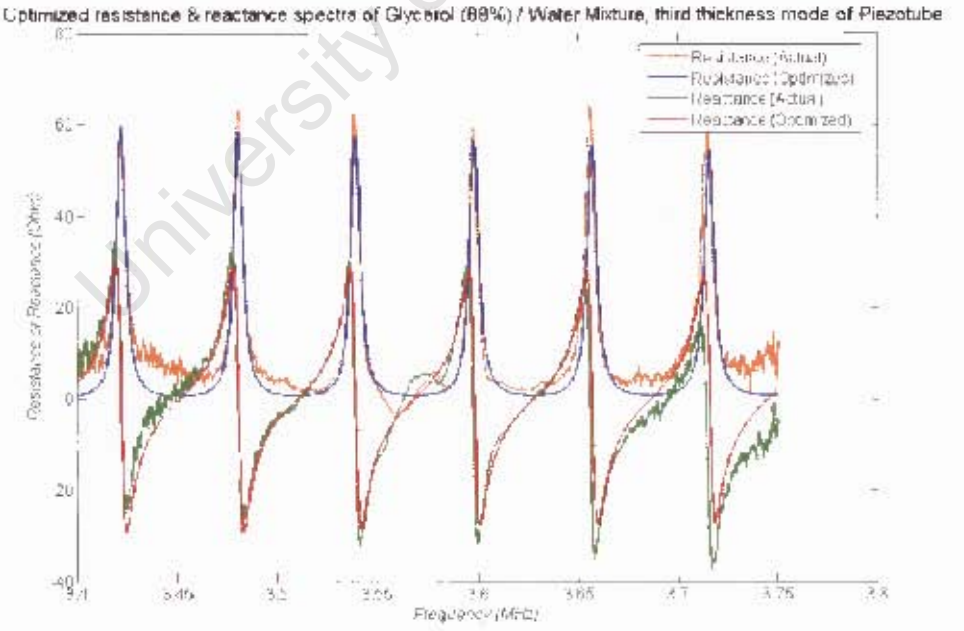

Figure 10.9: Resistance and reactance spectra for actual and modelled glycerol (88%) / water mixture sample at 30°C over the third thickness mode of the piezotube.

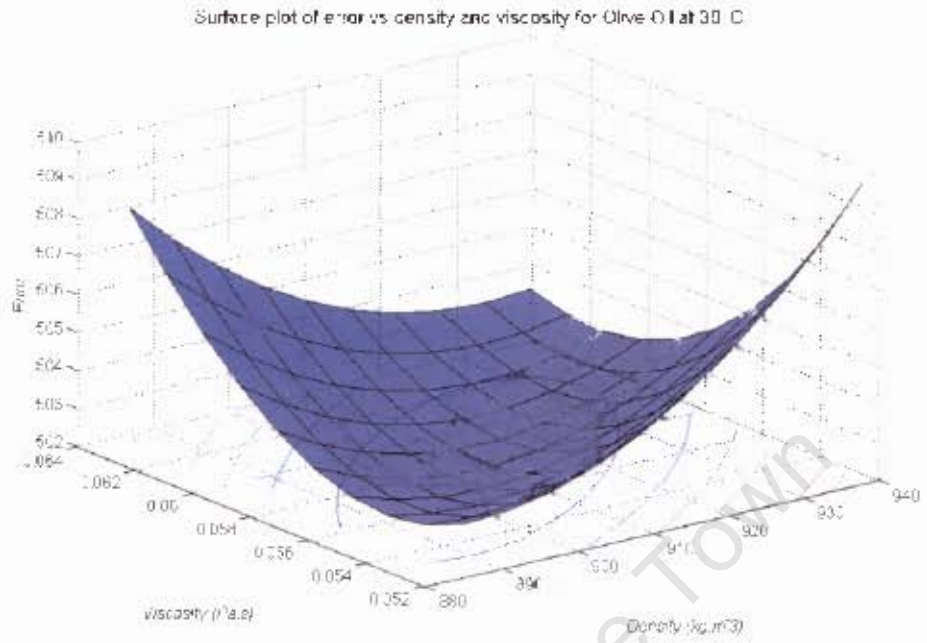

Figure 10.10: Surface plot of the error vs simulated density and viscosity for a olive oil sample at $30°C$.

10.2.3 Olive Oil

Olive oil is quite regularly used as a reference for viscosity in liquids and it was the least dense sample used. The modelled spectra fitted the real data very accurately.

The speed of sound was determined to be $1424.9 m.s^{-1}$ compared to a reference values of $1445 m.s^{-1}$ [2] and $1465 m.s^{-1}$ at $25°C$ [36]. For this speed of sound, the density optimized to a $909.01 kg.m^{-3}$ compared to reference measurement of $910 kg.m^{-3}$ and the viscosity optimized to $0.0573 Pa.s$ compared to a reference measurement of $0.0526 Pa.s$.

Although this sample's modelled density and real density are very close, a detailed look at the surface of error shows how insensitive the error plot of this sample (figure 10.10), and that for the other samples, is to changes in density, compared to that for changes in viscosity.

10.2.4 Linseed Oil

In order to evaluate if small changes in parameters - particularly density - can be determined, a sample of linseed oil was used in comparison with that of olive oil. Later it was noticed that linseed oil had an unfortunate further influence on the peizoceramic

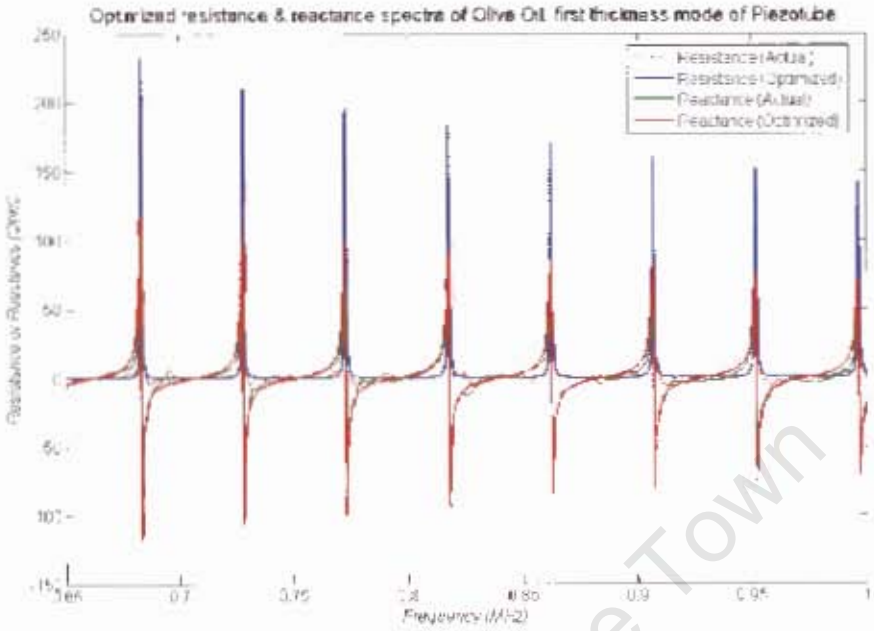

Figure 10.11: Resistance and reactance spectra for actual and modelled olive oil sample at $30°C$ over the first thickness mode of the piezotube.

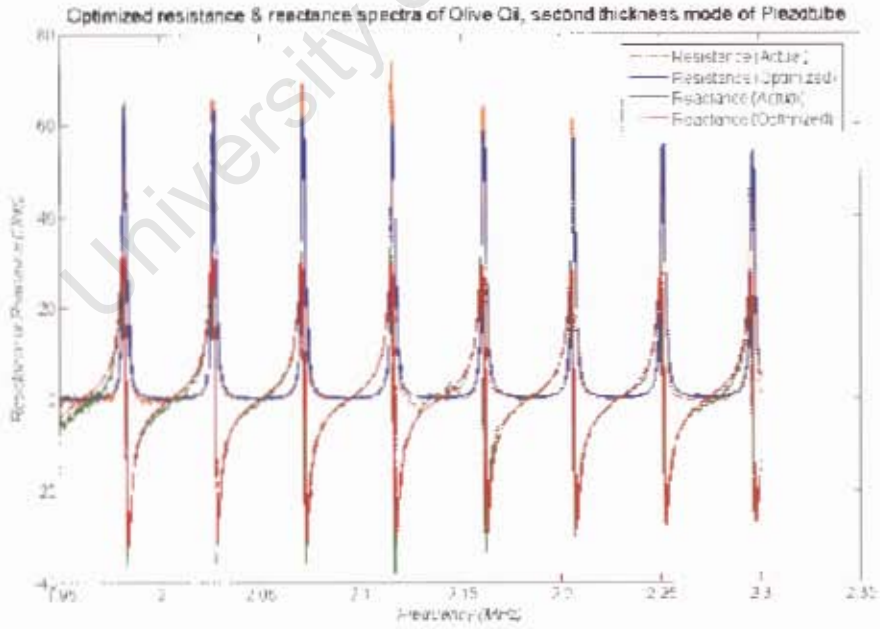

Figure 10.12: Resistance and reactance spectra for actual and modelled olive oil sample at $30°C$ over the second thickness mode of the piezotube.

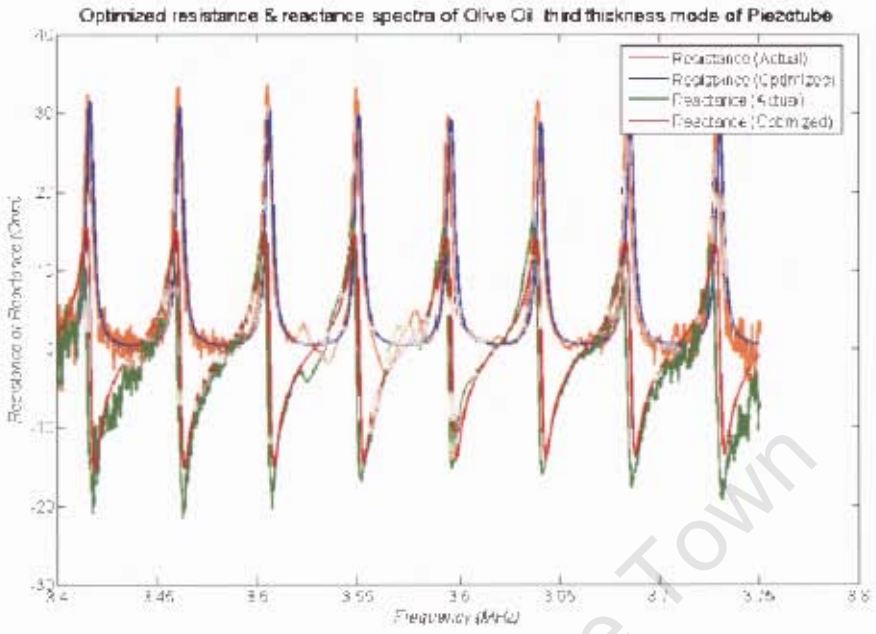

Figure 10.13: Resistance and reactance spectra for actual and modelled olive oil sample at 30°C over the third thickness mode of the piezotube.

tube. It influenced the effect of coupling between the tube and the next liquid sample used after the linseed oil sample was removed. One of linseed oil's applications is as a varnish, so a prolonged influence on the surface of the tube should have been no surprise. This influence, however, was only apparent for a day or two; after that the response of the peizoceramic tube returned to that of an unaffected tube.

The speed of sound was determined to be $1437.6m.s^{-1}$ compared to a reference value of $1460m.s^{-1}$ [2]. For this speed of sound, the density optimized to $914.86kg.m^{-3}$ compared to reference reading of $920kg.m^{-3}$ and the viscosity optimized to $0.0360Pa.s$ compared to a reference reading of $0.0332Pa.s$.

10.3 Discussion

As a proof of concept, this system worked better than initially anticipated. It was definitely able to discern between the different sample liquids tested, and to extract the physical parameters with some accuracy.

The effect of density on the error surface is far less than that of viscosity; this means that values determined for density hold less credibility than those determined for viscosity. Yet values for density are actually determined to be quite close to the

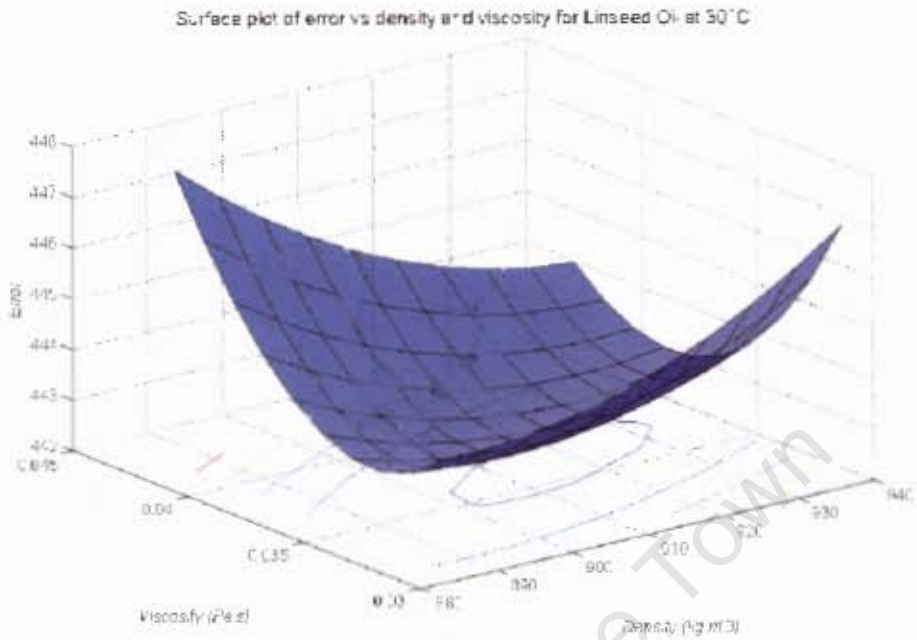

Figure 10.14: Surfance plot of the error vs simulated density and viscoity for a linseed oil sample at $30°C$.

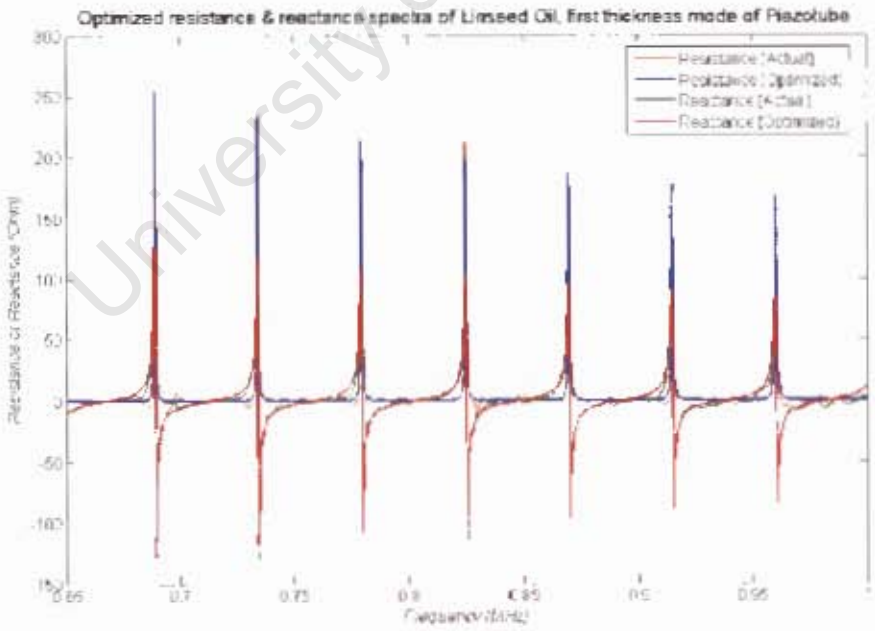

Figure 10.15: Resistance and reactance spectra for actual and modelled linseed oil sample at $30°C$ over the first thickness mode of the piezotube.

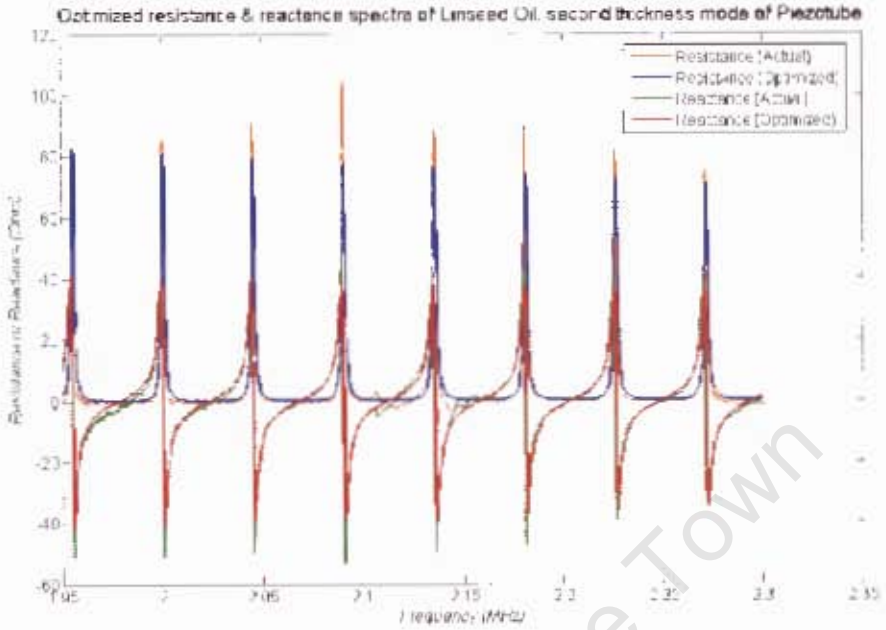

Figure 10.16: Resistance and reactance spectra for actual and modelled linseed oil sample at 30°C over the second thickness mode of the piezotube.

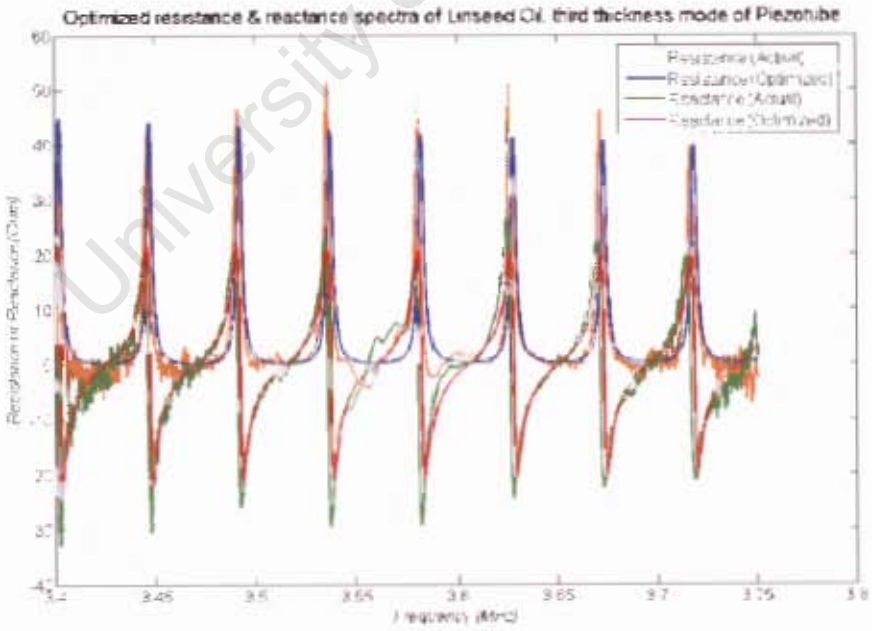

Figure 10.17: Resistance and reactance spectra for actual and modelled linseed oil sample at 30°C over the third thickness mode of the piezotube.

true value. It was also found that if the density of the liquid was known, the optimized value for viscosity was far more accurate.

Another interesting point is how similar the spectra of linseed oil and olive oil are in relation to each other, with only a liquid mode size difference visible, primarily around the third thickness harmonic of the peizoceramic tube, and yet, the optimizer was able to discern between the slight changes in characteristics of these liquids. A similar comparison can be made for the spectra of linseed oil and the glycerol mixture, as their mode sizes are very similar; nonetheless the optimizer was able to determine that the glycerol mixture was substantially more dense than the linseed oil.

The coupling ratios were assumed to be the same for all samples. However, it is very unlikely that this will be accurate, as each sample will most likely produce its own dynamics at the wall of the peizoceramic tube. The impact that this had on the results is unknown, and future work will have to determine a method to minimize this effect.

Chapter 11

Conclusions

This thesis aimed to show that the impedance spectrum of a liquid filled piezoelectric tube could be used to measure not only the speed of sound, but also the density and viscosity of the liquid. However, such an impedance response contains not only the liquid modes, but also the tube's modes. It was possible to exploit an understanding of the tube resonance to acquire an accurate response of the liquid. By modelling of these responses and optimizing the model to real data, a sensor was produced. The following conclusions were drawn:

- The fitting of actual data to a simulated spectrum allowed for density, viscosity and speed of sound to be determined, with an error of 3% in density and 10% for viscosity. This implies that a piezoceramic tube can be used as a low cost in-line sensor for these variables.
- The use of impedance subtraction to remove the response of the piezoceramic tube from a impedance spectrum produces sufficiently accurate spectra for successful optimization to obtain liquid parameters. Although one of the other models used, namely the derivation from continuum equations, showed a relatively good fit when comparing liquid coupled to piezoceramic spectra, the system struggled computationally and only allowed for the comparison of coupled spectra, which led to poor results.
- The derived equation for the liquid response and the actual data had a good fit, both in respect to mode placement and mode size for Newtonian liquids.
- The resonant mode produced by the case capacitance and the cable impedance can be successfully removed using an RLC equivalent circuit, as long as the mode is made to be at a high frequency, in comparison with the sampled spectra.

- It was shown that the determination of error between actual and simulated spectra was not a clear-cut calculation. It order to allow for equal influence of both mode size and placement of liquid modes, a nearest neighbour distance error reading was implemented which showed reasonable accuracy during optimization.

- Results were determined through optimization. It was found that breeder algorithms gave a significant benefit for models that had many system variables; however, with the reduction of the model complexity, a search algorithm was preferred as it required fewer evaluations and thus less time to return a result.

- Coupling between the liquid and the piezoceramic tube has been found to have a significant impact on the spectra for different liquids. The impact of this was reduced through the use of a soapy liquid to rinse out the tube before it was filled with a new sample. Although this effect still remained, the results for the sensor's viscosity and density measurements showed that its contribution seemed to remain constant.

Chapter 12

Future work

The work done here was part of a proof of concept. I did show that the implementation of this type of sensor is at least feasible. However, further research would need to be done into the more intricate aspects of the sensor's final design in order to make it practical.

- Currently the impedance readings are taken with an impedance analyzer. It had the benefit of giving very accurate impedance readings, but it was also very time consuming. During the time taken to make a reading, the liquid needed to remain at constant temperature. The use of a fast impedance capturing system would reduce the amount of time between samples, and remove the need for thermal regulation, as it can be assumed that a sample's temperature cannot change significantly in a few microseconds.

  The proposed method is a time-pulsed impedance measurement system. Here an extremely narrow pulse of voltage is applied to the piezoceramic tube, and the current in the tube is measured. By dividing the Fourier transforms of the voltage and the current measured, the impedance of the tube can be determined. This system requires a sampling rate of at least 20MHz, in order to capture impedances of up to 10MHz. Thus this requires a rather complicated circuit. Also, the sensor might benefit in computation time from the use of a FPGA. The calculation of impedances for the simulated spectra at 50000 sample points lends itself well to parallel processing. It should also be noted that the, sensor for this work, was based on a stable system. Whether the equations approximate such a quasi-stable system, is yet to be determined.

- Further work needs to be done into the study of the wetting phenomena and the impact of the coupling components to the spectral response of the piezotube-liquid system. Test should be done to see whether a coupling layer could be used

to minimize or stabilize the effect, in order to remove the need for washing the tube with a soapy liquid.

- Another factor that will have an impact is surface roughness, and its impact should be determined. Also the RC model used to simulate these effects could be improved by studying the impact of different surface roughness on the spectrum, and deriving governing equations for the effect.

- During this work, only one piezotube was taken though to a final implementation. However, a change in tube shape will have a significant impact on the placement of the liquid and the piezoceramic tube modes. This allows for the deliberate tuning of the thickness modes of the tube in relation to the liquid modes, effectively tuning the response of the tube to the characteristic of the liquids that are to be measured. Thus the dimension of the wall thickness in relation to the inner diameter is important. A study should also be done to determine the impact of increasing the length of the piezoceramic on the coupling components measured, as the percentage of sound that escapes out of the ends of the tube will diminish with a longer tube.

- The evaluation of error has an important role to play in the determination of what liquid parameters will produce the optimal answer. Only two error techniques were attempted in this work; however many more variations have been applied to other fields of study like image recognition. Thus a study should be implemented to determine which error metric will produce the most reliable results.

- As this was a proof of concept, a static environment was used to take readings. However, if this sensor was to be used in an in-line application, the impact of flow on the spectra would need to be evaluated. The impact is assumed to be small for low flow rates. If the sensor was to be used to determine properties of a suspended media, the flow rate would need to be quite high to ensure that the sample does not settle. The impact of these high flow rates has yet to be determined. Another impact of flow could be a change in temperature profile through the tube. This would adversely impact the spectra taken and the liquid modes would be blurred over a certain region. The exact impact of this should also be determined.

- The cable that connects the piezoceramic tube to the network analyzer produces a substantial mode in the measured spectra. This mode was removed by subtracting a model for that behaviour. With the current construction, the liquid's electrical characteristics had an impact on both the resistance of the mode and

the placement of the mode. This impact can be removed both through careful design of the housing of the tube to minimize the impact of the liquid's physical capacitance, and through placing multiple contact points on the tube to reduce the slight change in resistance experienced. Also work should be done on the seal that is used to locate the tube, to reduce the impact of its damping.

- As could be seen in the glycerol sample, not all liquids are ideal; they can change both in speed of sound and in viscosity, with frequency and even with flow rates. These impacts are described in the literature and can be included in the model for the liquid. This increase in the complexity of the model will allow more liquids to be characterized accurately. This system should be very good at determining the behaviour of liquids whose speed of sound relaxes; yet it is less likely that the spectral response due to viscosity can be determined.

Lists of symbols

$\frac{B}{A}$	Non-linearity parameter for liquids
ρ	Density
m	Mass of liquid
V	Volume of liquid
B	Bulk Modulus
p	Pressure
c_l	Speed of sound for longitudinal waves travelling in a liquid
d	Distance that sound traveled
t	Time
η	Viscosity
τ	Shear Stress
$\dot{\gamma}$	Strain Rate
σ	Stress
ε	Strain
C^E	Stiffness Matrix
e^{φ}	Piezoelectric Constant Matrix
q	Charge Density
E	Electric Field
f_r	Resonant Frequency

N Frequency Constant

r_o Outer Radius of tube

r_i Inner Radius of tube

L Length of tube

A Area

t Plate Thickness

ε_{33}^{s} Clamped permittivity

h_{33} Piezoelectric constant

c_{33}^{D} Speed of sound in the ceramic

ω Angular frequency

C_o Capacitance of Piezoceramic

u Displacement

λ Lamé Constant

μ Lamé Constant

$\frac{dy(r)}{dr}$ Radial displacement

J_o Bessel's equation

Y_o Bessel's equation

Z_i Acoustic Impedance on Inner surface

Z_o Acoustic Impedance on Outer surface

R Resistance

L Impedance

C Capacitance

n Transformer Ratio

Z Impedance

v Viscosity

k Bulk modulus

φ Displacement field

j $\sqrt{-1}$

d Earthmover Distance

Bibliography

[1] http://www.ferroperm-piezo.com/definitions.html, August 2003.

[2] http://www.ondacorp.com/tables/liquids.pdf, April 2007.

[3] L. Allegra and A. Hawley. Attenuation of sound in suspensions and emulsions - theory and experiments. *J. Acoust. Soc. Am.*, 51:1545, 1972.

[4] B. Antohe and B. Wallace. The determination of the speed of sound in liquids using acoustic resonance in piezoelectric tubes. *Meas. Sci. Technol.*, 10:994–998, 1999.

[5] J. Auge, P. Hauptmann, J. Hartmann, S. Rösler, and R. Lucklum. New design qcm sensor in liquids. *Sensors and Actuators B*, 24-25:43–48, 1995.

[6] F. Barez, W. Goldsmith, and J. Sackman. Longitudinal waves in liquid-filled tubes-i: Theory. *Int. J. Mech. Sci*, 21:213–221, 1978.

[7] R. Beyer. Parameter of nonlinearity in fluids. *J. Acoust. Soc. Am.*, 32(6):719–721, 1960.

[8] V. Buckin, B O'Discoll, and C. Smyth. Ultrasonic spectroscopy for material analysis. recent advances. *Spectroscopy Europe*, 15(1):20–25, 2003.

[9] S. Butterworth. On electrically maintained vibrations. *Proc. Phys. Soc.*, 27:410–424, 1915.

[10] W. Cady. Piezoelectric equations of state and their application to thickness-vibration transducers. *J. Acoust. Soc. Am.*, 22(5):579, 1950.

[11] W. Cady. Graphical aids in interpreting the performance of crystal transducers. *J. Acoust. Soc. Am.*, 25(4):687–696, 1953.

[12] T. Christensen and N. Olsen. Determination of the frequency-dependent bulk modulus of glycerol using a piezoelectric spherical shell. *Phys. Rev. B*, 49(21):15396–15399, 1994.

[13] P. Coghill, M. Millen, and B. Sowerby. On-line particle size analysis using ultrasonic velocity spectroscopy. *Particle and Particle Systems Characterisation*, 14:116–121, 1997.

[14] T. Cover. Nearest neighbor pattern classification. *IEEE Transactions on information technology*, IT-13(1):21–27, 1967.

[15] J. Davies. *Continuous wave mode locking for the determination of the acoustic nonlinearity parameter B/A*. PhD thesis, University of Cape Town, 2001.

[16] K. Deb. *Multi-Objective Optimization using Evolutionary Algorithms*. John Wiley & sons, LTD, 2003.

[17] J. Dion, E. Cornieles, F. Galindo, and K. Agbossou. Exact one-dimensional computation of ultrasonic transducers with several piezoelectric elements and passive layers using the transmission line analogy. *IEEE Trans. Ultrason. Ferro. Freq. Control*, 44(5):1120–1131, 1997.

[18] D. Ebenezer and L. Joseph. Frequency-dependant open-circuit acoustic sensitivity of fluid-filled, coated, radially polarised piezoelectric ceramic cylindrical shells of arbitary thickness and infinite lenght. *IEEE Trans. Ultrason. Ferro. Freq. Control*, 48(4):914–921, 2001.

[19] R. Etchenique and A. Weisz. Simultaneous determination of mechanical moduli and mass of thin layers using nonadditive quartz crystal acoustic impedance analysis. *J. Appl. Phys.*, 86(4):1994–2000, August 1999.

[20] E. Everbach and R. Apfel. An interferometric technique for b/a measurement. *J. Acoust. Soc. Am.*, 98(6):3428–3438, 1995.

[21] M. Greenspan and C. Tschiegg. Sing-around ultrasonic velocimeter for liquids. *Rev. Sci. Instrum.*, 28(11):897–901, 1957.

[22] J. Haskins and J. Walsh. Vibrations of ferroelectric cylindrical shells with transverse isotropy. i. radially polarized case. *J. Acoust. Soc. Am.*, 29(6):729–734, June 1957.

[23] T. Hertz, S. Dymling, K. Lindström, and H. Persson. Viscosity measurement of an enclosed liquid using ultrasound. *Rev. Sci. Instrum.*, 62(2):457–462, 1991.

[24] T. Hueter and R. Bolt. *Sonics: Techniques for the use of sound and ultrasound in engineering and science*. John Wiley & sons, 1955.

[25] J. Hunter. The absorbtion of ultrasonic waves in highly viscous liquids. *J. Acoust. Soc. Am.*, 13:36–40, July 1941.

[26] S. Karim and L. Rosenhead. The second coefficient of viscosity liquids and gases. *Reviews of Modern Physics*, 24:108–116, 1952.

[27] V. Kremlevskii and A. Stepichev. Measurement of viscosity and density of a liquid by means of a vibratory transducer. *Soviet Physics - Acoustics*, 21(1):37–40, 1975.

[28] R. Krimholz, D. Leedom, and G. Matthaei. New equivalent circuit for elementary piezoelectric transducers. *Electron. Letters*, 6:398–399, 1970.

[29] V. Krutin and I. Smirnitskii. Measurement of the viscosity of newtonian fluids by means of vibratory probes. *Soviet Physics - Acoustics*, 12(1):42–45, 1966.

[30] T. Ledwidge and G. Hughes. Gas density measurement by the natural damping of a vibrating reed. *J. Phys. E: Sci. Instrum.*, 44:385–387, 1967.

[31] T. Lin and G. Morgan. Wave propagation through fluid contained in a cylindrical, elastic shell. *J. Acoust. Soc. Am.*, 28(6):1165–1176, 1956.

[32] G. Lévêque, J. Ferrandis, J. van Est, and B. Cros. An acoustic sensor for simultaneous density and viscosity measurement in liquids. *Rev. Sci. Instrum.*, 71(3):1433–1440, 2000.

[33] W. Mason and M. Hill. Measurement of the viscosity and shear elasticity of liquids by means of a torsionally vibrating crystal. *Transactions of A.S.M.E.*, pages 359–370, May 1947.

[34] W. P. Mason. *Electromechanical Transducers and Wave Filters.* Van Nostrand, Princeton, NJ, 1948.

[35] F. May and J. Dual. Focusing of pulses in axially symmetric elastic tubes with fluid filling and piezo actuator by a finite difference simulation and a method of time reversal. *Wave Motion*, 43:311–322, 2006.

[36] J. McClements and M. Povery. Ultrasonic analysis of edible fats and oils. *Ultrasonics*, 30(6):383–388, 1992.

[37] H. McSkimmin. Measurement of dynamic shear viscosity and stiffness of viscous liquids by means of traveling torsional waves. *J. Acoust. Soc. Am.*, 24(4):355–365, 1952.

[38] H. McSkimmin. Variations of the ultrasonic pulse-superposition method for increasing the sensitivity of delay-time measurements. *J. Acoust. Soc. Am.,*, 37(5):864–871, 1965.

[39] B. Mert, H. Sumali, and O. Campanella. A new method to determine viscosity of liquids using vibration principles. *Rheol Acta*, 42:534–543, 2003.

[40] B. Mert, H. Sumali, and O. Campanella. A new method to measure viscosity and intrinsic sound velocity of liquids using impedance tube principles at sonic frequencies. *Rev. Sci. Instrum.*, 75:2613–2619, 2004.

[41] T. G. Mezger. *The Rheology Handbook.* Vincentz Verlag, 2002.

[42] B. Prenzlow. Design of a low pressure system to determine the acoustic nonlinearity parameter b/a for small volumes of sample liquids. Master's thesis, University of Cape Town, 2003.

[43] V. Rama Rao and J. Vandier. Acoustics of fluid-filled boreholes with pipe: Guided propagation and radiation. *J. Acoust. Soc. Am.*, 105(6):3057–3066, 1999.

[44] M. Redwood. Transient performance of a piezoelectric transducer. *J. Acoust. Soc. Am.*, 33:527–536, 1961.

[45] W. Roth and S. Rich. A new method for measurement of continuous viscosity measurement. general theory of the ultra-viscoson. *J. Appl. Phys.*, 24:940–950, 1953.

[46] Y. Rubner, C. Tomasi, and L. Guibas. The earth mover's distance as a metric for image retrieval. Technical Report STAN-CS-TN-98-86, Computer Science Department, Stanford University, 1998.

[47] T. Schneider and S. Martin. Influence of compressional wave generation on thickness-shear mode resonator responce in a fluid. *Anal. Chem.*, 67:3324–3335, 1995.

[48] C. Sehgal, R. Bahn, and J. Greenleaf. Measurement of the acoustic nonlinearity parameter b/a in human tissue by a thermodynamic method. *J. Acoust. Soc. Am.*, 76(4):1023–1029, 1984.

[49] H. Shen and A. Wong. Generalized texture representation and metric. *Computer, Vision, Graphics and Image Processing*, 23:187–206, 1983.

[50] S. Sherrit, S. Leary, B. Dolgin, and Y. Bar-Cohen. Comparison between the mason and klm equivalent circuits for piezoelectric resonators in the thickness mode. *IEEE Ultrasonics Symposium*, 1999.

[51] S. Sherrit, H. Wiederick, B. Mukherjee, and M. Sayer. An accurate equivalent circuit for the unloaded piezoelectric vibrator in the thickness mode. *J. Phys. D: Applied Phys.*, 30:2354–2363, 1997.

[52] B. Sinha, T. Plona, S. Kostek, and S. Chang. Axisymmetric wave propagation in fluid-loaded cylindrical shells. i: Theory. *J. Acoust. Soc. Am.*, 92(2):1132–1143, 1992.

[53] R. Timme. Speed of sound in castor oil. *J. Acoust. Soc. Am.*, 52:989–992, 1972.

[54] J. Vollmann. *Wave Propagation in Viscoelastic and Anisotropic, Cylindrical Structures.* PhD thesis, Swiss Federal Institute of Technology, 1996.

[55] J. Woodward. A vibrating-plate viscometer. *J. Acoust. Soc. Am.*, 25(1):147–151, 1953.

[56] R. Zangger and D. Bell. Viscosity measurement. *Control & Instrumentation*, pages 28–31, February 1975.